UNCLASSIFIED

12

SECU [illegible] nlered)

AD-A257 907

| | READ INSTRUCTIONS BEFORE COMPLETING FORM |
|---|---|
| 1. RI [illegible] PAGE / GOVT ACCESSION NO. | 3. RECIPIENT'S CATALOG NUMBER |
| 4. TI Three-Terminal Superconducting Device Research | 5. TYPE OF REPORT & PERIOD COVERED FINAL TECHNICAL REPORT Sept. 16, 1985- Jan. 15, 1991 |
| | 6. PERFORMING ORG. REPORT NUMBER N/A |
| 7. AUTHOR(s) Dr. William J. Gallagher | 8. CONTRACT OR GRANT NUMBER(s) N00014- 85- C- 0361 |
| 9. PERFORMING ORGANIZATION NAME AND ADDRESS IBM Thomas J. Watson Research Center P.O. Box 218 Yorktown Heights, NY 10598 | 10. PROGRAM ELEMENT, PROJECT, TASK AREA & WORK UNIT NUMBERS Task No. NR 604-006 |
| 11. CONTROLLING OFFICE NAME AND ADDRESS Office of Naval Research Dept. of the Navy 800 N. Quincy St., Arlington, VA 22217-5000 | 12. REPORT DATE Sept. 18, 1992 |
| | 13. NUMBER OF PAGES 6 plus attachments |
| 14. MONITORING AGENCY NAME & ADDRESS(if different from Controlling Office) | 15. SECURITY CLASS. (of this report) UNCLASSIFIED |
| | 15a. DECLASSIFICATION/DOWNGRADING SCHEDULE N/A |

16. DISTRIBUTION STATEMENT (of this Report)

Approved for public release; distribution unlimited.

17. DISTRIBUTION STATEMENT (of the abstract entered in Block 20, if different from Report)

Same



18. SUPPLEMENTARY NOTES

19. KEY WORDS (Continue on reverse side if necessary and identify by block number)

20. ABSTRACT (Continue on reverse side if necessary and identify by block number)



DD FORM 1 JAN 73 1473 EDITION OF 1 NOV 65 IS OBSOLETE

UNCLASSIFIED

OFFICE OF NAVAL RESEARCH

FINAL REPORT

for

Contract N00014-85-C-0361

Task No. NR 604-006

# Three-Terminal Superconducting Device Research

William J. Gallagher, Principal Investigator

IBM Thomas J. Watson Research Center
P.O. Box 218
Yorktown Heights, NY 10598

September 18, 1992

# Final report

# Three-Terminal Superconducting Device Research


## William J. Gallagher, Principal Investigator



## Contract N00014-85-C-0361, Task No. NR 604-006

## Contract period: September 16, 1985 to January 15, 1991


**Technical Objective**

The goal of this cost-shared contract research was to investigate potential new three-terminal cryogenic device structures in order to explore new regimes of device physics and ultimately to develop better cryogenic superconducting devices.

**Approach**

There were three principal thrusts during the term of this contract:

1. submicron injection-controlled weak links,
2. ultrashort FET's with superconducting source and drain contacts which induce superconductivity in the channel, and
3. electric field induced changes in the carrier densities of high-Tc materials.

In each case our approach was to fabricate, study, and analyze experimental structures with the aim of understanding device potential.

In addition to the above three terminal device thrusts, because of the enormous new opportunity that the discovery of high temperature superconductivity offered, a portion of the contract effort was directed at elucidating the basic properties of these materials with the aim of understanding their device potential. This actually led to the third line of inquiry above, and also indirectly to another jointly IBM/ONR-funded research effort, one directed at developing high-Tc SQUIDs.

**Accomplishments on submicron injection-controlled weak links**

The initial thrust of this contract was to develop the processes that would enable us to evaluate the ultimate device potential of submicron injection-controlled weak links. We initially estimated from energy dissipation and quasiparticle injection times that we could achieve a transistor-like characteristic, modestly high gain ($\sim$10) and switching speeds of a few tens of picoseconds.

We developed the ultrathin NbN film process and an edge structure fabrication process that allowed us to fabricate a 0.3 $\mu$m long NbN link, 35 nm in thickness with a critical current density of $3 \times 10^5$ A/cm$^2$ at 4.2 K. DC characteristics were along the lines of our expectations, namely we were able to suppress a critical current of 600 $\mu$A to zero with an injection current of 55 $\mu$A, although about 15 percent of the operating range had hysteretic characteristics. Input and output impedances were reasonable and devices were made well matched to coplanar 50 ohm transmission lines for high-speed testing.[1]

The switching response displayed an initial fast spike followed by a more gradual turn on to the voltage state which took 0.5 to 2.6 ns to reach 80 percent of the final output value.[1] The spike was determined to be due to a kinetic inductance effect like one seen in the turn-on characteristics of microbridges driven by supercritical current pulses. A quantitative model for these effects was developed.[1]

Overall, we learned that only at the very extremes of what it might be possible to fabricate (well beyond what we had achieved in our experiments) is the gain-speed potential of such devices possibly competitive with modern semiconducting and conventional Josephson superconducting devices.

**Accomplishments on FET's with superconducting source and drain contacts and semiconducting channels**

Our superconducting FET efforts concentrated on III-V materials because the characteristic length scale for the proximity effect is relatively long and, in addition, materials such as InAs form contacts to metallic superconductors without Schottky barriers which act to limit supercurrent. In our initial work we studied niobium-based superconducting-weak-link devices fabricated on MBE-grown n-InAs films on GaAs substrates[2]. The only earlier published InAs weak links had poor properties due to an inability to isolate devices, a problem eliminated with our structure. Our devices exhibited almost ideal critical current behavior. Unfortunately, it is difficult to form effective gates on InAs FET devices, and our efforts to address this problem with a novel pseudomorphic InGaAs/InAs capacitor structure, though initially encouraging, ended up having unacceptably high surface state densities.

To over come this surface pinning problem, we switched to a field-effect structure that combined an established technology, InGaAs on lattice matched InP substrates with the superconducting link being through an InGaAs layer[3]. To simplify things in order to get at the essential physics, we pursued a back-gated JFET structure, the main advantage of the back-gated structure being that we could make direct contact between Nb and fresh InGaAs surface. (No processing on this surface meant no possibility of contamination leading to undesired barriers.) This approach allowed us to study channel thickness and length dependencies. We successfully fabricated gate-controlled superconducting proximity effect FET's with the JFET structure and niobium source and drain contacts. The $In_{0.47}Ga_{0.53}As$ channel material which we used was attractive for this application because it combined a large coherence length with highly transmissive Schottky barrier contacts. At large voltages the devices behaved as conventional semiconductor FET's. Below the $T_c$ of the Nb electrodes, the source-drain characteristics showed superconducting effects at voltages of order ($\sim$ 1 mV) the superconducting energy gap voltage. Gate voltages swings of order 1 volt were required to switch from characteristics in which supercurrents were observed, to characteristics in which no supercurrents were seen.

Fortunately from a physics viewpoint, and unfortunately from a device viewpoint, the overall superconducting proximity FET characteristics were pretty much as expected. From the physics point of view, this was a very good device structure for systematically studying the effects of varying channel length, carrier concentration, mobility, etc. For instance, we made a study of the effects of varying the Schottky barrier thickness by varying the interfacial dopant concentration, and observed a cross-over from tunneling behavior to metallic behavior

in the superconducting semiconducting contacts[4]. From a device viewpoint, gate voltages were of the order of volts and output swings where superconductivity made a difference were of order millivolts. It is possible to lower the control voltage, perhaps by more than an order of magnitude, and, with high-Tc electrodes, to possibly increase the output swings, but it appears extremely difficult to really make these voltage levels compatible. The best practical application for this type of device may be as a gate-controlled SQUID or other Josephson device, not as a device from which one is looking for large signal gain.

**Basic properties of high-Tc superconductors and electric field induced changes in high-Tc materials**

The discovery of high temperature superconductors was an unprecedented breakthrough in the field of superconductivity and condensed matter physics in general. Some contract effort was spent in joint activities clarifying some of the basic properties of these new materials in order to facilitate consideration of their appropriateness for three-terminal superconducting devices. Key contributions we made to the field were the elucidation of the basic anisotropy of the transport properties of $YBa_2Cu_3O_7$[5,6] and of the basic anisotropic superconducting parameters[7] of this prototypical high-Tc material.

The key property of the new superconductors as far as potential transistor-like device possibilities was their relatively low carrier densities, 2 to $5x10^{21}$ $cm^{-3}$. Although this range is low for a metal or superconductor, it is still high compared to that in any semiconductor. Our approach to trying to electrically modulate the carrier density and thereby the superconducting properties was to try to work with oxygen-depleted material. Oxygen depletion lowers the carrier concentration (as well as Tc). The notion was that it would be easier to achieve a significant fractional surface carrier density modulation, as well as to induce a more significant fractional change in Tc.

Indeed, in our first experiments[8] (done jointly within the Consortium for Superconducting Electronics with a student A. Levy funded by the CSE's DARPA funds), we did observed electric field induced modulation of the (normal state) conductivity of semiconducting YBaCuO films using $SrTiO_3$, the substrate on which the films were grown, as the gate insulator. It was possible to modulate the conductivity on two of the $SrTiO_3$ substrates tried. The gate voltage dependence showed a conductivity increase for negative voltages (holes added to the YBaCuO) and little increase for positive voltages (negligible influence on the total conductivity of the thick films.) The best sample showed a conductivity increase of 0.07 $e^2/h$ (200 %). A field effect mobility of 70 $cm^2/V$-s was inferred at 250 K, which is nearly as large as values found from Hall measurements of the normal state of superconducting $YBaCu_3O_7$. We thus had one example of a rather decent interface from the point of view of trapped charge and near-surface mobility, but in the same materials system we also produced several examples of poorer interfaces. Due to a ferroelectric transition in the $SrTiO_3$ substrate at 125 K, it was not possible, however, to get meaningful data at temperatures lower about 125 K, and thus not to seriously look for electric field induced superconductivity. Attempts to modulate the conductivity in additional back-gated samples made with MgO, $LaGaO_3$, and $LaAlO_3$ substrates, as well as with the other $SrTiO_3$ substrates, were not successful, indicating that better control of the insulator-YBaCuO interface was needed.

Most of our follow-on efforts (the first round jointly supported by the CSE, IBM, and this contract and the later rounds continued by the CSE and IBM after the contract ended) were aimed at achieving improved insulator-YBaCuO interfaces. Efforts included deposition of high quality PECVD $SiO_2$ and $Si_3N_4$ dielectrics on $(LaSr)_2CuO_4$ single crystal substrates[9] and $YBa_2Cu_3O_6$ thin films. Unfortunately there were significant interfacial interactions in these systems, although some (e.g., $Si_3N_4$ on $La_2CuO_4$) were better than others. While continuing to work on improved multilayer thin film approaches (e.g. high quality deposited $SrTiO_3$ thin insulators on doped $SrTiO_3$ substrates on which YBaCuO was subsequently grown[10]) we also pursued an approach which avoided high temperature interface interaction complexities completely to try to get at some of the physics involved. We performed experiments using oxygen depleted films using a pressed-on Kapton dielectric. These experiments gave us a means to make the first measurement the binding energy of the hole to the oxygen acceptor, basically the energy level of a narrow localized level in these materials.[11]

Our overall assessment of the potential for high-Tc FET's is that based on our best mobility for the surface layer in this system, and on the best achieved charge moved with an electric field ($\varepsilon E$), electric field-induced superconductivity should be possible at low temperatures. Again, however, the best one could practically hope for in the region of the device characteristics where superconductivity plays a role is for something like a gate controlled Josephson device, not a high gain digital device.

**Summary**

A comprenensive review of three termial superconducting device research as of the end of 1989 was written and published.[12]

In the course of this contract our initial optimism for realizing a practical transistor-like digital device operating at superconducting temperatures has turned into a realistic assessment that such a device is not possible based on any known concrete device proposal. Over the course of the contract we pursued three avenues that had appeared most promising to us: nonequilibrium superconductivity, hybrid semiconductor-superconductor FET's, and electric field induced changes in high-Tc superconductors. We learned a lot from our inquiries, and there are some interesting devices that might have specialized uses that could be realized with these approaches, but there won't be the "holy grail" high performance superconducting transistor.

A new avenue we did not pursue in our own work is low voltage control based on harnessing quantum confinement effects. Such an approach is new, interesting, and does address the key issued of the high control voltage required in device proposals involving semiconductors. Much remains to be learned in this area, including the possible means by which control on, say, the 10 mV scale could be achieved in a device with an output swing that exceeds this voltage scale.

Our general conclusion is therefore that further exploratory device research in these areas is certainly important for both fundamental and applied reasons (and is being continued by us at a lower level since the contract ended). However, it should be undertaken with an appreciation for the extreme challenge it is to obtain a widely useful cryogenic transistor, and, in view of what we know about harnessing better understood physical phenomena, it should contain exploration of newer, less well understood phenomena.

**References (key contract publications, copies appended)**


1. R. Sprik, W.J. Gallagher, S.I. Raider, B. Bumble, and C.-C. Chi "Transient Response of Quasiparticle Injected Superconducting Links," Appl. Phys. Lett. 55, 489 (1989).
2. A.W. Kleinsasser, T.N. Jackson, G.D. Pettit, H. Schmid, J.M. Woodall, and D.P. Kern, "n-InAs/GaAs Heterostructure Superconducting Weak Links with Nb Electrodes", Appl. Phys. Lett. **49**, 1741 (1986).
3. A.W. Kleinsasser, T.N. Jackson, D. McInturff, F. Rammo, G.D. Pettit, and J.M. Woodall, "Superconducting InGaAs junction field-effect transistors with Nb electrodes," Appl. Phys. Lett, **55**, 1090 (1989).
4. A.W. Kleinsasser, T.N. Jackson, D. McInturff, F. Rammo, G.D. Pettit, and J.M. Woodall, "Crossover from tunneling to metallic behavior in superconducting-semiconducting contacts," Appl. Phys. Lett, **57**, 1811 (1990).
5. T. R. Dinger, T. K. Worthington, W. J. Gallagher and R. L. Sandstrom, "Direct Observation of Electronic Anisotropy in Single Crystal $Y_1Ba_2Cu_3O_{7-x}$," Phys. Rev. Lett. **58** , 2687 (1987).
6. S.W. Tozer, A.W. Kleinsasser, T. Penney, D. Kaiser, and F. Holtzberg, "Measurement of Anisotropic Resistivity and Hall Constant for Single-Crystal $YBa_2Cu_3O_{7-x}$," Phys. Rev. Lett. 59, 1768 (1987).
7. T. K. Worthington, W. J. Gallagher, and T. R. Dinger, "Anisotropic Nature of High Temperature Superconductivity in Single-Crystal $Y_1Ba_2Cu_3O_{7-x}$," Phys. Rev. Lett. 59, 1160 (1987).
8. A. Levy, J.P. Flack, M.A. Kastner, W.J. Gallagher, A. Gupta, and A.W. Kleinsasser, "Field-effect conductance of $YBa_2Cu_3O_6$," J. Appl. Phys. **69**, 4439 (1991).
9. A. Levy, M.J. Lercel, J.P. Flack, M.A. Kastner, A.A. Bright, and A.W. Kleinsasser, "Chemical and electrical properties of interfaces between deposited insulators and $La_2CuO_4$," J. Appl. Phys. **71**, 1764 (1992).
10. W. Eidelloth, A. Levy, B.P. Chang, and W.J. Gallagher "$SrTiO_3/YBa_2Cu_3O_7$ Bilayers: Fabrication and Characterization," Physica C (Netherlands) **194**, 92 (1992).
11. A. Levy, J.P. Falck, M. Kastner, R.J. Birgeneau, A.T. Fiory, A.F. Hebard, W.J. Gallagher, A. Kleinsasser, and A.C. Anderson "Field and Hall Effects in Semiconducting $YBa_2Cu_3O_{6-\delta}$," Phys. Rev. **B46** 520, (1992).
12. A.W. Kleinsasser and W.J. Gallagher, "Three-Terminal Devices," in **Superconducting Devices**, S. Ruggiero and D. Rudman, eds. Academic Press, Inc. (New York, 1990), pp. 325-372.

# Transient response of quasiparticle injected superconducting links

R. Sprik,[a] W. J. Gallagher, S. I. Raider, B. Bumble, and C.-C. Chi
*IBM Research Division, Thomas J. Watson Research Center, Yorktown Heights, New York 10598-0218*

(Received 22 March 1989; accepted for publication 26 May 1989)

We have fabricated submicron injection-controlled NbN links with gain and measured their injection-triggered superconducting-to-normal transition to occur in 0.5–2.6 ns at 4 K, governed by condensate dynamics. The transient pulse shape displays a rising-edge kinetic-inductance spike and a strong dependence on the amplitude of the injected quasiparticle current similar to microbridges driven by supercritical currents. A modified dynamic effective-temperature model is used to interpret the transient time and the pulse shape.

Out of many proposals[1] for superconducting devices that might serve as alternatives to the Josephson device or as analogs of transistors, only one type has been constructed and operated in a manner in which a large power gain was achieved. This is the injection-controlled link operated in a latching mode in which quasiparticle injection through a tunnel junction triggers a superconducting-to-normal transition in a current-carrying superconducting line. In the first demonstration of such a device, Wong *et al.*[2] showed that 1.2 mA of quasiparticle current injected at a few millivolts was able to trigger the switching of 23 mA of supercurrent in a long line that eventually developed up to a 200 mV voltage drop. In fact, voltage gain can be made arbitrarily large by increasing device length, but the transition time governed by "hot spot" propagation increases proportionally. Intrigued by the possibility of large gains, but interested in obtaining fast response as well, we have been investigating submicron versions of quasiparticle-injection-controlled links. Considerations of superconducting condensation energy relative to the power available from joule heating in a link (once in the normal state) indicate that sub-100 ps switching times might be possible in small devices with optimum materials. If the switching could be governed by direct quasiparticle injection, there are predictions of even faster responses on a 5 ps time scale.[3] In this letter we report our experimental results on the switching behavior of submicron injection-controlled links. We believe this is the first study of the dynamical properties of this type of device on a subnanosecond time scale. Our results show that the main switching behavior occurs on a 0.5–2.6 ns time scale and is governed by condensate dynamics. Switching time estimates based on steady-state energy dissipation considerations or on quasiparticle injection times are not reliable.

We fabricated a short injection-controlled NbN link using the edge structure shown in Fig. 1. The NbN link reported on here is 0.3 $\mu$m in length, 6 $\mu$m in width, and $\simeq$350 Å thick and carried a critical current density at 4.2 K of $3\times10^5$ A/cm$^2$. The quasiparticles are injected from the Nb injector to the NbN link through a $Nb_2O_5$ edge junction. The dc characteristics of the link show a critical current of $\simeq$600 $\mu$A, which can be suppressed to zero by an injection current of $I_{inj} = 55\ \mu$A. The link has a small hysteretic region; for link currents larger than 500 $\mu$A, the link will remain normal after injection current is removed (i.e., the device is latching). Our devices, incorporated in on-chip $\simeq 50\ \Omega$ coplanar transmission-line structures, were mounted in a high-speed cryogenic probe for measurements with $\simeq$70 ps time resolution using standard sampling scope techniques.

A schematic timing diagram for the transient measurements is given in Fig. 2. At *A* the link bias is applied with a level such that the link still remains superconducting. When a pulse is applied to the injector (*B*), a voltage starts to develop across the link as it switches to the normal state. Since the leading edge of the injector pulse is much steeper than the response of the output, the latter is a direct measure of the transient time of the device. At *C* the injector is removed and, when the link is operated in the hysteretic region, the link remains resistive until the bias is removed (*D*). Figure 3 shows an example of the observed leading edge of the output as function of injector current at fixed link bias current. The leading edge displays a short spike and then a steady rise over 0.5–2.6 ns to 80% of the final value. The final 10–20% of the response develops rather slowly over several nanoseconds. The short spike is not due to electrical cross talk. It is much larger than what can be expected for any electrical inductance in the circuit. Furthermore, it is much smaller when the device remains superconducting and shows an abrupt increase once the current is sufficient to drive the link normal. The overall rise time depends strongly on the injector current and increases when the sum of the injector current and the bias current approaches the critical current of the link.

Microbridges driven by supercritical currents display similar turn-on characteristics.[4–6] Both the rise time and the initial spike observed in these have been interpreted most

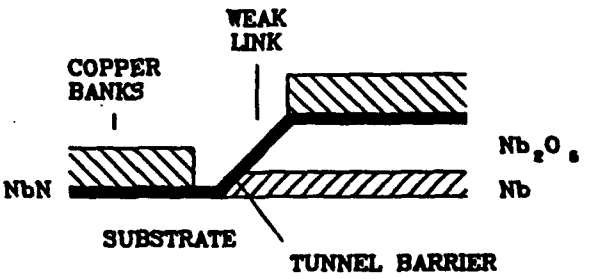


FIG. 1. Edge structure used for the quasiparticle injected NbN link.

[a] Permanent address: Natuurkundig Laboratorium, Universiteit van Amsterdam, Valckenierstraat 65, 1018 XE Amsterdam, The Netherlands.

 0003-6951/89/310489-03$01.00  

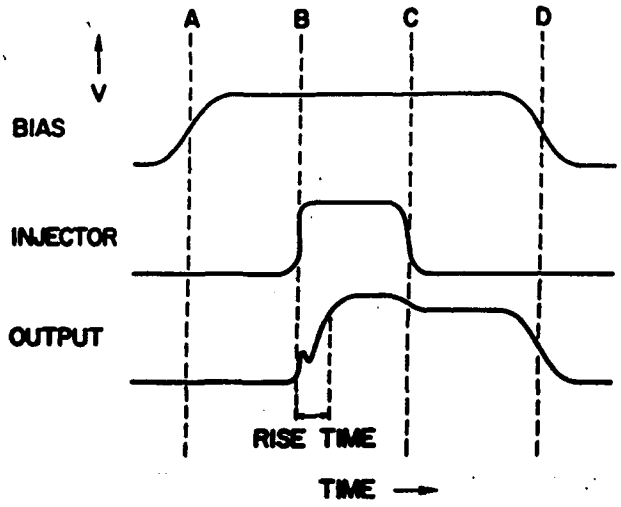


FIG. 2. Schematic transient response of the link to a bias current in combination with an injector current when operated in the hysteretic region.

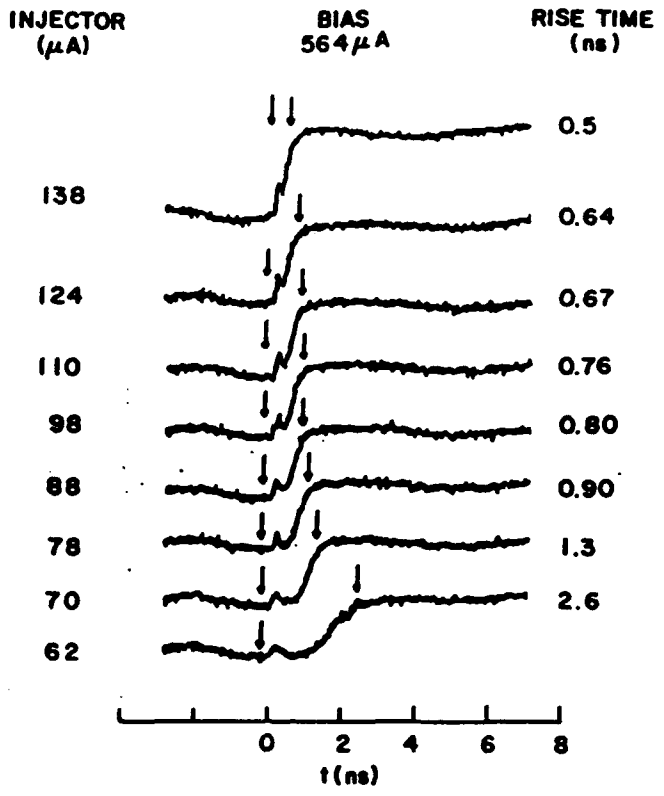


FIG. 3. Observed transient response at 4.2 K for different injection currents at a fixed link bias current.

simply by Tinkham using a model that combines a time-dependent Ginzburg–Landau equation with an effective-temperature description of the quasiparticles.[7] This model captures the essence of more elaborate solutions of the time-dependent Ginzburg–Landau equation.[5,8] In the following discussion we will introduce and extend Tinkham's phenomenological model in order to interpret the observed dynamics of quasiparticle injected links. The quasiparticle distribution is described by an effective temperature $T^*$ defined as the temperature at which the BCS gap $\Delta(T^*)$ equals the gap caused by the change in quasiparticle density $\delta f$. It is assumed that the quasi-static Ginzburg–Landau equation can be applied. The change $\delta f$ leads to a change in the normalized effective quasiparticle temperature, $\alpha^* = (T/T_c - 1) + \delta T^*/T_c = \alpha + \delta\alpha^*$, and results in an additional time-dependent term in the Ginzburg–Landau equation. Together with the current equation this gives[7]

$$1 - \psi^2 - q^2 = -\delta\alpha^*/\alpha, \tag{1}$$

$$J = (3\sqrt{3}/2)\psi^2 q, \tag{2}$$

where $\psi = \Delta/\Delta_0$ is the reduced order parameter, $q = Q\xi$ is the reduced condensate momentum (with $\xi$ the Ginzburg–Landau coherence length and $Q$ the superfluid momentum), and $J = I/I_c$, the ratio of the driving current to the link critical current. The change in effective temperature can be approximated by[7]

$$\frac{-\delta\alpha^*}{\alpha} = a\int_{-\infty}^{t} \dot{\psi}(t')\exp\left(\frac{t'-t}{\tau_E}\right)dt', \tag{3}$$

where $a = 2\tau_\Delta/\tau_E \simeq 2.41(1 - T/T_c)^{-1/2}$, with $\tau_\Delta$ the relaxation time of the superconducting gap and $\tau_E$ the inelastic scattering time of the electrons near the Fermi surface. Equation (3) describes the change in $T^*$ due to the changing order parameter. The change in $T^*$ is negative for decreasing $\psi$ and tends to increase temporarily the supercurrent that can be carried by the link. The voltage across the link is proportional to $\dot{q}$.

To include the effect of quasiparticle injection we assume that the time dependence of $\delta f$ due to a quasiparticle injection current $I_{inj}$ in a link with a volume $V$ obeys a simple relaxation equation with a relaxation time $\tau_R$. In general, $\tau_R$ depends on the relaxation dynamics of the quasiparticles and the phonons in the link.[9] In the numerical calculations discussed later, we take a lower limit, namely that $\tau_R$ is the same as the inelastic scattering time $\tau_E$. Equation (3) and the assumption that the quasiparticles are injected at an energy $\Delta \approx (\Delta_{Nb} + \Delta_{NbN})$ lead to an additional term $a_{inj}$ in Eq. (1) of the form

$$a_{inj} = \frac{1}{I_{inj}^c \tau_R}\int_{-\infty}^{t} I_{inj}\exp\left(\frac{t'-t}{\tau_R}\right)dt', \tag{4}$$

where $I_{inj}^c = 2eVN(0)\Delta/\tau_R$ is the critical quasiparticle injection current and $N(0)$ is the single-spin density of states. Thus Eq. (1) becomes

$$1 - \psi^2 - q^2 = -\delta\alpha^*/\alpha + a_{inj}. \tag{5}$$

The extra term $a_{inj}$ includes most of the effects anticipated for quasiparticle injection. For example, in a steady-state situation with negligible bias current, $d\psi/dt = 0$ and the order parameter ($\psi^2 = 1 - a_{inj}$) reduces and finally vanishes as $a_{inj} = I_{inj}/I_{inj}^c$ approaches 1.

Figure 4 displays the solution of Eqs. (2) and (5) for the case of the same total current $J = J_{bias} + J_{inj} = 1.1$ in the link with (solid curve, $a_{inj} = 0.2$) and without (dashed curve, $a_{inj} = 0.0$) quasiparticle injection. The inductive spike is evident for the duration of the ramp-up time of the injection current ($0.5\,\tau_E$). This is similar to purely supercri-

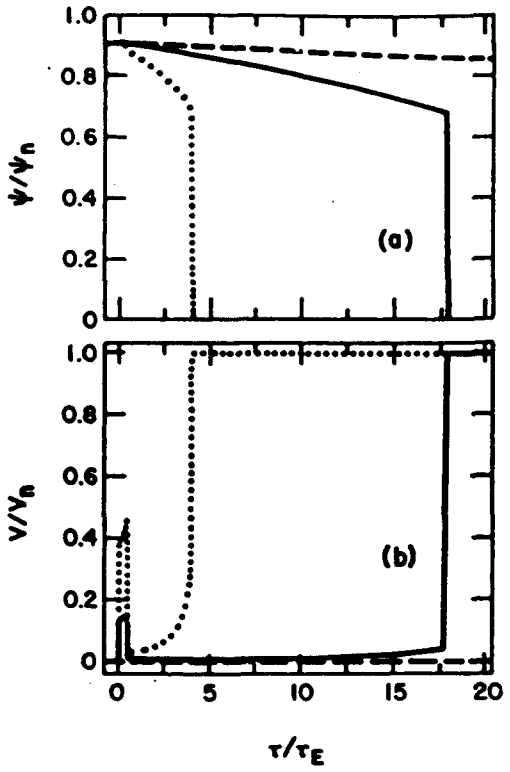


FIG. 4. Time-dependent Ginzburg–Landau predictions for (a) the normalized order parameter $\psi$ and (b) the voltage $V$ scaled by the normal state voltage $V_n$ as a function of $\tau/\tau_E$. The transient time of the injection current is 0.5 $\tau_E$, $\tau_R \simeq \tau_E$ and $a = 25$, and the total maximum current in the pulse $J = J_{bias} + J_{inj} = 0.9 + 0.2 = 1.1$. The solid curve is with injection ($a_{inj} = 0.2$). The dashed curve is without injection ($a_{inj} = 0.0$). For the dotted curve $a_{inj} = 0.2$ and $J_{bias} = J_{inj} = 0.9$.

tical current driven bridges. However, the magnitude of the spike is smaller in the case of quasiparticle injection. The overall response with quasiparticle injection is much faster than without quasiparticle injection, but still slower than $\tau_E$. The response can be accelerated by a higher current in the link as is illustrated by the dotted curve in Fig. 4. Additional calculations show that the response time slows down when the combination of injected current and quasiparticle density is close to the critical conditions in the link. The abrupt change in the calculated results at the critical conditions is due to the approximate model we used for the Ginzburg–Landau equation. Additional terms make the predictions smoother.[5] Furthermore, thermal processes have to be considered.[2,10,11] Heating of the injected area due to the growing dissipation in the link will speed up the transition. It is also the source of the latching behavior of the device. The absence of these effects in the model precludes more than a qualitative comparison to the data.

In conclusion, the measurements and the model indicate that the transition time in injection-controlled superconducting links is limited by condensate dynamics and occurs on a time scale several times $\tau_E$ for injection currents close to the critical conditions in the link. Overdrive will enhance speed, but this is at the expense of current gain.

This work was partly supported by Office of Naval Research contract No. N00014-85-C-0361.

[1]W. J. Gallagher, IEEE Trans. Magn. MAG-21, 709 (1985).
[2]T.-W. Wong, J. T. C. Yeh, and D. N. Langenberg, Phys. Rev. Lett. 37, 150 (1976); IEEE Trans. Magn. MAG-13, 743 (1977).
[3]C. C. Chi, M. M. T. Loy, D. C. Cronemeyer, and M. L. Thewait, IEEE Trans. Magn. MAG-17, 88 (1981).
[4]J. A. Pals and J. Wolter, Phys. Lett. A 70, 150 (1979).
[5]D. J. Frank, M. Tinkham, A. Davidson, and S. M. Faris, Phys. Rev. Lett. 50, 1611 (1983); D. J. Frank, thesis, Harvard, 1982.
[6]J. Bindslev Hansen, A. Davidson, M. Brady, and N. F. Pederson, Jpn. J. Appl. Phys. LT-18, Suppl. 26-3, 1603 (1987).
[7]M. Tinkham, in *Non-equilibrium Superconductivity, Phonons, and Kapitza Boundaries*, edited by K. E. Gray, NATO Advanced Studies Institute Series B 65, 231 (1981).
[8]A. Geier and G. Schön, J. Low Temp. Phys. 46, 151 (1982); M. Octavio, S. Frota-Pessoa, I. F. Oppenheim, and J. A. Blackburn, Phys. Lett. A 82, 365 (1981); I. F. Oppenheim, S. Frota-Pessoa, and M. Octavio, Phys. Rev. B 25, 4495 (1982); A. Schmid, G. Schön, and M. Tinkham, Phys. Rev. B 21, 5076 (1980).
[9]S. B. Kaplan, C. C. Chi, D. N. Langenberg, J. J. Chang, S. Jafarey, and D. J. Scalapino, Phys. Rev. B 14, 4854 (1976).
[10]S. B. Kaplan, J. Appl. Phys. 51, 1682 (1980).
[11]W. J. Skocpol, M. R. Beasley, and M. Tinkham, J. Appl. Phys. 45, 4054 (1974); W. J. Skocpol, in *Non-equilibrium Superconductivity, Phonons, and Kapitza Boundaries*, edited by K. E. Gray, NATO Advanced Studies Institute Series B 65, 559 (1981).

# *n*-InAs/GaAs heterostructure superconducting weak links with Nb electrodes

A. W. Kleinsasser, T. N. Jackson, G. D. Pettit, H. Schmid, J. M. Woodall, and D. P. Kern
*IBM T. J. Watson Research Center, P.O. Box 218, Yorktown Heights, New York 10598*

(Received 8 September 1986; accepted for publication 21 October 1986)

We report on the fabrication and characterization of planar superconductor-normal-superconductor (SNS) weak links in which the normal region is deposited *n*-InAs. The InAs is part of a heterostructure consisting of 100 nm of *n*-InAs grown on an undoped GaAs buffer layer on a semi-insulating GaAs substrate. The superconductor is Nb, patterned by electron beam lithography with interelectrode spacings as small as 260 nm. Device behavior is well explained by SNS weak link theory, with coherence lengths calculated from measured material parameters. These heterostructure weak links can be the basis for superconducting field-effect devices. They have the significant advantage of allowing simple device isolation compared with bulk InAs, which has been used in previous attempts to make such devices.

Recognition of the need for three-terminal devices for cryogenic circuit applications has resulted in renewed interest in superconducting field-effect transistors (FET's),[1–4] which were first proposed a number of years ago.[5–7] These are superconductor-normal-superconductor (SNS) weak links in which the link is a semiconductor, allowing the strength of the Josephson coupling (i.e., the supercurrent) to be controlled by adjusting the carrier concentration in the link (or FET channel) via a gate.

The original superconducting FET proposals[5–7] emphasized the use of materials such as InAs for the channel because, in these materials, the pinning of the Fermi level in the conduction band at surfaces and interfaces results in Schottky barrier-free contacts; the presence of such barriers in a superconducting FET device would decrease the maximum available supercurrent, reduce the degree of control of the supercurrent via the gate, and represent a significant series resistance in the device. Both Si[1,2] and InAs[3,4] have been used in the recent superconducting FET experiments. The absence of Schottky barriers, low effective mass, and high carrier mobility in InAs allow significantly larger device lengths and/or lower dopings for InAs compared with Si (for a given Josephson critical current). However, the InAs devices have two major drawbacks, namely, very poor response to applied gate bias and lack of device isolation. The application of several volts to the gate of a Nb/*p*-InAs/Nb device changes the critical current or device resistance by considerably less than a factor of 2,[3,4] due to strong pinning of the surface Fermi level at the channel-gate insulator interface. As for device isolation, the use of *p*-InAs allows vertical isolation, since a surface inversion layer is separated from the conductive substrate by a depletion region, but the presence of a conducting layer over the entire surface of both *n*- and *p*-type InAs crystals, even after etching of mesas, results in low values for the critical current-resistance ($I_C R_N$) product (which is an important figure of merit for Josephson weak links)[3,4,8] and makes it difficult to laterally isolate devices.

The semiconductor-coupled SNS weak link structure which forms the basis for these superconducting FET's is of interest in its own right for some potential applications of Josephson devices. Weak links, particularly SNS junctions, are attractive primarily due to their low capacitance. In order to achieve reasonable resistances and large $I_C R_N$ products, many workers have advocated using semiconductors as a link material.[9,10] Semiconductor-coupled weak links have been made, primarily on Si[2,10,11]; however, the behavior of these devices is not well understood; in particular the $I_C R_N$ values are considerably larger than expected,[11,12] possibly due to a SINIS structure (S and N are the superconductor and normal semiconductor layers and I is the insulating depletion region due to the Schottky barrier at the metal-semiconductor interface). InAs-coupled links have been made[8]; however, they suffer from low $I_C R_N$ values.

In this letter, we describe the use of an *n*-InAs/GaAs heterostructure to produce Nb/InAs/Nb weak links with high $I_C R_N$ products and excellent isolation. In addition to their potential as high quality Josephson devices, these links can form the basis for improved Josephson FET devices. This scheme also introduces the possibility of modulation-doped superconducting FET's and similar device structures.

The heterostructures consisted of 100 nm of *n*-InAs, grown on undoped GaAs buffer layers on semi-insulating GaAs substrates by molecular beam epitaxy and schematically illustrated in the inset to Fig. 1. Although there is a large ($\simeq$7%) lattice mismatch between GaAs and InAs, excellent layers were obtained. The films were mirrorlike with only occasional small surface defects. It was possible to dope the layers *n* type with Si over several orders of magnitude of dopant concentration. Room-temperature Hall-effect electron mobilities were 5000, 2000, and 1900 $cm^2/V\,s$ for dopings of $3.5\times10^{17}$, $3.5\times10^{18}$, and $3.1\times10^{19}$ $cm^{-3}$, with no significant change on cooling to liquid-nitrogen temperature. For comparison, in the weak link experiment on bulk *n*-InAs,[8] mobilities of 16 900 and 10 000 $cm^2/V\,s$ for dopings of $2.5\times10^{17}$ and $2.6\times10^{18}$ $cm^{-3}$ were reported. The mobilities in the lightly doped layers were below those expected for bulk InAs, possibly due to defects resulting from the large lattice mismatch; however, growths on lattice-matched substrates (e.g. *p*-InAs) for comparison have

 0003-6951/86/511741-03$01.00  

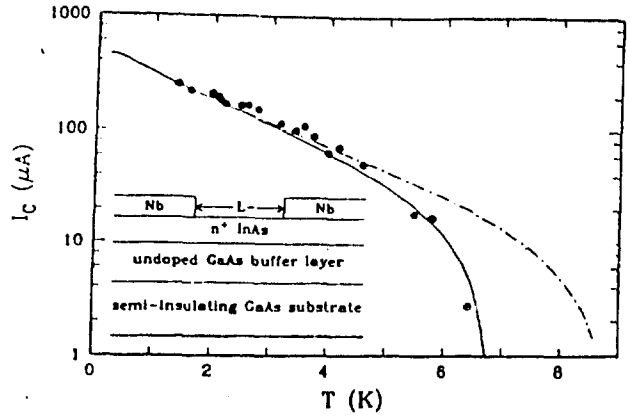


FIG. 1. Temperature dependence of critical current for a weak link on $3.5\times10^{17}$ cm$^{-3}$ $n$-InAs. The low-temperature dependence, dominated by the $T^{-1/2}$ dependence of $\xi_N$, is sensitive to the value of $L/\xi_N(T_C)$. A value of 60 nm is obtained for $\xi_N$ at 4.2 K. The curves are fitted to the data using Eq. (2) with an adjustable prefactor. $T_C$ values of 8.84 and 6.8 K were assumed for the dashed and solid curves, respectively. The inset is a schematic diagram of the device structure. The InAs and Nb layers are 100 and 60 nm thick, respectively, and link length $L$ is as small as 260 nm.

not been done. In the layers with the heaviest doping, electron mobilities were closer to those expected for bulk InAs at that doping.

The use of thin InAs allowed both vertical and lateral isolation of the devices, since device mesas could be formed by etching through the InAs layer to the insulating substrate. Also, channel thickness could be controlled by the InAs film thickness, and is not limited to a thin surface inversion layer.

Device processing involved three masking levels. First, the device mesas were patterned using optical lithography and etched with an Ar ion beam. Next a lift-off stencil for the Nb superconducting electrodes was defined in a double layer resist by electron beam lithography. Gaps between the Nb electrodes (device lengths) ranged from 0.26 to 3 $\mu$m. The device widths ranged from 25 to 200 $\mu$m. The Nb electrodes, 50–65 nm thick, were deposited by electron beam evaporation. $T_C$ was 8.8–9 K; essentially the same value was obtained in InAs as on accompanying oxidized Si substrates. An rf sputter preclean of the InAs (2.6 Pa Ar, $-200V_{dc}$, 3 min) was used prior to Nb deposition by electron beam evaporation. Au/Cr wiring, patterned by optical lithography, was used to connect devices to bonding pads on a periphery of the chip.

The $3.5\times10^{17}$ sample was processed to completion. Current-voltage ($I$-$V$) measurements were made at 4.2 K on 21 devices. Device lengths were measured in a scanning electron microscope after the electrical measurements. The gaps between the Nb pads defining the weak links were uniform, with an estimated roughness of approximately 0.03 $\mu$m. The measured resistivities were in reasonable agreement with the Hall-effect results down to the smallest gaps, indicating that the contact resistance was quite low. Supercurrents were observed at 4.2 K in the four shortest devices. Any supercurrents in the longer links were below $\simeq 1\,\mu$A. The $I$-$V$ characteristics exhibited the excess current characteristic of SNS weak links. The $I$-$V$ curves were nonhysteretic, except that the $I$-$V$ for the smallest sample (0.26 $\mu$m) became hysteretic at temperatures below 3 K.

The critical current of a semiconductor-coupled SNS weak link varies with device length $L$ as $\exp(-L/\xi_N)$, where

$$\xi_N = (\hbar^3\mu/6\pi mek_BT)^{1/2}(3\pi^2 n)^{1/3} \quad (1)$$

is the normal metal coherence length ($\mu$,$m$, and $n$ are the electron mobility, effective mass, and density in the semiconductor).[10] The $I_CR_N$ product for SNS weak links was obtained by Likharev.[13] For long links ($L \gg \xi_N$) not too far from $T_C$,

$$I_CR_N = [4\Delta^2(T)L/\pi ek_BT\xi_N]e^{-L/\xi_N}, \quad (2)$$

where $I_C$ is the maximum Josephson supercurrent and $R_N$ is the normal state resistance.

At low temperatures, the temperature dependence of the critical current is dominated by the $T^{-1/2}$ variation of $\xi_N$, and is therefore very sensitive to $L/\xi_N$, providing a good method for determining $\xi_N$ (fits to the data become very poor if the $L/\xi_N$ ratio deviates by more than $\simeq 10\%$ from the value used for an optimum fit). Figure 1 is a plot of the temperature dependence of critical current for the shortest link ($L = 0.26\,\mu$m). Fitting the low-temperature data (below $\simeq 4$ K) to the temperature dependence implied by Eq. (2) gives a value of 4.35 for $L/\xi_N$ at 4.2 K, implying a value of 0.060 $\mu$m at 4.2 K. To obtain the value $\xi_N(4.2\text{ K}) = 0.060$ $\mu$m from Eq. (1), using the measured values of mobility and carrier density for this wafer, requires an effective mass of 0.048 for the InAs. The textbook value[14] is 0.023; however, at $3.5\times10^{17}$ cm$^{-3}$ the Fermi level is well into the conduction band, and the effective mass is larger than the value at the band minimum,[15] and the value 0.048 is not unreasonable. The dashed line in Fig. 1 is a fit to the data using the temperature dependence of Eqs. (1) and (2), using $L/\xi_N(4.2\text{ K}) = 4.35$ and a prefactor chosen to fit the data at 1.4 K. The data drop significantly below the theory curve above $\simeq 4$ K. This sort of deviation is common in SNS junctions, and may be related to the proximity effect on the superconductor.[9] The solid line in the figure was obtained in the same way, but using $T_C = 6.8$ K, the temperature at which the observed critical current disappears; this lower $T_C$ presumably represents the transition temperature of the SN bilayer. Note, however, that the electrode $T_C$ is 8.84 K; at this temperature the $I$-$V$ characteristic changes resistance dramatically as large areas of Nb go normal. Thus, the meaning of the lower $T_C$ is not completely clear.

Figure 2 is a plot of critical current (divided by electrode width) as a function of device length. The solid circles are our data, while the open circles were obtained from Ref. 8 from links on bulk $n$-InAs with essentially the same doping (the data given in that paper were for 2 K; the 4.2 K values were obtained from the known temperature dependence). There appears to be some consistency between the two experiments. Unfortunately, although all of the data in the figure are for essentially the same doping, the coherence lengths for the bulk sample and our thin InAs sample are different, due to the differing mobilities. The two lines in the figure are included to show consistency with the expected $\exp(-L/\xi_N)$ dependence (the lines are drawn arbitrarily

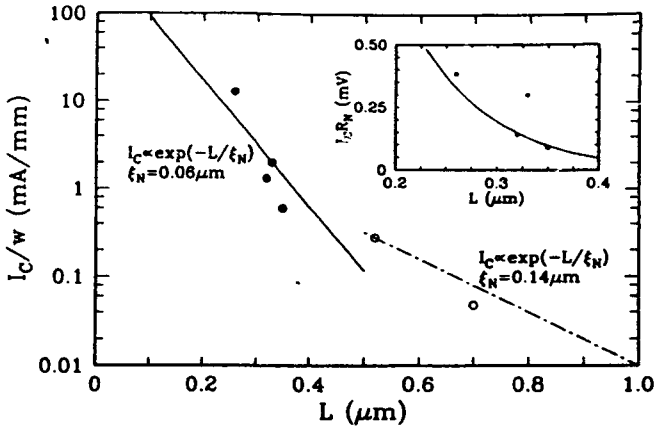


FIG. 2. Critical current (normalized by device width) vs measured link length for $N_D = 3.5\times10^{17}$ cm$^{-3}$. The solid circles are our data; the open circles are from Ref. 8, for Nb weak links on bulk InAs for a similar doping. The lines, of the form $\exp(-L/\xi_N)$, are drawn through one data point from each experiment, using appropriate values for $\xi_N$, to illustrate consistency with the expected length dependence. The inset shows the length dependence of the $I_C R_N$ product at 4.2 K. The solid curve is the prediction of Ref. 13; no adjustable parameters are used.

through data points; only the slopes are relevant). The values of $\xi_n$ used were 0.14 $\mu$m for the bulk sample[8] (dashed line) and 0.060 $\mu$m for our sample (solid line).

The $I_C R_N$ product at 4.2 K is shown in the inset to Fig. 2. The $R_N$ values are the differential resistances at voltages large enough that the $I$-$V$'s are linear, $\simeq$10 mV. The solid curve is the theory of Likharev [Eq. (2)], with $\xi_N(4.2\text{ K}) = 0.060\,\mu$m and no adjustable parameters. The good agreement with the data is remarkable in that we know of no case in which the full theoretical value of $I_C R_N$ was obtained experimentally for an SNS junction. In fact, there is some argument as to the validity of Likharev's result.[9] Clearly studies of more samples having different dopings would be very useful.

In summary, we have grown thin InAs layers on semi-insulating GaAs substrates with a wide range of dopings and reasonable mobility values. SNS weak link devices fabricated on a $3.5\times10^{17}$ cm$^{-3}$ $n$-type sample demonstrate that critical currents comparable to those obtained with bulk InAs devices can be achieved, with the advantages of easy device isolation and channel thickness control. Device behavior can be understood with simple SNS weak link theory. The $I_C R_N$ values obtained in this work are quite high, suggesting that semiconductor-coupled Josephson SNS weak links are indeed promising. This structure is intended to be applicable to low voltage FET devices, and should lead to modulation-doped superconducting FET's and other similar devices.

The authors wish to acknowledge the technical assistance of C. Jessen and G. Pepper in processing of the multilayers, and the services of J. Speidell, who fabricated the masks for optical lithography. Partial support for this work was provided by the Office of Naval Research under contract N00014-85-C-0361.

[1]T. Nishino, M. Miyake, Y. Harada, and U. Kawabe, IEEE Electron Device Lett. EDL-6, 297 (1985).
[2]T. Nishino, E. Yamada, and U. Kawabe, Phys. Rev. B 33, 2042 (1986).
[3]H. Takayanagi and T. Kawakami, Phys. Rev. Lett. 54, 2449 (1985).
[4]H. Takayanagi and T. Kawakami, *International Electron Devices Meeting Digest* (IEEE, Piscataway, NJ, 1985), p. 98.
[5]A. H. Silver, A. B. Chase, M. McColl, and M. F. Millea, in *Future Trends in Superconductive Electronics*, edited by B. S. Deaver, C. M. Falco, J. H. Harris, and S. A. Wolf (American Institute of Physics, New York, 1978), p. 364.
[6]T. D. Clark, R. J. Prance, and A. D. C. Grassie, J. Appl. Phys. 51, 2736 (1980).
[7]T. D. Clark, Ph.D. thesis, University of London, 1971 (unpublished).
[8]T. Kawakami and H. Takayanagi, Appl. Phys. Lett. 46, 92 (1985).
[9]R. B. van Dover, A. de Lozanne, and M. R. Beasley, J. Appl. Phys. 52, 7327 (1981).
[10]R. C. Ruby and T. van Duzer, IEEE Trans. Electron Devices ED-28, 1394 (1981).
[11]A. Serfaty, J. Aponte, and M. Octavio, J. Low Temp. Phys. 63, 23 (1986).
[12]A. W. Kleinsasser (unpublished).
[13]K. K. Likharev, Pis'ma Zh. Tekh. Fiz. 2, 29 (1976) [Sov. Tech. Phys. Lett. 2, 12 (1976)].
[14]S. M. Sze, *Physics of Semiconductor Devices* (Wiley, New York, 1981), Appendix G.
[15]N. A. Semikolenova, I. M. Nesmelova, and E. N. Khabarov, Fiz. Tekh. Poluprovodn. 12, 1915 (1978) [Sov. Phys. Semicon. 12, 1139 (1978)].

# Superconducting InGaAs junction field-effect transistors with Nb electrodes

A. W. Kleinsasser, T. N. Jackson, D. McInturff, F. Rammo, G. D. Pettit, and J. M. Woodall
*IBM Research Division, T. J. Watson Research Center, P. O. Box 218, Yorktown Heights, New York 10598*

(3)

(Received 29 June 1989; accepted for publication 21 August 1989)

We describe the design, fabrication, and characterization of superconducting $In_{0.47}Ga_{0.53}As$ junction field-effect transistors (JFETs) with Nb source and drain electrodes. $In_{0.47}Ga_{0.53}As$ has the advantage of combining large coherence length and high Schottky barrier transmission, making it a very attractive material on which to base superconducting FETs. At large voltages these devices behave as normal FETs in either enhancement or depletion modes, while at small voltages they act as Josephson junctions or super-Schottky diodes. Both normal and supercurrents are controlled by the gate.

A field-effect transistor (FET) in which the source and drain metallizations are superconductors can exhibit superconducting properties (at source-drain voltages of order the electrode energy gap) which are controlled by varying the gate voltage. In short-channel devices with suitable superconductor-semiconductor contacts, the channel becomes superconducting by the proximity effect, and Josephson effects occur. Such Josephson FETs (JOFETs) were first proposed over a decade ago.[1] Recently, gate-controlled supercurrents have been demonstrated,[2] and true superconducting FETs, exhibiting a wide range of gate control of both super and normal currents, have been built.[3] In this letter, we report on the design, fabrication, and initial characterization of superconducting $In_{0.47}Ga_{0.53}As$ junction field-effect transistors (JETs) with Nb electrodes. These are the first junction-type JOFETs and the first JOFETs based on this very attractive materials system.

At this early stage of research on JOFETs, the choice of superconducting electrode material is of secondary importance; Nb was used for this work. The major materials-related concern is the choice of semiconductor. The semiconductor materials system chosen should be one which allows the fabrication of high quality FETs. Beyond that most basic concern, this work was motivated by a desire to address two fundamental issues which dominate JOFETs: (1) The channel length scale, which is set by the normal coherence length of the semiconductor, and (2) the superconductor-semiconductor source and drain contacts, in particular the transmission coefficient for tunneling through the Schottky barriers. $In_{0.47}Ga_{0.53}As$, grown epitaxially on InP substrates, was chosen as the semiconductor for this work because it offers large coherence lengths and Schottky barrier transmission coefficients, as discussed in the following paragraphs.

(1) In order to have a supercurrent in a JOFET, the separation $L$ of the source and drain electrodes must be no more than a few times the normal coherence length $\xi_n$ in the semiconductor channel since, under typical conditions, the critical current $I_c$ varies as $\exp(-L/\xi_n)$. For a material with Fermi velocity $v_F$, carrier diffusion constant $D$, and elastic mean free path $l$, $\xi_n$ is given by $\hbar v_F/2\pi k_B T$ and $(\hbar D/2\pi k_B T)^{1/2}$ in the clean ($l \gg \xi_n$) and dirty ($l \ll \xi_n$) limits, respectively. In both cases $\xi_n \propto v_F = \hbar k_F/m^*$, where $m^*$ is the carrier effective mass, and the desire to maximize $\xi_n$ leads to the selection of low effective mass materials. In $n$-type InAs, $In_{0.47}Ga_{0.53}As$, GaAs, and Si, the values of $\xi_n$ have the ratios 3.4:2.4:2.0:1 in the dirty limit, for a given carrier concentration and mobility. (Of course, the larger mobilities in low mass materials make these ratios even larger.) In the clean limit, the corresponding ratios are 11.3:5.9:3.9:1, again for fixed carrier density. InAs materials technology is not well developed, and high quality FETs are very difficult to obtain, and we therefore chose $In_{0.47}Ga_{0.53}As$ for this work.

(2) The superconductor-semiconductor interfaces should be as transmissive as possible.[4] This led early workers[1] to suggest InAs as a suitable material, since Schottky barrier-free contacts are possible. For materials with which high quality FETs have been built, Schottky (tunneling) barriers at metal-semiconductor contacts are expected. Supercurrent transport in JOFETs is a coherent process involving two tunneling events (one at each superconductor-semiconductor interface) so the critical supercurrent is proportional to $P^2$, where $P$ is the transmission probability for a single interface. In the WKB approximation,[5] $P = \exp(-E_B/E_{00})$, where $E_B$ is the Schottky barrier height and $E_{00} = (e\hbar/2)(N_D/\epsilon_s m^*)^{1/2}$, with $N_D$, $\epsilon_s$, and $m^*$ being the dopant density, dielectric constant, and carrier effective mass of the semiconductor, respectively. For $n$-type $In_{0.47}Ga_{0.53}As$, GaAs, and Si, using barrier heights of 0.2, 0.7, and 0.2 eV, we have $P^2 = 9.2\times10^{-2}$, $3.4\times10^{-6}$, and $4.6\times10^{-5}$, respectively, for a carrier density of $5\times10^{19}$ cm$^{-3}$ at the interface. Again, $In_{0.47}Ga_{0.53}As$ appears to be desirable for JOFET devices, compared with other materials from which FETs are fabricated. It is the combination of low barrier height and low carrier mass relative to the other materials which is responsible for this great disparity in favor of $In_{0.47}Ga_{0.53}As$ (the disparity increases with decreasing doping). Although the WKB approximation breaks down for large doping,[6] this calculation should indicate the correct qualitative trend.

Most studies of JOFETs and ungated semiconductor-coupled weak links have focused on the coherence length in the semiconductor through measurements of the critical current. Systematic studies of the influence of the contact properties are only beginning. In contrast to the situation with normal FETs, the superconductor-semiconductor contacts in JOFETs have an importance as great as that of the contacts between the gate and the channel. Thus we chose

 0003-6951/89/441909-03$01.00  

for our initial studies an inverted device structure, with the gate underneath the channel, allowing the superconductor to be deposited on the as-grown semiconductor surface. The device is a JFET with a $p$-type $In_{0.47}Ga_{0.53}As$ gate. A depletion-mode device is illustrated schematically in Fig. 1. The channel is conducting in absence of gate bias. Application of a negative voltage to the gate terminal (with the source grounded) increases the width of the gate depletion region (shaded in Fig. 1), thereby decreasing the conducting channel thickness, and eventually pinching it off completely. Application of a positive gate voltage increases the channel width. Enhancement-mode devices, which are pinched off at zero gate bias, were also built.

The $In_{0.47}Ga_{0.53}As$ layers were grown on a $p^+$-InP substrate by molecular beam epitaxy (MBE). At the time of this work, we were unable to deposit the Nb film in the MBE system. The wafers were transferred to a separate system immediately after growth of the $In_{0.47}Ga_{0.53}As$ layers, and Nb was deposited by electron beam evaporation. Device mesas were etched by ion milling. A narrow gap between the Nb electrodes was defined by reactive ion etching using an $NF_3$-based chemistry and an Al mask, which was patterned by optical lithography and liftoff. The minimum source-drain separation on the photomask was 0.5 $\mu$m.

Design values for the layer thicknesses and dopant densities for the initial fabrication run are shown in Fig. 1. The gate depletion layer thickness is estimated to be 64 nm (21 nm on the $n$ side), leaving a channel thickness of 49 nm. Low-temperature Hall measurements were consistent with this, with a Hall mobility of 2500 $cm^2/V$ s. Calculated device parameters include 510 $\Omega/\square$ resistance (0.51 $\Omega$ mm for a 1-$\mu$m-long channel), 50 nm electron mean free path, and 62 nm coherence length at 4.2 K.

The 5 nm $n^+$ layer was used to ensure good ohmic contacts. Based on a Schottky barrier height of $\sim$0.2 eV, this layer is completely depleted of carriers over the entire device, as indicated by the shading in Fig. 1. Thus it improves

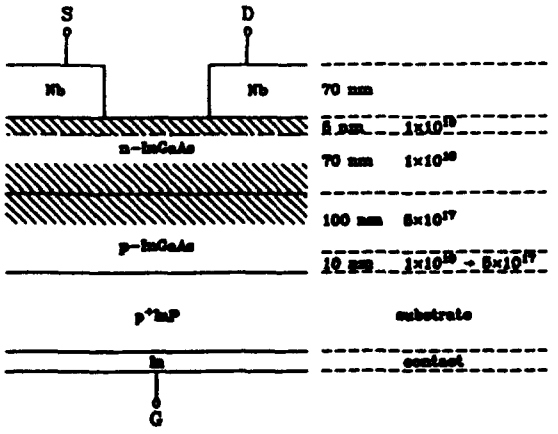


FIG. 1. Schematic of inverted-gate JFET structure. The left portion of the figure illustrates the vertical structure, with the source ($S$), drain ($D$), and gate ($G$) terminals indicated. Regions depleted of carriers are shaded. The clear $n$-type region in between is the channel. At the right, the layer thicknesses and dopings (in $cm^{-3}$) for the first fabricated device are shown. Note the use of a thin, heavily doped contact layer, which is completely depleted and does not participate in lateral current transport, but which reduces the thickness of the contact Schottky barriers.

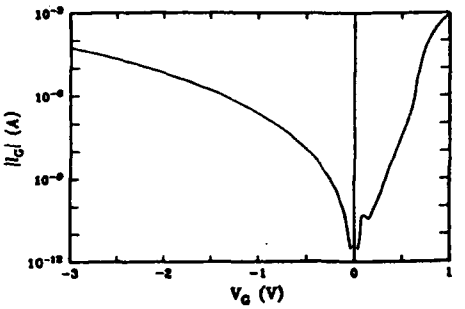


FIG. 2. Magnitude of gate current vs voltage for a typical large-area $p$-$n$ junction at 4.2 K. Note the negative-resistance feature associated with interband tunneling in the forward direction. The low leakage of these junctions allows several volts of reverse bias to be applied, pinching off the conducting channels of the FETs.

electron transmission at the contact interface without contributing to lateral current transport.

Large-area gates were used in this work in order to simplify the fabrication process. Device mesas were etched into the $p$-$In_{0.47}Ga_{0.53}As$ layer. Heavy doping was used at the interface between InP and $In_{0.47}Ga_{0.53}As$ in order to minimize its contribution to the gate characteristics. The current-voltage ($I$-$V$) characteristics of a representative large-area ($>10^{-4}$ $cm^2$) gate are shown in Fig. 2. The low leakage of these $p$-$n$ junctions is important to the function of the JFETs. The gate current is due to interband tunneling. Forward gate bias, which increases the conducting channel thickness, is limited to less than $\sim$1 V, but several volts can be applied in the reverse direction, depending on the doping of the $p$ and $n$ layers. A device designed with a sufficiently thin channel can be completely pinched off.

The source-drain $I$-$V$ characteristics of a representative depletion-mode JFET, for several values of gate voltage at 4.2 K, are shown in Fig. 3. On the voltage scale shown, the device acts as a normal JFET[7]; the fact that the electrodes are superconducting does not significantly alter the characteristics. In this particular device, the doping was low enough that the channel was pinched off with a reverse gate bias of $-1$ V, and a forward bias of $\simeq$1 V could be applied without excessive gate current.

When cooled below the electrode transition temperature, the characteristics of virtually all of the devices we have studied exhibit effects due to superconductivity in the source and drain electrodes. The effects were limited to a voltage

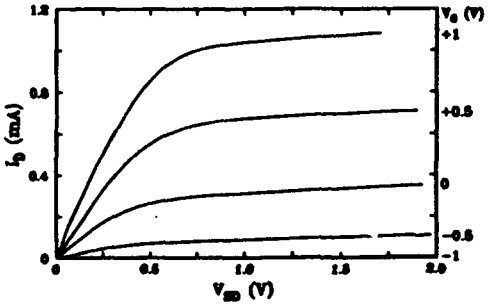


FIG. 3. Source-drain $I$-$V$ characteristics of a representative JFET at 4.2 K for various values of gate bias. On a scale of volts, these devices behave as ordinary FETs, with channel conductance and saturation current controlled by the gate. In this enhancement-mode JFET, positive (negative) voltages increase (decrease) channel current.

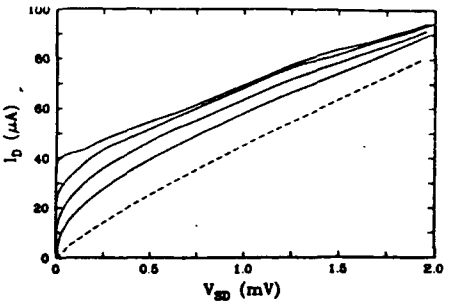


FIG. 4. Source-drain $I$-$V$ characteristics of a JFET which exhibits a supercurrent at 1.6 K. Note the 1000 times reduction of the voltage scale compared with Fig. 3. On this scale, $I(-V) = -I(V)$. In the device shown, a gate-controlled supercurrent is seen, along with an excess current and a conductance peak at subgap voltages (solid curves, for $V_G = 0$, $-2$, $-2.5$, and $-3$ V). The dashed curve was taken above the electrode transition temperature with no gate bias.

scale which is on the order of the superconducting energy gap of the electrodes. Devices with relatively high resistances act as back-to-back super-Schottky diodes,[8] exhibiting an increased resistance at subgap voltages. Their characteristics are dominated by tunneling between the superconducting electrodes and the normal channel through the Schottky barriers at the contacts. The tunneling current at each contact is suppressed for contact voltage drops smaller than the superconducting energy gap due to the absence of states in the superconductor at subgap energies.

Low-resistance devices (those having very transmissive or low resistance contacts) with short channels exhibit gate-controlled Josephson supercurrents. Figure 4 shows the $I$-$V$ characteristics for one such device on a mV scale (a 1000-fold sensitivity increase in the voltage scale compared with Fig. 3). The four solid curves in the figure are for gate voltages of 0, $-2$, $-2.5$, and $-3$ V at 1.6 K. Gate current was negligible. In this particular device, the relatively high channel doping, close to that indicated in Fig. 1, led to a large supercurrent. However, the channel could not be pinched off completely. Greater sensitivity to gate voltage was achieved in devices with somewhat lower channel dopings and shorter channels (in the present work such channel lengths were at the limit of what we could attain with optical lithography). Thus, both gate-controlled supercurrent and channel pinchoff have been observed in the same device. The dotted curve in Fig. 4 was obtained at 10 K (above the electrode transition temperature $T_c$) with no applied gate voltage. Below $T_c$, the current was linear in voltage for voltages much larger than the superconducting energy gap, exhibiting an excess current when extrapolated back to zero voltage. This behavior is common in superconducting junctions involving normal metals, and is due to Andreev scattering at the superconductor-normal metal interface(s).[9]

Typical critical current-normal resistance products $I_cR_n$ in these devices varied between 1 and 2 mV at low temperatures. This is close to the value expected for an ideal Josephson junction with Nb electrodes (2.4 mV). In semiconductor or normal metal-coupled junctions, this value should be reduced by a factor of order $\exp(-L/\xi_n)$, where $L$ is the electrode separation and $\xi_n$ is the normal coherence length.[4,10] In these devices, $L$ was 0.5–1 $\mu$m (recall that optical lithography was used to define the electrodes), and $\xi_n$ was estimated to be 90 nm at 2 K, so that the expected $I_cR_n$ product is less than $\sim 10\,\mu$V. This sort of discrepancy has been reported by a number of workers in semiconductor-coupled weak links reported by a variety of workers, and is an important subject for future investigations. Resistances in the devices exhibiting supercurrents were consistent with expectations for channels of the measured dimensions and carrier densities. Thus it is the critical current which is anomalously large in these devices. Critical currents in devices of this type are known to be very sensitive to contact quality. Thus, we have been able to obtain the very high quality contacts expected with this materials system.

In conclusion, we have fabricated superconducting JFETs with Nb electrodes, based on $In_{0.47}Ga_{0.53}As$ lattice matched to InP substrates. $In_{0.47}Ga_{0.53}As$ appears to represent a well-optimized choice of a semiconductor material on which to perform device investigations, due to the highly transmissive contacts and long coherence lengths which are possible. The devices reported on here represent a good starting point for the study of JOFETs in this materials system. Understanding of the behavior of Josephson FETs and semiconductor-coupled weak links has been hampered by a lack of experiments on well-defined structures (e.g., with known length, channel thickness, carrier concentration, and mobility), which can be compared with theory in detail. The structure described here is one which makes such investigations possible. Finally, the largest problem with JOFETs, when considering possible applications, is the large disparity between the input (gate) and output (source-drain) voltage scales.[11] In the future, we hope to reduce the gate voltage swing required to pinch off the devices by optimizing doping and channel thickness.

The authors wish to acknowledge the help of B. Bumble, C. Jessen, and G. Pepper on aspects of these experiments. Partial support for this work was provided by the Office of Naval Research under contract N00014-85-C-0361.

[1] A. H. Silver, A. B. Chase, M. McColl, and M. F. Millea, in *Future Trends in Superconductive Electronics*, edited by B. S. Deaver, C. M. Falco, J. H. Harris, and S. A. Wolf (American Institute of Physics, New York, 1978), p. 364; T. D. Clark, R. J. Prance, and A. D. C. Grassie, J. Appl. Phys. 51, 2736 (1980).

[2] T. Nishino, M. Miyake, Y. Harada, and U. Kawabe, IEEE Electron Device Lett. EDL-6, 297 (1985); H. Takayanagi and T. Kawakami, Phys. Rev. Lett. 54, 2449 (1985).

[3] Z. Ivanov and T. Claeson, Jpn. J. Appl. Phys. 26, Suppl. 26-3, 1617 (1987); T. Nishino, M. Hatano, H. Hasegawa, F. Murai, T. Kure, A. Hirawa, K. Yagi, and U. Kawabe, IEEE Electron Device Lett. EDL-10, 61 (1989).

[4] A. W. Kleinsasser and T. N. Jackson, Jpn. J. Appl. Phys. 26, Suppl. 26-3, 1545 (1987).

[5] F. A. Padovani, in *Semiconductors and Semimetals*, edited by R. K. Willardson and Albert C. Beer (Academic, New York, 1971), Vol. 7, Part A p. 75.

[6] W. J. Boudville and T. C. McGill, J. Vac. Sci. Technol. B 3, 1192 (1985).

[7] See, for example, S. M. Sze, *Physics of Semiconductor Devices* (Wiley, New York, 1981), p. 312.

[8] M. McColl, M. F. Millea, and A. H. Silver, Appl. Phys. Lett. 23, 263 (1973).

[9] G. E. Blonder, M. Tinkham, and T. M. Klapwijk, Phys. Rev. B 25, 4515 (1982); M. Octavio, M. Tinkham, G. E. Blonder, and T. M. Klapwijk, Phys. Rev. B 27, 6739 (1983); K. Flensberg, J. Bindsley Hansen, and M. Octavio, Phys. Rev. B 38, 8707 (1988).

[10] T. van Duzer and C. W. Turner, *Principles of Superconductive Devices and Circuits* (Elsevier, New York, 1981), p. 302.

[11] A. W. Kleinsasser and T. N. Jackson, IEEE Trans. Magn. MAG-25, 1274 (1989).

# Crossover from tunneling to metallic behavior in superconductor-semiconductor contacts

A. W. Kleinsasser, T. N. Jackson, D. McInturff, F. Rammo, G. D. Pettit, and J. M. Woodall
*IBM Research Division, T. J. Watson Research Center, P.O. Box 218, Yorktown Heights, New York 10598*

(Received 5 July 1990; accepted for publication 20 August 1990)

We describe current-voltage measurements on superconducting Nb/InGaAs junction field-effect transistors which reveal a crossover from tunneling-dominated to Andreev scattering-dominated transport at the superconductor-semiconductor contacts as Schottky barrier thickness decreases with increasing interfacial dopant concentration. These measurements are the first demonstration of such a crossover in a thin-film structure, and are of interest for investigations of hybrid superconductor-semiconductor devices, proximity effect boundary conditions, and transport in ohmic contacts to semiconductors.

The behavior of hybrid devices,[1] such as semiconductor-coupled weak links, superconducting field-effect transistors (FETs), and super-Schottky diodes, is sensitive to the quality of the superconductor-semiconductor contacts, and techniques which allow direct measurements of contact properties are therefore of interest. In this letter, we describe measurements which demonstrate dramatic qualitative changes in the source-drain current-voltage ($I$-$V$) characteristics of superconducting FETs as the transmittance of the superconductor-semiconductor contacts is improved by increasing the interfacial dopant concentration. These changes are caused by a crossover from normal tunneling to Andreev reflection-dominated transport at the contacts. This work is the first demonstration of such a crossover in a thin-film structure. In addition to connecting superconducting device performance with ohmic contact quality, measurements of this type are of interest for fundamental studies of the proximity effect and of transport in ohmic contacts to semiconductors.

The superconducting junction FETs (JFETs) used in this work are described elsewhere.[2] The device structure is illustrated schematically in the inset to Fig. 1 . Nb source and drain contacts are separated by 0.5–1 $\mu$m. The substrate is InP, the channel is lattice-matched $n$-InGaAs, and the channel conductance is controlled by the bias applied to the $p$-InGaAs gate. The Nb/InGaAs ohmic contacts are of crucial importance. In the extreme cases of low or high contact transmittance the devices act as back-to-back super-Schottky diodes[3] or as gated Josephson junctions, respectively. In the latter case, a long coherence length and highly transmissive nonalloyed ohmic contacts have made record gated supercurrents[2] possible. This work, however, deals with single particle currents in the semiconductor, and supercurrents are suppressed by applying a magnetic field or a gate voltage.

Since the semiconductor channel acts as a normal metal, the contacts are SN interfaces (in this letter, S, N, Sm, and I denote superconductor, normal metal, semiconductor, and insulator, respectively). There is ample evidence for a proximity effect between superconductors and semiconductors,[1,4,5] but it is well known that even a thin tunnel barrier at an SN interface destroys the proximity effect.[6] The Schottky barriers at most SSm contacts make them SIN tunnel junctions, or super-Schottky diodes.[3] The thickness (and thus the transmittance) of the Schottky barrier at an SSm interface is determined by the dopant concentration near the surface of the semiconductor. We varied this doping in order to study the expected crossover from SN to SIN character. This resulted in changes in the $I$-$V$ characteristics, as illustrated in Fig. 1 and discussed below. A crossover from SN to SIN behavior has been studied in Cu-Nb point contacts,[7] and these earlier experiments demonstrated the validity of a simple theoretical picture;[8] however, this sort of crossover has not been studied previously in a thin-film structure.

The $I$-$V$ characteristics of a SIN contact are influenced by two scattering processes.[8] Figure 2 (a) shows an electron ($I$) incident on the interface from the $N$ side at a subgap energy. It cannot propagate into the superconductor so it reflects, either as an electron ($R1$) contributing zero junction current, or as a hole ($R2$) with a Cooper pair ($T2$) propagating in the superconductor (Andreev reflection) and contributing twice the current expected from Ohm's law. Above the gap energy, both normal tunneling and Andreev scattering contribute current. For a highly

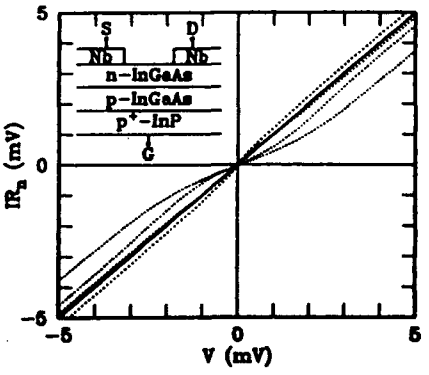


FIG. 1. Source-drain characteristics at 4.2 K of several JFETs without gate bias (dashed curves). The transmittance of the Nb/$n$-InGaAs contacts was varied using different doping levels in top few nm of the InGaAs. The lowest curve (in the first quadrant) corresponds to the lowest doping and the uppermost curve to the higest doping. The solid line represents the normal state ($R_n$ is the device resistance). Inset: Schematic of the JFET structure. $S$, $D$, and $G$ are the source, drain, and gate terminals, respectively.

 0003-6951/90/431811-03$02.00  

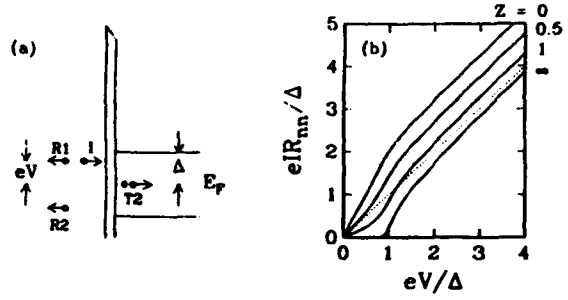


FIG. 2. (a) Scattering processes at a SN contact. A low-energy electron ($I$) incident from $N$ reflects as an electron ($R1$), or Andreev reflects as a hole ($R2$) with a Cooper pair ($T2$) propagating into $S$, contributing zero or two units of current, respectively, rather than one. (b) $I$-$V$ characteristics of an SN contact at $T = 0.1T_c$. $Z = 0$ and $\infty$ are the thin and thick limits for the interfacial tunnel barrier. $Z = 0.5$ and 1 are intermediate cases. The dashed line represents a normal junction (after Ref. 8).

transmissive barrier, the relative contributions of these processes determines the form of the $I$-$V$ characteristics, which thus contain information about interface transmission probability. This is shown in Fig. 2(b), which qualitatively resembles Fig. 1. With no barrier ($Z = 0$, $Z$ being a dimensionless parameter characterizing the amount of interfacial scattering), there is a conductance peak at subgap voltages and an excess current (the $I$-$V$ curve at large voltages extrapolates to a finite current at zero voltage). There is a gradual crossover to the thick barrier extreme ($Z = \infty$), in which case there is a conductance minimum at subgap voltages and no excess current. In the absence of a barrier the Andreev process dominates. However, Andreev scattering involves two traversals of any tunnel barrier, and is thus second order in the transmission probability. Normal tunneling is first order, and dominates for thick barriers.

In the present experiment there are two superconducting electrodes, so that the structure is SNS or SINIS. Both SN interfaces are involved in the scattering processes described above, with significant effects on device behavior. The $I$-$V$ characteristics at 2 K of a device with high doping in the contact region are shown in Fig. 3 (a). This device had doping levels of $\simeq 10^{19}$ cm$^{-3}$ in the top 5 nm and $10^{18}$ cm$^{-3}$ in the next 70 nm. The channel thickness was $\simeq 50$ nm. Above 9.2 K, the $I$-$V$ curve was linear at low voltages, with a normal resistance consistent with estimates based on doping, mobility, and device dimensions which assumed a very small contact resistance ($< 10^{17}$ $\Omega$ cm$^2$). All such low-resistance devices exhibited two features visible in Fig. 3, the effects being largest in the lowest resistance devices: (1) an excess current and (2) a sharp peak in the dynamic conductance at low voltages. This peak was never wider than $2\Delta$, and was considerably sharper at low temperatures in the lowest resistance devices. At voltages beyond $\simeq 2$ mV the conductance approached the normal-state value. We identify as "SNS-like" devices which exhibit these features.

For devices in which the top 5 nm of the InGaAs film (the contact region) had a doping level between $\simeq 10^{19}$ cm$^{-3}$ and $10^{18}$ cm$^{-3}$ (the doping level in the channel),

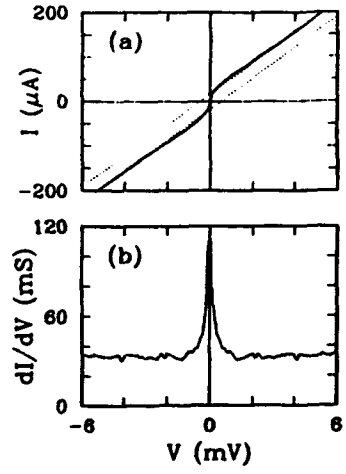


FIG. 3. (a) $I$-$V$ characteristics at 2 K of a low-resistance device which exhibits SNS-like behavior. The excess current is shown by the dashed lines extrapolated from large voltages ($|V| > 20$ mV). (b) Dynamic conductance of the same device.

the resistance was considerably larger, due to the exponential dependence of tunneling current on barrier width (device resistance becomes increasingly dominated by the contacts as interface doping is reduced). These devices exhibit what we term "SINIS-like" behavior, as shown in Fig. 4. Clearly visible are (1) a deficit current/excess voltage (the current extrapolated from voltages many times the energy gap voltage has a negative intercept) and (2) a low-voltage minimum in the dynamic conductance with a full width of $\simeq 4\Delta$. This minimum resembles that expected for two series SIN junctions; however, the zero-bias conductance does not fall exponentially at low temperatures. This is consistent with very transmissive tunnel barriers. Again, the $I$-$V$ curves above the Nb transition temperature were linear at low voltages, and the low-temperature conductance approached the normal-state value for voltages above $\simeq 5$ mV.

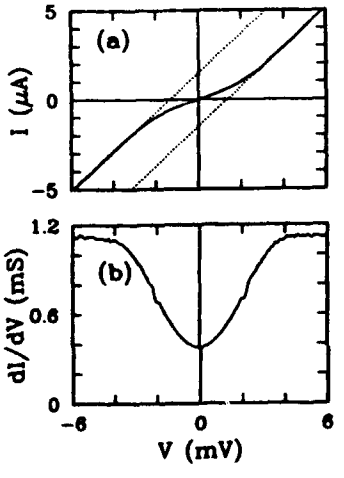


FIG. 4. (a) $I$-$V$ characteristics at 4.2 K of a high-resistance device which exhibits SINIS-like behavior. The deficit current is shown by the dashed lines extrapolated from large voltages ($|V| > 20$ mV). Dynamic conductance of the same device.

We observed a gradual crossover from SNS-like to SINIS-like behavior, with a transition from excess to deficit current and from a sharp subgap conductance peak to a broader conductance minimum, as the doping level in the contact region was reduced to roughly that of the channel. There were two major differences between this behavior and that of SN or SIN junctions[8] (our samples consist of two junctions in series): (1) the "SNS-like" conductance peak was considerably sharper than the Nb energy gap and larger in amplitude than twice the normal conductance of the device, and (2) the "SINIS-like" devices not only had no excess current, they also exhibited deficit currents. We believe that these features are inherent in SNS (or SINIS) structures.

Most of the work aimed at extending the theory for SN and SIN contacts[8] to SNS and SINIS structures[9,10] has tried to explain the subharmonic gap structure observed in various types of Josephson weak links (in the case of high critical current density tunnel junctions, the basic correctness of this approach has been established[11]). The most recent work[10] also predicts just what we are reporting: an excess current and a sharp (compared with $\Delta$) conductance peak for devices with high transmittance interfaces, a deficit current, and a conductance minimum of (full) width $4\Delta$ for devices with low transmittance barriers, and a gradual transition between these extremes. The model treats SNS and SINIS structures with all (elastic) scattering lumped into two $\delta$ function potential barriers at the SN interfaces, with no scattering within the normal material. Our devices had electrode separation well in excess of the elastic mean free path, but the inelastic scattering length is considerably longer. Evidently the model contains the essential physics behind the behavior of our JFETs as long as inelastic scattering is not important.

In principle, the form of the $I$-$V$ characteristic at a given temperature determines the value for the interface parameter[8,10] $Z$, and therefore the contact transmission coefficient. However, the present model is limited by the use of $\delta$-function barriers. Nevertheless, the fact that $I$-$V$ measurements such as these might be used to determine the transmission probability of a metal (superconductor)-semiconductor contact makes them interesting for ohmic contact studies, since transport measurements of high transmittance normal ohmic contacts are complicated by the parasitic resistance of the semiconductor.

For devices with apparent $Z$ values exceeding approximately unity, the temperature dependence of the characteristics (e.g., the zero-bias conductance) agrees with the model predictions, with $Z$ as a fitting parameter. Such comparisons have not been made for devices having $Z$ values less than unity. At present, the analysis is limited by the fact that the voltage between superconductor and semiconductor is not constant along the contact, washing out the $I$-$V$ characteristic. This does not affect the excess or deficit currents, whose temperature dependences appear to scale with the energy gap as expected. We observed no subharmonic gap structure in our devices. Such structure occurs in the model due to multiple Andreev reflections, but is presumably washed out in these devices due to the spatially varying voltage drop across the interface and to the proximity effect, which results in a graded energy gap in both the superconductor and the normal material.

The measurements described here allow relationships to be established between weak link (and FET) critical currents and ohmic contact transmittance. What is now required is to perform these types of measurements on well-characterized samples spanning various materials systems and contact schemes, and to further improve the theory in this area. It would also be desirable to know the value of the boundary condition for the superconducting order parameter at the contacts, since this quantity is proportional to the critical current of a weak link. Transition temperature[4] and tunneling measurements[5,12] on SSm bilayers can provide such information. SSm samples offer a much wider range of boundary conditions for proximity effect studies than do the more familiar SN ones, allowing further generalization of earlier investigations.[13] Finally, our results imply limits on the specific resistance of super-Schottky diodes, since increasing barrier transmittance results in degraded characteristics (increased subgap currents).

In conclusion, we have described a dramatic crossover in the $I$-$V$ characteristics of gated semiconductor-coupled weak links as the contact transmittance is varied. These measurements are important for understanding hybrid superconductor-semiconductor devices, for fundamental studies of transport in ohmic contacts, and for improving our understanding of the proximity effect.

The authors wish to acknowledge the technical assistance of C. Jessen and G. Pepper and conversations with W. J. Gallagher. Partial support for this work was provided by the Office of Naval Research under contract N00014-85-C-0361.

[1] For a recent review, see A. W. Kleinsasser and W. J. Gallagher, in *Superconducting Devices*, edited by S. T. Ruggiero and D. A. Rudman (Academic, Boston, 1990), p. 325.
[2] A. W. Kleinsasser, T. N. Jackson, D. McInturff, F. Rammo, G. D. Pettit, and J. M. Woodall, Appl. Phys. Lett. 55, 1909 (1989).
[3] M. McColl, M. F. Millea, and A. H. Silver, Appl. Phys. Lett. 23, 263 (1973).
[4] M. Hatano, T. Nishino, and U. Kawabe, Appl. Phys. Lett. 50, 52 (1987).
[5] T. Nishino, M. Hatano, and U. Kawabe, Jpn. J. Appl. Phys. 26, Suppl. 26-3, 1543 (1987).
[6] G. Deutscher and P. G. de Gennes, in *Superconductivity*, edited by R. D. Parks (Marcel Dekker, New York, 1969), Vol. 2, p. 1005.
[7] G. E. Blonder and M. Tinkham, Phys. Rev. B 27, 112 (1983).
[8] G. E. Blonder, M. Tinkham, and T. M. Klapwijk, Phys. Rev. B 25, 4515 (1982).
[9] T. M. Klapwijk, G. E. Blonder, and M. Tinkham, Physica 109–110, 1657 (1982); M. Octavio, M. Tinkham, G. E. Blonder, and T. M. Klapwijk, Phys. Rev. B 27, 6739 (1983).
[10] K. Flensberg, J. Bindslev Hansen, and M. Octavio, Phys. Rev. B 38, 8707 (1988).
[11] G. B. Arnold, J. Low Temp. Phys. 68, 1 (1987).
[12] A. Kastalsky, L. H. Greene, J. B. Barner, and R. Bhat, Phys. Rev. Lett. 64, 804 (1990).
[13] H. J. Fink, M. Sheikholeslam, A. Gilalbert, J. P. Laheurte, J. P. Romagnan, J. C. Noiray, and E. Guyon, Phys. Rev. B 14, 1052 (1976).

# Direct Observation of Electronic Anisotropy in Single-Crystal $Y_1Ba_2Cu_3O_{7-x}$

T. R. Dinger, T. K. Worthington, W. J. Gallagher, and R. L. Sandstrom
*IBM Thomas J. Watson Research Center, Yorktown Heights, New York 10598*
(Received 14 May 1987)

We report direct observation of the anisotropic electronic behavior of the high-temperature superconductor $Y_1Ba_2Cu_3O_{7-x}$. Critical-field and critical-current measurements performed on single crystals show anisotropies of 10 and greater. Critical supercurrent densities in favorable directions in single crystals are $3\times10^6$ A/cm$^2$ in low fields at 4.5 K and remain above $10^6$ A/cm$^2$ to beyond 40 kG.

PACS numbers: 74.70.Ya, 74.60.Ec

Feverish activity on high-$T_c$ superconductivity in Cu-O-based perovskite-type materials has followed the breakthrough discovery of superconductivity at ~35 K in $La_{2-x}Ba_xCuO_4$ by Bednorz and Müller.[1] A highlight of this activity was the attainment of superconductivity at ~95 K, first achieved by Wu *et al.*[2] in mixed-phase compositions of Y-Ba-Cu-O, and the later isolation of $Y_1Ba_2Cu_3O_{7-x}$ as the superconducting phase.[3-5] The commonality of Cu-O layers to both the $K_2NiF_4$ structure of $La_{2-x}Ba_xCuO_4$ superconductors and the layered perovskite $Y_1Ba_2Cu_3O_{7-x}$ compounds suggests strongly that these two-dimensional layers are tied to the attainment of high transition temperatures. Indeed, Hidaka *et al.*[6] recently reported upper-critical-field anisotropies of 5 in single crystals $La_{2-x}Ba_xCuO_4$ and thus confirmed the anisotropic nature of the superconductivity in the ≃35-40-K based superconductors. In this Letter we report the observation of even larger anisotropies in lower critical field and in the critical current density of single crystals of $Y_1Ba_2Cu_3O_{7-x}$. Furthermore, our measurements demonstrate that $Y_1Ba_2Cu_3O_{7-x}$ can carry large supercurrent densities (≃$3\times10^6$ A/cm$^2$) in favorable directions at 4.5 K, and that the large supercurrent-carrying capability can persist in modest fields.

Single crystals of $Y_1Ba_2Cu_3O_{7-x}$ were grown by a technique similar to that used by Iwazumi *et al.*[7] for $La_{1.85}Sr_{0.15}CuO_4$. A sintered powder containing three phases, $Y_1Ba_2Cu_3O_{7-x}$, CuO, and $BaCuO_2$, and having a nominal composition in the molar ratio (0.125 $Y_2O_3$):(0.61 BaO):(1.00 CuO), was formed into a 1.27-cm-diameter pellet and fired in a slightly reducing atmosphere at 975 °C for 12 h. During the 975-°C soak, an oxidizing atmosphere was introduced to promote growth of the $Y_1Ba_2Cu_3O_{7-x}$ crystallites already present in the particle compact. This technique routinely produced highly faceted crystals with dimensions of approximately 200 μm (Fig. 1) with occasional crystals approaching 0.5 mm in size.[8] Precession-camera x-ray results (Fig. 1) using Mo radiation ($\lambda=0.71069$ Å) showed the crystals to be of high quality with unit-cell dimensions of $a=3.88$ Å and $b=3.84$ Å given by the $a^*\times b^*$ net in Fig. 1. Rotation of the crystal by 90° gave the $a^*\times c^*$ net of Fig. 1 showing the three-layer modulation of the structure in [001] with $c=11.63$ Å. The degree of orthorhombism of the single crystals based on the precession-camera photograph was $a/b=1.01$ which is close to the 1.016 measured by Beyers *et al.*[9] Twinning of the crystals was not observed either optically or in the single-crystal diffraction experiment although transmission electron microscopy of similar crystals showed large amounts of twinning after the mechanical grinding used in the specimen preparation.[10] This result suggests that the crystals are unstable to mechanical stress and deform through the twinning process in order to minimize their strain energy. Such behavior has been previously noted and well documented in other ceramics such as $BaTiO_3$ and $ZrO_2$.[11,12]

We characterized our crystals by performing extensive magnetic measurements using a SHE 905 magnetometer equipped with a 40-kG superconducting solenoid. As grown, our crystals typically displayed superconducting diamagnetic transitions in the 40-50-K region. Annealing in flowing oxygen for extended periods at 450 to 500 °C raised the transition temperatures to ≃85 K. Extensive measurements were performed on two 85-K crystals. One had dimensions ≃400×370×120 μm$^3$; the other had dimensions ≃300×300×180 μm$^3$. The larger crystal was the same one used in point-contact tunneling studies that indicated essentially no difference in the superconducting energy gap as determined from tunneling into different orientations of the crystal from a probe tip dug ≃1000 Å into the crystal surface.[13]

We first investigated the low-field magnetization of our crystals with the field applied both parallel to and perpendicular to the Cu-O planes. The zero-field-cooled diamagnetism in several crystals in low fields (20 G) was essentially 100% after correction for demagnetizing factors. The Meissner flux expulsion expressed as a fraction of the diamagnetic shielding was small, varying from ≃4% in the parallel orientation to ≃17% in the perpendicular orientation. The 100% diamagnetic shielding is as expected; the low Meissner effect is somewhat surprising, although not without precedent. For example, small Meissner fractions in single crystals were observed some time ago in single crystals of $TaS_2$(pyridine)$_{1/2}$,[14] and more recently they were observed in single crystals of $La_{1.85}Sr_{0.15}CuO_4$.[9] Incomplete Meissner effects are generally associated with inhomogeneities in superconduct-

 

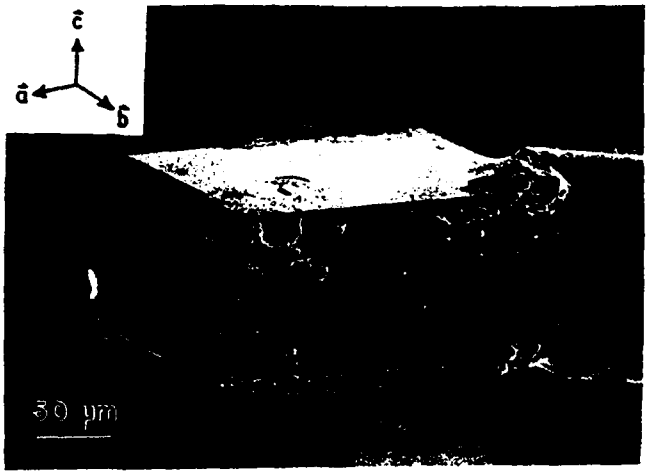


(a)

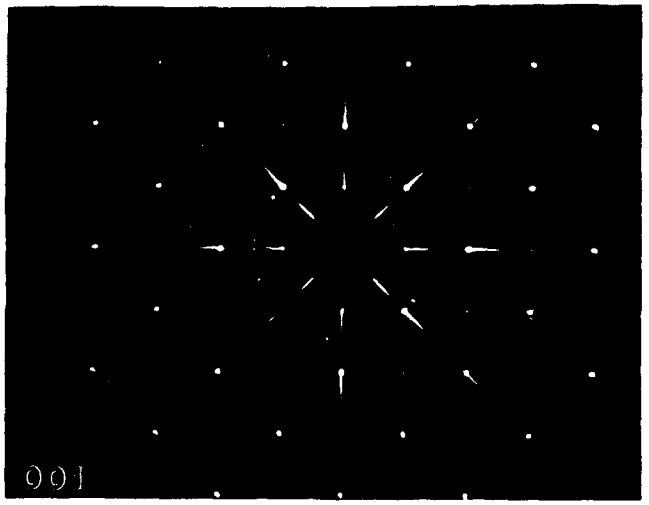


(b)

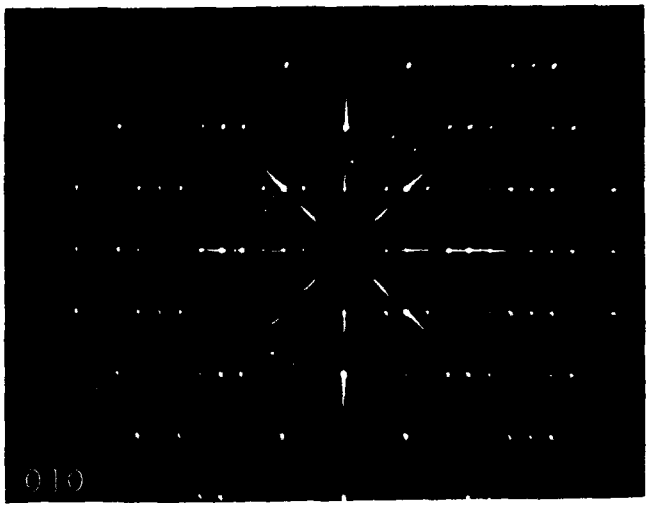


(c)

FIG. 1. Secondary-electron image and [001] and [010] zone-axis precession-camera photographs of a $Y_1Ba_2Cu_3O_{7-x}$ single crystal after extraction from the crystal mass. The [010] pattern shows the three-layer stacking of the perovskite blocks along [001].

ing materials. In doped materials, such as $La_{2-x}Sr_x$-$CuO_4$, concentration variations are a likely source of inhomogeneities. In $Y_1Ba_2Cu_3O_{7-x}$ the inhomogeneities might be variations in the oxygen-defect ordering. Our crystals, with $T_c$ slightly below the 92–95-K maximum achieved for $Y_1Ba_2Cu_3O_{7-x}$, likely possess some imperfections in the defect ordering. We are not yet sure of the significance of the difference in Meissner fractions between the parallel and perpendicular orientations.

Studies of magnetization hysteresis as an applied field is swept allow the determination of the lower critical field and provide a noncontact way of determining critical density from the magnetic moment resulting from induced screening currents. Antonova, Medvedev, and Shebalin[15] used such measurements to study the critical field and critical current anisotropy in $NbSe_2$ and we found the technique to work well for $Y_1Ba_2Cu_3O_{7-x}$.

Figure 2 shows magnetic hysteresis loops at 4.5 K for the larger crystal mounted with the Cu-O planes perpendicular to the field lines [Fig. 2(a)] and parallel to the field lines [Fig. 2(b)]. The differences in the scale and in the shape of the magnetization for the two orientations are very striking. The lower critical fields, $H_{c1}^{\perp}$ and $H_{c1}^{\parallel}$, for crystals oriented such that the applied field is perpendicular and parallel to the Cu-O planes, respectively, can be determined from the point in the initial part of each loop at which the departure from linearity begins. The departures occur at fields of 4 kG for the perpendicular orientation and at 600 G for the parallel orientation. Corrected for the demagnetizing factors we get $H_{c1}^{\perp}=8$ kG and $H_{c1}^{\parallel}=800$ G, giving a ratio of 10. This large lower-critical-field anisotropy was cross checked by measurements on a second crystal. In this case we repeatedly cycled the low-field magnetization curve to find the lowest field at which the magnetization was not reversible. This procedure yielded values of $H_{c1}^{\perp}=5.2$ kG and $H_{c1}^{\parallel}\lesssim 530$ G for this crystal, again giving a ratio of 10.

The difference in the magnitudes of the hysteresis in the two loops in Fig. 2 is even larger. In the perpendicular orientation the gradual departure of the magnetization curve from perfect diamagnetism indicates that there is strong pinning. In contrast, the sharp break at $H_{c1}^{\parallel}$ in the parallel orientation is indicative of weak pinning. According to the critical-state model of Bean[16] applied to a disk-shaped sample in an applied field $H_a$ much in excess of the magnetization, the magnitude of the critical current density is related to the magnetization by the simple relation[17] $J_c=30M/r$, where $M$ is the magnetization in electromagnetic units per cubic centimeter, $r$ is the disk radius in centimeters, and $J_c$ is the critical current density in amperes per square centimeter. We use this relationship and approximate $r$ as the geometric mean of half of the sample dimensions perpendicular to the field. From the peaks in the 4.5-K magnetization curves, we estimate the maximum critical current densities in the two directions as $J_c^{\perp}=2.9\times10^6$ A/cm$^2$

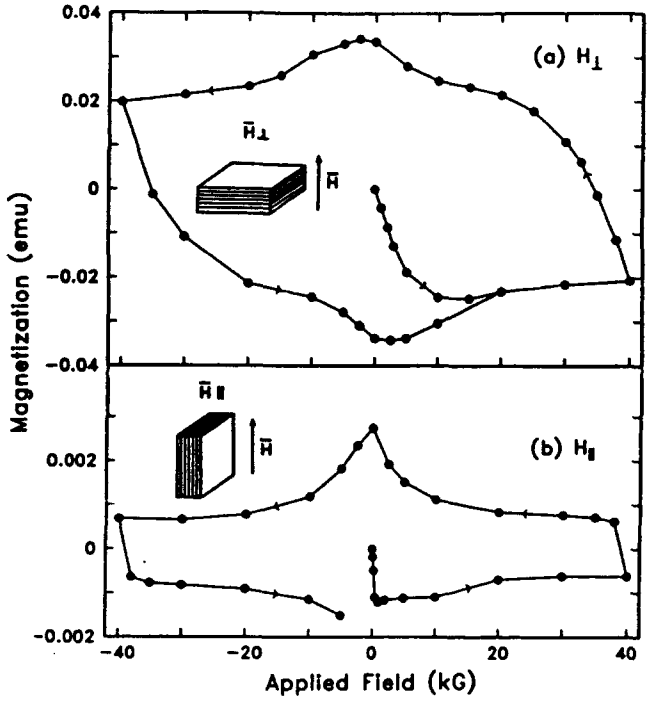


FIG. 2. Magnetization hysteresis loops at 4.5 K for a single crystal of $Y_1Ba_2Cu_3O_{7-x}$ with the Cu-O planes oriented (a) perpendicular to the applied magnetic field and (b) parallel to the applied field.

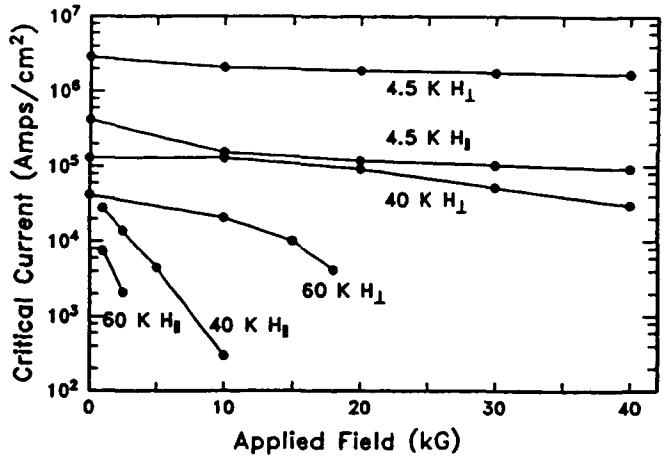


FIG. 3. Critical current densities deduced from magnetization hysteresis at various temperatures as a function of magnetic field applied either parallel or perpendicular to the Cu-O planes.

and $J_c^\parallel = 4.2\times10^5$ A/cm$^2$. (Note that our nomenclature is such that $J_c^\parallel$ is the critical current inferred from fields applied parallel to the Cu-O planes such that the induced screening currents actually flow perpendicular to the planes and $J_c^\perp$ is the critical current determined from currents induced along the direction of the planes by fields applied perpendicular to the planes.) In Fig. 3 we show the field and temperature dependence of the critical current density as determined from the hysteresis curves in Fig. 2 and similar curves taken at higher temperatures. From this plot one can see that the falloff of critical current density with applied field is not too severe. At 40 kG, $J_c^\perp = 1.7\times10^6$ A/cm$^2$ and $J_c^\parallel = 9.2\times10^4$ A/cm$^2$. The falloff with temperature is much more rapid. By 40 K in zero field, the perpendicular critical current density $J_c^\perp = 1.3\times10^5$ A/cm$^2$ and by 60 K this has fallen to $J_c^\perp = 4.2\times10^4$ A/cm$^2$. The critical-current anisotropy increases considerably at higher temperatures and fields.

Measurements taken on a second crystal at 4.5 K confirmed the same general anisotropic critical-current behavior, giving approximately three times greater anisotropy at zero field ($J_c^\perp = 3.2\times10^6$ A/cm$^2$ and $J_c^\parallel = 1.6\times10^5$ A/cm$^2$) and still larger critical-current anisotropies in larger fields. For instance, at 20 kG, $J_c^\perp = 2.2\times10^6$ A/cm$^2$ and $J_c^\parallel = 3.2\times10^4$ A/cm$^2$, for a ratio of 70. We observed in the course of these measurements that the hysteresis curves were extremely sensitive to slight misalignments from the parallel orientation. An estimated 5° misalignment of the crystal reduced the inferred critical-current anisotropy at 20 kG by more than an order of magnitude. It is possible that the smaller anisotropy observed in the first crystal was due to some slight misalignment, but we cannot rule out the possibility that it was a less perfect crystal.

Above $H_{c1}$ we observed a slow time-dependent change in the magnetization similar to that observed in $La_{2-x}Ba_xCuO_4$ by Müller, Takashige, and Bednorz.[18] The magnetization was seen to change by as much as 20% and the time dependence was consistent with logarithmic behavior for times longer than 1000 min. For practical reasons, the magnetization points reported in this paper were typically taken a few minutes after establishing the field.

These critical-current and lower-critical-field measurements prove that the $Y_1Ba_2Cu_3O_{7-x}$ superconductor is strongly anisotropic with the good conducting directions being along the Cu-O planes. Refined structural analyses[19] show that there are one-dimensional Cu-O chains in the $Y_1Ba_2Cu_3O_{7-x}$ structure as well as two-dimensional Cu-O planes. Band-structure calculations[20] indicate that both one-dimensional and two-dimensional features may be making contributions to the high-transition-temperature superconductivity. However, it seems unlikely to us that the large supercurrents that we have observed at low temperatures could be carried by the one-dimensional chains.

From studies of intercalation superconductors, much is known both experimentally and theoretically about the behavior of anisotropic layered superconductors. Theoretically, such superconductors can be described either by a Ginzburg-Landau theory with an anisotropic $\kappa$[21] or as an array of Josephson-coupled layers[22] (which can be reduced in some limits to an anisotropic Ginzburg-Landau description). Consistent with our findings for $Y_1Ba_2Cu_3O_{7-x}$, this class of superconductors is known

to possess anisotropic critical fields with $H_{c1}^{\perp}$ much larger than $H_{c1}^{\parallel}$ and differences in magnetization hysteresis loops and inferred critical-current densities. Though we have not studied the upper critical fields in our $Y_1Ba_2Cu_3O_{7-x}$ crystals, they can be expected to behave like those in other anisotropic layered superconductors, in which case $H_{c2}^{\parallel}$ is much larger than $H_{c2}^{\perp}$. Such behavior in $Y_1Ba_2Cu_3O_{7-x}$ would explain some disparate aspects of the early data on this material. In particular, measurements of the resistive transitions in high magnetic fields have indicated drastic broadening of the transition as field is applied.[2,23] In a ceramic composite of $Y_1Ba_2Cu_3O_{7-x}$, some grains oriented with their layers perpendicular to the field would possess modest critical fields. Other grains with their layers oriented parallel to the field would have enormous critical fields. The resulting resistive transition, as field is applied, would broaden in a manner consistent with the early observations. Pinning between weakly Josephson-coupled layers would be very weak resulting in small depinning critical currents perpendicular to the layers. The critical currents so far observed for ceramic materials have been in all cases small. To our knowledge the $\simeq 3\times 10^6$-A/cm$^2$ values for critical current density in the direction of the Cu-O planes in our crystals at 4.5 K are the largest values yet seen in the $Y_1Ba_2Cu_3O_{7-x}$ materials. In general, pinning in perfect crystals is not expected to be strong, and so it is reasonable to expect that still higher critical current densities can be achieved. Indeed, recent results with epitaxial films,[24] with the epitaxy such that the large supercurrents flow along the direction of the Cu-O planes, have demonstrated larger high-temperature values of critical current density than ours, although the drop off with increasing field is more rapid.

In summary, our measurements on single crystals of $Y_1Ba_2Cu_3O_{7-x}$ demonstrate conclusively that its superconductivity is strongly anisotropic. At low temperatures in fields out to 40 kG, critical currents along the direction of the Cu-O planes were observed to be in excess of $10^6$ A/cm$^2$. The large supercurrent-carrying capability and the anisotropy will be important aspects of most application considerations.

This work was supported in part by the U.S. Office of Naval Research Contract No. N00014-85-C-0361. We thank S. J. LaPlaca for single-crystal x-ray results, H. R. Lilienthal, T. R. McGuire, S. S. P. Parkin, and K. P. Roche for experimental assistance in the magnetic-susceptibility measurements. We acknowledge informative discussions with R. Schwall, A. Davidson, R. L. Greene, F. Hotzberg, T. N. Jackson, A. W. Kleinsasser, A. P. Malozemoff, M. W. Shafer, T. M. Shaw, and A. R. Williams.

[1]J. G. Bednorz and K. A. Müller, Z. Phys. B 64, 189 (1986).

[2]M. K. Wu, J. R. Ashburn, C. J. Torng, P. H. Hor, R. L. Meng, L. Gao, Z. J. Huang, Y. Q. Wang, and C. W. Chu, Phys. Rev. Lett. 58, 908 (1987).

[3]R. J. Cava, B. Batlogg, R. B. van Dover, D. W. Murphy, S. Sunshine, T. Siegrist, J. P. Remeika, E. A. Rietman, S. Zahurak, and G. P. Espinosa, Phys. Rev. Lett. 58, 1676 (1987).

[4]P. M. Grant, R. B. Beyers, E. M. Engler, G. Lim, S. S. P. Parkin, M. L. Ramirez, V. Y. Lee, A. Nazzal, J. E. Vazquez, and R. J. Savoy, Phys. Rev. B 35, 7242 (1987).

[5]W. J. Gallagher, R. L. Sandstrom, T. R. Dinger, T. M. Shaw, and D. A. Chance, Solid State Commun. 63, 147 (1987).

[6]Y. Hidaka, Y. Enomoto, M. Suzuki, M. Oda, and T. Murakami, Jpn. J. Appl. Phys. 26, L377 (1987).

[7]T. Iwazumi, R. Yoshizaki, H. Sadawa, H. Uwe, T. Sakudo, and E. Matsuura, Jpn. J. Appl. Phys. 26, L386 (1987).

[8]Alternative growth techniques are now giving significantly bigger crystals; cf. D. Kaiser, F. Holtzberg, and B. A. Scott (unpublished).

[9]R. B. Beyers, G. Lim, E. M. Engler, R. J. Savoy, T. M. Shaw, T. R. Dinger, W. J. Gallagher, and R. L. Sandstrom, Appl. Phys. Lett. (to be published).

[10]T. M. Shaw, unpublished.

[11]T. Malis and H. Gleitner, J. Appl. Phys. 47, 5195 (1976).

[12]A. G. Evans and A. H. Heuer, J. Am. Ceram. Soc. 63, 241–248 (1980).

[13]J. R. Kirtley, R. T. Collins, Z. Schlesinger, W. J. Gallagher, R. L. Sandstrom, T. R. Dinger, and D. A. Chance, Phys. Rev. B (to be published).

[14]D. E. Prober, M. R. Beasley, and R. E. Schwall, Phys. Rev. B 15, 5245 (1977).

[15]E. A. Antonova, S. A. Medvedev, and I. Yu. Shebalin, Zh. Eksp. Teor. Fiz. 57, 329 (1969) [Sov. Phys. JETP 30, 181 (1970)].

[16]C. P. Bean, Phys. Rev. Lett. 8, 250 (1962).

[17]This relation is approximate. It neglects the correction to the internal field in the superconductor caused by the current in the superconductor. This difference is small at high fields; at low fields we use average of the magnitudes of the magnetization at a given applied field. Corrections beyond this are inconsequential to our results.

[18]K. A. Müller, M. Takashige, and J. G. Bednorz, Phys. Rev. Lett. 58, 1143 (1987).

[19]Structural refinements showing the vacancy ordering have been reported by a number of groups. See for example, F. Beech, S. Miraglia, A. Santoro, and R. S. Roth, Phys. Rev. B (to be published).

[20]L. F. Mattheiss and D. R. Hamann, Solid State Commun. (to be published).

[21]R. C. Morris, R. V. Coleman, and R. Bhandari, Phys. Rev. B 8, 895 (1972).

[22]W. E. Lawrence and S. Doniach, in *Proceedings of the Twelfth International Conference on Low Temperature Physics*, edited by E. Kanda (Academic, Kyoto, 1971), p. 361.

[23]T. P. Orlando, K. A. Delin, S. Foner, E. J. McNiff, Jr., J. M. Tarascon, L. H. Greene, W. R. McKinnon, and G. W. Hull, Phys. Rev. B 35, 7249 (1987).

[24]P. Chaudhari, R. H. Koch, R. B. Laibowitz, T. McGuire, and R. Gambino, Phys. Rev. Lett. 58, 2684 (1987) (this issue).

(6)

# Measurement of Anisotropic Resistivity and Hall Constant for Single-Crystal $YBa_2Cu_3O_{7-x}$

S. W. Tozer, A. W. Kleinsasser, T. Penney, D. Kaiser, and F. Holtzberg
*IBM Thomas J. Watson Research Center, Yorktown Heights, New York 10598*
(Received 7 August 1987)

The resistivity of single-crystal $YBa_2Cu_3O_{7-x}$ has been found to be anisotropic, with magnitude and temperature dependence similar to ceramic samples in directions parallel to the Cu-O planes, and with a 30 times larger room-temperature value and a much smaller temperature dependence in the orthogonal direction. The Hall coefficient, with a magnetic field applied parallel to the Cu-O planes, is negative (electronlike) and essentially temperature independent in these crystals, in direct contrast to the behavior of other types of samples.

PACS numbers: 74.70.Ya

The report of superconductivity at unprecedented high temperatures in $La_{2-x}Ba_xCuO_4$ by Bednorz and Müller[1] led to the discovery of superconductivity at temperatures above 90 K in $YBa_2Cu_3O_{7-x}$ and numerous related compounds.[2] The layered perovskite structure[3] of these materials indicates that they should be quite anisotropic. Transport measurements on single crystals are thus an important step towards gaining an understanding of these materials. Anisotropic magnetic properties (critical fields, critical current density) have been reported in single crystals of both $La_{2-x}Ba_xCuO_4$ and $YBa_2Cu_3O_{7-x}$-type materials,[4-7] as has an anisotropy in resistivity in $La_{2-x}Sr_xCuO_4$ single crystals[8] and in oriented films[9] of $YBa_2Cu_3O_{7-x}$. In addition to being anisotropic, these new superconductors represent a state of matter significantly different from those which are presently understood. A fundamental question is whether or not the normal state from which the superconducting one condenses is a Fermi liquid, as is believed to be the case with all other known superconductors. One signature of the Fermi-liquid state is a quadratic dependence of electrical resistivity on temperature below the range in which phonon scattering dominates. The linear temperature dependence of the resistivity characteristic of these materials in ceramic form[3] appears, in this context, to be rather mysterious, implying a breakdown of the Fermi-liquid description. For example, Lee and Read[10] infer both nonphonon and $d$-wave pairing from this linear dependence.

In this paper we report measurements of the anisotropic resistivity and Hall coefficient in bulk single-crystal $YBa_2Cu_3O_{7-x}$. We find that the resistivity in the $a$ and $b$ directions (i.e., parallel to the Cu-O planes) is approximately 450 $\mu\Omega$ cm at room temperature, decreasing linearly with temperature above the superconducting transition with a slope of 1.3 $\mu\Omega$ cm/K. This is similar to the resistivity behavior of ceramic samples, for which slopes of 1.7–2.5 $\mu\Omega$ cm/K are typical.[3] Thus we can state that the relatively large magnitude and the linear temperature dependence of resistivity are bulk properties and not artifacts of the granular nature of the ceramic materials. In the $c$ direction (i.e., orthogonal to the Cu-O planes), we find a room-temperature resistivity 30 times larger than in the in-plane direction, with only a weak temperature dependence, confirming the highly anisotropic nature of the material. The Hall coefficient, measured with a magnetic field applied parallel to the Cu-O planes, is electronlike and virtually temperature independent, in contrast to the holelike and temperature-dependent Hall constant observed in ceramic samples[11] and epitaxial thin films.[12]

The crystal-growth process, described elsewhere,[13] yields crystals in the shape of rectangular parallelpipeds. One typical form is thin platelets, as large as several millimeters in size in the basal (Cu-O) plane by a few tens of micrometers in the orthogonal ($c$ axis) direction. The other common shape is euhedral, with dimensions of up to $0.5\times0.5$ mm$^2$ by 0.2 mm.

Low-resistance Ohmic contacts to these crystals proved to be difficult to form. Contact resistance values in the range $10^{-3}$ to 10 $\Omega$ cm$^2$ were obtained by ultrasonic bonding of Al or Au wires and by direct probing. The presence of a poorly conducting surface layer, possibly residual melt, often made even four-terminal measurements of the underlying superconducting crystal impossible in many cases. We developed a process, to be described elsewhere,[14] which results in Ohmic contacts with specific resistance values in the range $10^7$ to $10^6$ $\Omega$ cm$^2$. The crystal is masked with only the contact areas exposed during the contact process.

For measurement of the resistivity anisotropy, $\simeq 10$ $\mu$m$\times 10$ $\mu$m$^2$ contacts were formed on the corners of a rectangular crystal face containing the $c$ axis. The two directions in the face used in the measurement and the one orthogonal to it will be denoted by subscripts 1, 2 (along the $c$ axis), and 3, respectively, with corresponding lengths of 275, 97, and 290 $\mu$m for the sample reported here. The standard Montgomery[15] and van der Pauw[16] techniques were used to extract the anisotropic resistivity and Hall coefficient.

Four-terminal ac measurements yielded two resistances, $R_1$ with the current terminals parallel to the $a$-$b$ planes (perpendicular to the $c$-axis direction) and $R_2$ with the current terminals along the $c$-axis direction, as

illustrated in Fig. 1. The two resistances have very different values and temperature dependences, as shown in Fig. 2. The small dots in Fig. 2 are data taken with an rms measurement current of 500 $\mu$A (peak current density 710 A/cm$^2$ at the contacts). In the low-resistance direction, $R_1$ falls rapidly with decreasing temperature. In the high-resistance ($c$ axis) direction, $R_2$ is $\simeq$100 times larger than $R_1$ at room temperature and increases with decreasing temperature, attaining a value about 60% above its room-temperature value just above the superconducting transition. The large solid resistance data points were obtained with an rms current of 20 mA (peak current density $2.8\times10^4$ A/cm$^2$ at the contacts) in a separate experiment. With the larger current, the superconducting transition was clearly seen in both $R_1$ and $R_2$. The good agreement with the lower-current data indicates that heating and critical current were not problems even with the larger current. There is a difference in $T_c$ between the two runs. The transition temperature of this sample was originally 91 K with a 10%-90% width of less than 1 K. It dropped to a value of approximately 80 K, still retaining the narrow transition width, after being tested several times. The reason for this decrease is not known; however, the normal-state resistances $R_1$ and $R_2$ did not change. $T_c$ was stable in other samples, which had contacts parallel to the $a$ and $b$ directions. $T_c$ varied from $\simeq$75 to 91 K from sample to sample, depending on the annealing conditions, without major differences in the normal-state resistivity.

The large difference between the resistances $R_1$ and $R_2$ indicates a substantial anisotropy between the in plane and $c$ directions, since the higher resistance corresponds to the shorter sample dimension. To extract the components of the resistivity tensor, the method developed by Montgomery[15] was used. In keeping with his notation, the potentials and currents present in an anisotropic sample with dimensions $l_1'$, $l_2'$, and $l_3'$ and (diagonal) resistivity tensor components $\rho_1$, $\rho_2$, and $\rho_3$, are mapped onto an equivalent isotropic sample with resistivity $\rho=(\rho_1\rho_2\rho_3)^{1/3}$ and dimensions $l_1$, $l_2$, and $l_3$. Given $R_1$ and $R_2$, the actual sample dimensions, and the assumption $\rho_1=\rho_3\neq\rho_2$, we obtain the components of resistivity. The magnitude and temperature dependence of $\rho_1$ which we obtain is in agreement with values obtained from measurements on other crystals involving contacts only in the $a$-$b$ plane. No $a$-$b$ plane anisotropy was observed, although a small anisotropy would be consistent with our measurements. These crystals exhibit twinning in the $a$-$b$ plane,[13] which would tend to cause the in-plane resistivity to appear more isotropic. Thus the assumption that there are only two components of resistivity, $\rho_{ab}$ ($=\rho_1=\rho_3$) and $\rho_c$ ($=\rho_2$), which we used in our analysis is a good one.

The rapid decrease in $R_1$ with decreasing temperature, which is essentially exponential, can be understood as being due to the increasing distance between the voltage leads and the current leads in the equivalent isotropic sample. As a result of the increasing value of the ratio $R_2/R_1$ with decreasing temperature, $l_2/l_1$ increases from 1.9 to 3.4 between 300 and 100 K ($l_2'/l_1'=0.35$). $l_2$ grows from 300 to 440 $\mu$m while $l_1$ changes only slightly, from 160 to 130 $\mu$m. The resistivity ratio $\rho_2/\rho_1$ increases from 30 to $\simeq$80 as temperature is lowered. In measurements on samples with all contacts in the $a$-$b$ plane, the measured *resistances* are much larger because of the more favorable effective sample geometry.

The resistivities $\rho_1$ (or $\rho_{ab}$) and $\rho_2$ (or $\rho_c$) are plotted as functions of temperature in Fig. 3. $\rho_1$ is 450 $\mu\Omega$ cm at room temperature, 180 $\mu\Omega$ cm at $T_c$, and extrapolates to 75 $\mu\Omega$ cm at $T=0$, with a slope of 1.3 $\mu\Omega$ cm/K. It

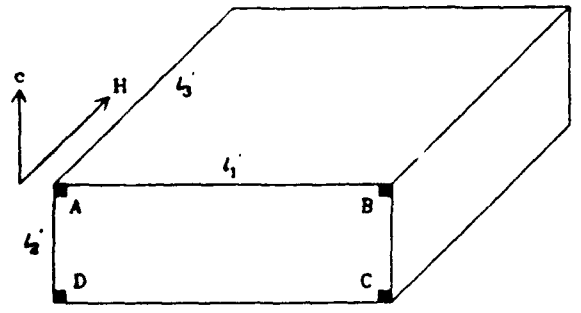


FIG. 1. Sample and contact geometry. The contacts are on a face which contains the $c$ axis. Four-terminal resistance measurements were made with the current contacts aligned perpendicular to the $c$ axis of the crystal ($R_1=V_{DC}/I_{AB}$), and parallel to it ($R_2=V_{BC}/I_{AD}$). For Hall measurements, $V_{AC}/I_{DB}$ is measured with a magnetic field, H, applied perpendicular to the contacted face.

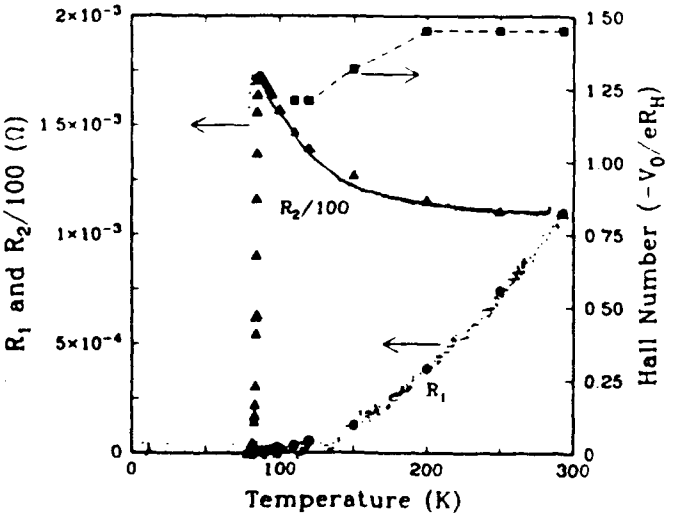


FIG. 2. Four-terminal resistances $R_1$ and $R_2$ as a function of temperature. Note the factor of 100 difference between $R_1$ and $R_2$ at room temperature. The small and large symbols represent data from different runs with currents of 500 $\mu$A and 20 mA, respectively. Also plotted is the Hall number ($V_0/eR_H$), corresponding to 1.2–1.5 electrons per unit cell.

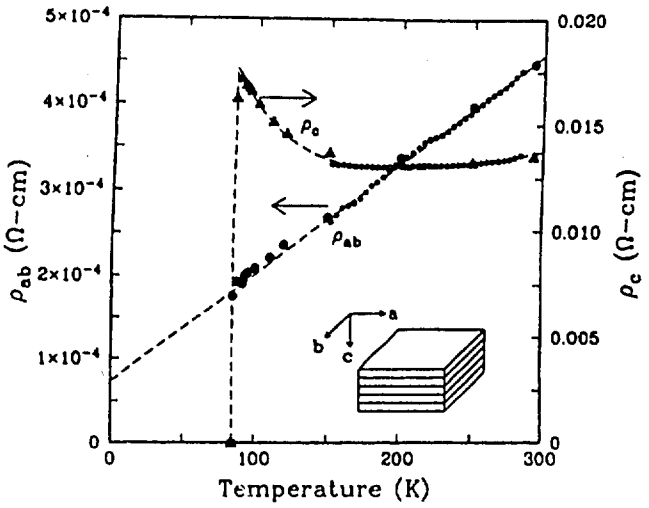


FIG. 3. Resistivity tensor components parallel to the Cu-O planes ($\rho_{ab}$ or $\rho_1$) and perpendicular to them, i.e., along the $c$ axis ($\rho_c$ or $\rho_2$). The small open and large solid symbols are for two different measurements with currents of 500 $\mu$A and 20 mA, respectively. Inset: Schematically illustrates the crystal directions with respect to the Cu-O planes which dominate the conductivity.

is similar in magnitude and temperature dependence to the resistivity of ceramic samples. In contrast, $\rho_2$, the resistivity in the $c$ direction, is much larger and increases somewhat with decreasing temperature. For a 500-$\mu$A current, the rapidly falling value of $R_1$ limits the temperature range of our analysis to above roughly 150 K. By assuming that $\rho_1$ is linear in temperature down to $T_c$, as observed in other samples with measurements along the $a$-$b$ planes and in ceramic samples, we can extrapolate the behavior of $\rho_2$, which increases slightly as temperature is lowered, as shown by the dashed line in Fig. 2. For this we used an extrapolation of $\rho_2/\rho_1$, which varied smoothly with temperature. The resistance values $R_1$ and $R_2$ calculated using the extrapolated resistivities were in good agreement with the measured ones so that, given the linear $\rho_1(T)$, the determination of $\rho_2(T)$ is unique all the way to $T_c$. The extrapolation is consistent with the 20-mA data. The $c$-axis resistivity is much larger than the in-plane resistivity, increasing somewhat with decreasing temperature, with a value of 13–17 m$\Omega$ cm.

In earlier measurements[8] on $La_{2-x}Sr_xCuO_4$, a large resistivity anisotropy between the $a$ and $c$ directions was inferred with use of two different bar samples. Both exhibited broad transitions and similar temperature dependences, with resistivity increasing with decreasing temperature above the onset of superconductivity. Zero resistance was not attained until 3.8 K. We observed similar temperature dependences on $YBa_2Cu_3O_{7-x}$ samples with poor contacts and attributed our results to a nonsuperconducting surface layer rather than to poor sample quality. Recent measurements on oriented $YBa_2Cu_3O_{7-x}$ thin films[9] show a factor-of-20 anisotropy between in-plane and out-of-plane resistivities at room temperature, increasing to about 40 near $T_c$. The in-plane resistivity is higher by roughly a factor of 2 than that of our crystals, possibly as a result the imperfect stoichiometry of the films. The $c$-axis resistivity fell slightly with decreasing temperature.

Hall measurements were made with the same sample which we discussed above. A magnetic field of $\pm 1$ T was applied perpendicular to the contacted face of the crystal (i.e., parallel to the $a$-$b$ planes). The Hall voltage was linear in $H$ at 0.5 and 1 T. It is convenient to normalize the Hall constant, $R_H$, to the unit cell volume, $V_0 = 174$ Å$^3$, and the electronic charge so that, in the case of one isotropic parabolic band the Hall number, $V_0/eR_H$, is the number of carriers per unit cell. For this sample, the Hall constant is in the range $-7.5\times10^{-10}$ to $-9\times10^{-10}$ m$^3$/C, giving a Hall number, shown in Fig. 2, which is electronlike (negative) and nearly temperature independent, as expected for a metal, indicating 1.2–1.5 electrons per formula unit. The thickness of the equivalent isotropic sample, 150 $\mu$m, and not the actual thickness of 290 $\mu$m was used to obtain this value. This behavior is in sharp contrast to that observed in ceramic[11] and polycrystalline epitaxial[12] samples, in which cases the Hall number is holelike and proportional to $T$. In ceramic $La_{2-x}Sr_xCuO_4$, a $p$-type Hall coefficient which was nearly temperature independent was found.[11] The behavior was purely holelike for $x < 0.15$ but mixed (both holes and electrons) for $x > 0.15$.

Recently, Allen, Pickett, and Krakauer[17] used a band-theory approach to calculate the anisotropic transport properties, including the resistivity and Hall tensors, of doped $La_2CuO_4$-based materials. This analysis has been extended[18] to $YBa_2Cu_3O_{7-x}$. Both positive (for $B$ parallel to the $c$ axis) and negative Hall coefficients (for B in the $a$ or $b$ direction) are predicted for both of these materials, depending on the field direction (due to the nonparabolic bands, $R_H \neq -1/ne$). For in-plane magnetic fields orthogonal to and along the ordered Cu-O chains, they predict Hall constants of $-3.5\times10^{-10}$ and $-11\times10^{-10}$ m$^3$/C, in reasonable agreement with our single in-plane number of $\simeq -8\times10^{-10}$ m$^3$/C. They also predict zero-temperature resistivity anisotropies of 5.6 and 15 between the in-plane and $c$ directions, somewhat smaller than we extrapolate from our measurements, and an anisotropy of 2.7 between the in-plane directions.

In summary, we have measured the anisotropic resistivity of single-crystal $YBa_2Cu_3O_{7-x}$. The in-plane behavior is like that of ceramic material, showing that the linear temperature dependence of resistivity is not an artifact of the granular materials. Along the $c$ axis the resistivity is much larger and increases with decreasing temperature. The Hall coefficient, measured with the B field perpendicular to the $c$ axis, is electronlike with a

value corresponding to 1.3 carriers per cell.

The authors wish to acknowledge the assistance of J. Rigotty and R. Picunko with the measurements and useful conversations with R. L. Greene, D. Newns, P. B. Allen, and A. R. Williams. T. N. Jackson was important in developing the Ohmic-contact process. Two of the authors (S.W.T. and A.W.K.) received partial support from the U. S. Office of Naval Research under Contracts No. N00014-85-C-0868 and No. N00014-85-C-0361, respectively.

[1]J. G. Bednorz and K. A. Müller, Z. Phys. B 64, 189 (1986).

[2]M. K. Wu, J. R. Ashburn, C. J. Torng, P. H. Hor, R. L. Meng, L. Gao, Z. J. Huang, Y. Q. Wang, and C. W. Chu, Phys. Rev. Lett. 58, 908 (1987).

[3]R. J. Cava, B. Batlogg, R. B. van Dover, D. W. Murphy, S. Sunshine, T. Siegrist, J. P. Remeika, E. A. Reitman, S. Zahurak, and G. P. Espinosa, Phys. Rev. Lett. 58, 1676 (1987).

[4]T. R. Dinger, T. K. Worthington, W. J. Gallagher, and R. L. Sandstrom, Phys. Rev. Lett. 58, 2687 (1987); T. K. Worthington, W. J. Gallagher, and T. R. Dinger, Phys. Rev. Lett. 59, 1160 (1987).

[5]S. Shamoto, M. Onoda, and M. Sato, to be published.

[6]Y. Hidaka, Y. Enomoto, M. Suzuki, M. Oda, A. Katsui, and T. Murakami, Jpn. J. Appl. Phys. Part 2 26, L726 (1987).

[7]Y. Iye, T. Tamegai, H. Takeya, and H. Takei, Jpn. J. Appl. Phys. Part 2 26, L1057 (1987).

[8]Y. Hidaka, Y. Enomoto, M. Suzuki, M. Oda, and T. Murakami, Jpn. J. Appl. Phys. Part 2 26, L377 (1987).

[9]Y. Enomoto, T. Murakami, M. Suzuki, and K. Moriwaki, Jpn. J. Appl. Phys. Part 2 (to be published).

[10]P. A. Lee and N. Read, Phys. Rev. Lett. 58, 2691 (1987).

[11]T. Penney, M. W. Shafer, B. L. Olsen, and T. S. Plaskett, Adv. Ceramic Mater. 2, 577 (1987).

[12]P. Chaudhari, R. J. Collins, P. Freitas, R. Gambino, J. Kirtley, R. Koch, R. Laibowitz, F. Legoues, T. McGuire, T. Penney, A. Segmüller, and Z. Schlesinger, to be published.

[13]D. L. Kaiser, F. Holtzberg, B. A. Scott, and T. R. McGuire (to be published).

[14]A. W. Kleinsasser, S. W. Tozer, and T. N. Jackson, unpublished.

[15]H. C. Montgomery, J. Appl. Phys. 42, 2971 (1971).

[16]L. J. van der Pauw, Phillips Res. Rep. 13, 1 (1958).

[17]P. B. Allen, W. E. Pickett, and H. Krakauer, 36, 3926 (1987).

[18]P. B. Allen, private communication.

# Anisotropic Nature of High-Temperature Superconductivity in Single-Crystal $Y_1Ba_2Cu_3O_{7-x}$

T. K. Worthington, W. J. Gallagher, and T. R. Dinger
*IBM Thomas J. Watson Research Center, Yorktown Heights, New York 10598*
(Received 24 June 1987)

We report the first contact-free measurements of the upper critical fields, $H_{c2}(T)$, of single-crystal $Y_1Ba_2Cu_3O_{7-x}$. In contrast to reported resistive measurements, we find that the anisotropy near $T_c$ is temperature independent in agreement with anisotropic Ginzburg-Landau theory. Estimates of the anisotropic Ginzburg-Landau and London parameters are reported. These indicate that despite the large anisotropy in $H_{c2}$ (5:1), the inferred low-temperature interplanar coherence length ($\xi_z = 7$ Å) remains larger than the Cu-O layer spacing of 3.9 Å. Superconductivity in $Y_1Ba_2Cu_3O_{7-x}$ thus remains fundamentally three dimensional in nature for a substantial temperature range below $T_c$.

PACS numbers: 74.60.Ec, 74.70.Ya

Despite the flurry of activity on high-$T_c$ superconductivity in Cu-O based perovskite-type materials that has followed the breakthrough discovery of superconductivity at $\simeq 35$ K in $La_{2-x}Ba_xCuO_4$ by Bednorz and Müller,[1] the macroscopic nature of the superconductivity in these new materials and the mechanism responsible for their superconductivity are not yet clear. The availability of single crystals of the new Cu-O based superconductors, and the anisotropy manifest in their resistivity,[2] critical current density,[3] and upper[2,4-6] and lower[3] critical fields, establish the importance of anisotropy to the macroscopic nature of the high-temperature superconductivity. In this paper we report the first inductive measurements of $H_{c2}$ as a function of orientation for single-crystal $Y_1Ba_2Cu_3O_{7-x}$. We use this and other data to estimate the anisotropic Ginzburg-Landau parameters, and to examine the degree to which existing theories of anisotropic superconductors are able to describe the observed behavior of $Y_1Ba_2Cu_3O_{7-x}$. We find that the anisotropic Ginzburg-Landau theory describes our data well near $T_c$, and that although the superconductivity in $Y_1Ba_2Cu_3O_{7-x}$ is strongly anisotropic, it is three dimensional in nature. Elaborations of available theories are needed to explain lower-temperature features of our data.

The $Y_1Ba_2Cu_3O_{7-x}$ single crystal used in this study was obtained from a partially melted pellet made with an off-stoichiometric composition according to a procedure described by Dinger *et al.*[3] This procedure routinely resulted in highly faceted crystals with dimensions of approximately 200 $\mu$m, with occasional crystals approaching 0.5 mm in size. The crystal studied here had dimensions of 340 by 280 by 160 $\mu$m.[3] Measurements in a scanning x-ray diffractometer showed this crystal to be of high quality with unit-cell dimensions of $a = 3.83$ Å, $b = 3.89$ Å, and $c = 11.71$ Å. The degree of orthorhombicity was $b/a = 1.016$. The crystal was macroscopically twinned in the $a$-$b$ plane. The diffraction peak widths were limited by instrumental resolution, indicating domains in excess of 500 Å in size and little compositional variation.

The inductive transition of the crystal was measured by means of a variation of a technique used by Dalrymple and Prober.[7] The crystal was tightly wrapped with eight turns of 30-$\mu$m-diam insulated copper wire. A 200-pF capacitor was connected in parallel with this inductor to form an $LC$ circuit which was resonant at about 70 MHz. The wrapped crystal, capacitor, and a carbon-glass thermometer (Lake Shore Cryotronics, encapsulation removed) were all affixed to an alumina TO-5 header which was mounted in a rotating fixture insert of a 15-T superconducting magnet. Variable temperatures were provided by helium gas flowing through a heated copper block below the sample. A Minicircuits ZSC-2-1 signal splitter, used as a directional coupler, and a HP4194A gain-phase analyzer were used to measure the reflected signal from the resonant circuit, as shown in the inset to Fig. 1(a). As the sample was slowly cooled through the transition, the change in inductance resulted in a change in resonant frequency. The transition temperature was determined by the measurement of the reflected power as a function of temperature at a fixed frequency. The frequency was chosen at the steepest point on the amplitude-versus-frequency curve above the transition temperature. The field due to the measurement current is estimated to be $\simeq 3$ G; smaller current values only reduced the signal-to-noise ratio. Figures 1(a) and 1(b) show a selection of the curves of the reflected power versus temperature for both parallel and perpendicular orientation. Data were taken for both warming and cooling to verify that the sample and the thermometer were at the same temperature. Each curve represents $\simeq 2$–$3$ h of data taking depending on the temperature span required.

The transition temperature at a given field was determined by the construction shown in the figures. Although our technique for extracting $T_c$ is somewhat arbitrary, the transitions are well defined and broaden only slightly with increasing field; any reasonable technique will yield same values for $dH_{c2}/dT$. The temperatures were corrected for magnetoresistance with use of data from Sample, Brant, and Rubin,[8] the corrections

 

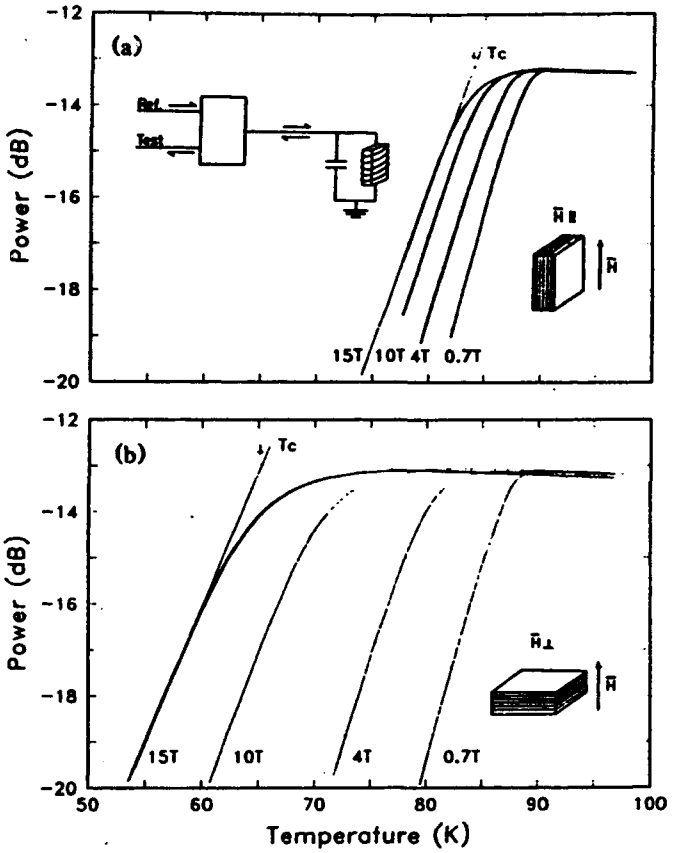


FIG. 1. Temperature dependence of the amplitude of the reflected signal from a resonant tank circuit with the $Y_1Ba_2Cu_3O_{7-x}$ crystal mounted with the Cu-O planes (a) parallel and (b) perpendicular to the applied field, for $H = 0.7$, 4, 10, and 15 T. The constructions indicate how $T_c$ at a given field was determined. Inset in (a): Schematic of the measurement apparatus.

amounting to $\simeq 1.5$ K at the highest field.

Figure 2 shows the temperature dependence of $H_{c2}$ for the Cu-O planes oriented parallel and perpendicular to the applied field. The zero-field transition temperature extrapolated from both the parallel and the perpendicular data is 88.8 K. The temperature dependence of $H_{c2}^{\parallel}$ is basically consistent with a straight line with a slope of $-2.3$ T/K, with the highest-field points possibly indicating some upward curvature. Extrapolation of the $H_{c2}^{\parallel}$ curve back to zero temperature according to the dirty-limit isotropic formula (with no Pauli paramagnetism limiting effects),[9] $H_c(0) = 0.69 T_c \, dH_c/dT$, gives $H_{c2}^{\parallel}(0) = 140$ T. {For a strongly anisotropic superconductor a more appropriate extrapolation might be linear [which would give $H_{c2}^{\parallel}(0) = 204$ T], and the correct extrapolation might be even higher than linear.} In contrast, the temperature dependence of the perpendicular field $H_{c2}^{\perp}$ shows a pronounced upward deviation from a linear dependence. Near $T_c$, $H_{c2}^{\perp}$ has a slope of $-0.46$ T/K, but below 78 K the data are consistent with a slope of $-0.71$ T/K. Extrapolating these two curves back to zero temperature using the isotropic dirty-limit formula,

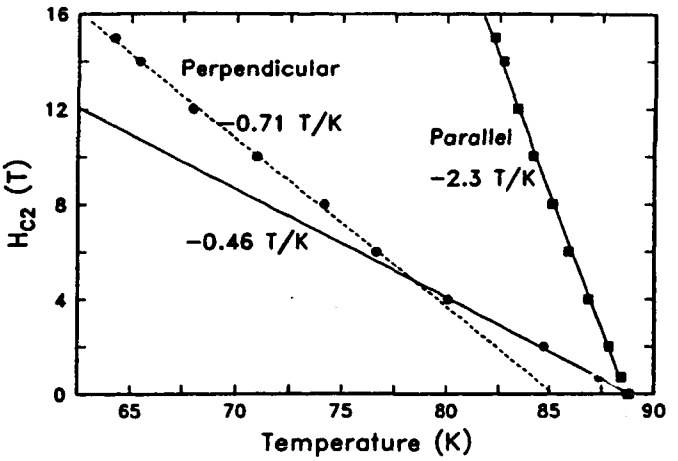


FIG. 2. Temperature dependence of the $H_{c2}$ for the $Y_1Ba_2Cu_3O_{7-x}$ crystal oriented with the Cu-O planes parallel and perpendicular to the applied field.

we get estimates for $H_{c2}^{\perp}(0)$ of 29 and 42 T.

Figure 3 shows the angular dependence of $dH_{c2}/dT$ for an applied field of 10 T. Here we define $dH_{c2}/dT$ as 10 T divided by the difference of the transition temperature at 10 T at a given angle and the zero-field transition temperature. The sharpness of the angular data near parallel orientation underscores the need for precise alignment of the sample. The two curves plotted in the figure are the angular dependences predicted for $H_{c2}$ at fixed temperature by the anisotropic Ginzburg-Landau theory,[10] $H_{c2}(\theta) = H_{c2}^{\perp}[\sin^2\theta + (m_{\perp}/m_{\parallel})\cos^2\theta]^{-1/2}$, for two values of $m_{\perp}/m_{\parallel}$. The value which fits the end points results in a curve that does not fit the data near the peak, and a value which fits the data near the peak results in a curve that is significantly below the data at

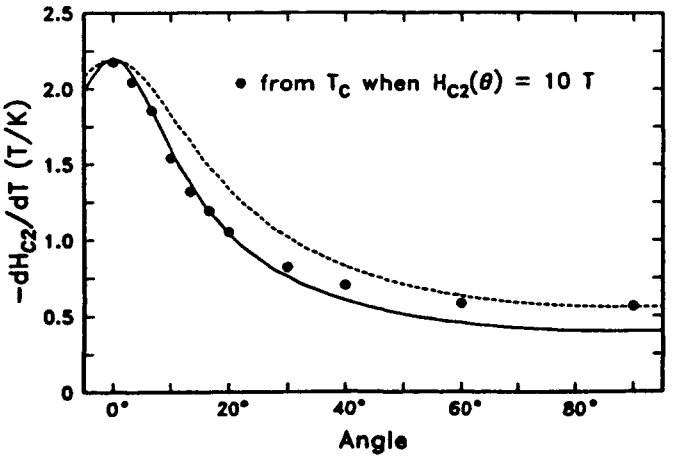


FIG. 3. Dependence of $dH_{c2}/dT$ on angle between the Cu-O planes and the applied field as calculated from data taken at 10 T. The two curves are the angular dependences predicted by the anisotropic Ginzburg-Landau theory for two sets of anisotropy parameters.

large angles. The deviation of the data from the latter theoretical curve would be significantly less if there were no break in the slope of $H_{c2}^{\perp}$ at $\simeq$78 K.

We looked for, but did not observe, any change in the transition temperature for rotations of 0°, 45°, and 90° in the *a-b* plane in a field of 10 T. We believe that we would have seen an anisotropy in our crystal if it were as large as the $\simeq$1-K change reported by Hidaka *et al.*[5] for their resistive measurements on single-crystal $Y_1Ba_2Cu_3O_{7-x}$ with a 70-K transition temperature. Iye *et al.*[6] likewise did not observe any *a-b* anisotropy in their resistive measurements on a $\simeq$90-K $Y_1Ba_2Cu_3O_{7-x}$ crystal.

Our results do not show any of the curvature near $T_c$ that was evident in the resistive measurements of $dH_{c2}/dt$ by Hidaka *et al.*[2] and Iye *et al.*[6] on single-crystal $Y_1Ba_2Cu_3O_{7-x}$ and in previous resistive measurements on $La_{2-x}Ba_xCuO_4$ by Shamoto, Onoda, and Sato[4] and Hidaka *et al.*[5] The resistive measurements are made by passing currents along the Cu-O planes and necessarily involve currents flowing on many planes. We know from our earlier work[3] that the critical currents at high temperature and fields between the planes are very small. These low critical currents and the possibility of damaged surface layers could be complicating the determination of $H_{c2}$ from resistive measurements.

Our measured values for some of the anisotropic parameters of $Y_1Ba_2Cu_3O_{7-x}$ are given in Table I along with various derived quantities. The coherence length in the Cu-O plane, $\xi_0$, is calculated from the estimate of $H_{c2}^{\perp}(0) = 29$ T and the relation[10] $H_{c2}^{\perp}(0) = \phi_0/2\pi\xi_0^2$. The ratio of $H_{c2}^{\parallel}/H_{c2}^{\perp} = \xi_z/\xi_0$ results in $\xi_z = 7$ Å. The coherence length perpendicular to the Cu-O layers, $\xi_z$, is significantly greater than the spacing between the Cu-O layers, 3.9 Å, indicating that although the superconductivity is strongly anisotropic, it remains three dimensional in nature down to very low temperatures. According to the Josephson-coupled layer model, the crossover to two-dimensional behavior is expected when $\xi_z = s/\sqrt{2} = 2.8$ Å, where $s$ is the Cu-O interplanar spacing.[11] The measurements of Freitas, Tsuei, and Plaskett[12] showed that the fluctuations near $T_c$ were also three dimensional in nature. $H_{c1}^{\perp}$ was used to calculate the penetration depth in the Cu-O planes, $\lambda_0$, from the relation $H_{c1}^{\parallel} = (\phi_0/4\pi\lambda_0^2)\ln(\lambda_0/\xi_0)$. From the penetration depth and $H_{c2}^{\perp}$ we calculate $H_c(0) = H_{c2}^{\perp}/\sqrt{2}\kappa_0$, where $\kappa_0 = \lambda_0/\xi_0$. The values for $\kappa_z$ and $\lambda_z$ are calculated from[13] $\kappa_z = (m_{\parallel}/m_{\perp})\kappa_0$ and $\kappa_z = (\lambda_z\lambda_0/\xi_z\xi_0)^{1/2}$. For these calculations we have used the anisotropy ratio given by the temperature dependence of $H_{c2}$ near $T_c$ and the dirty-limit isotropic relationship between the high-temperature data and the low-temperature parameters. Obviously, use of the larger anisotropy observed for $H_{c1}$ would alter the numerical results as would the use of extrapolations other than the conventional isotropic dirty-limit relationship.

TABLE I. Measured and derived anisotropic parameters for single-crystal $Y_1Ba_2Cu_3O_{7-x}$. Parallel and perpendicular refer to the direction of the field applied relative to the copper-oxygen planes. For the case of $J_c$, the currents are actually flowing perpendicular to the applied field.

| | Parallel | Perpendicular |
|---|---|---|
| | Measured parameters | |
| $T_c$ | 88.8 K | |
| $(dH_{c2}/dT)(T_c)$ | 2.3 T/K | 0.46 T/K |
| $H_{c1}(4.5\text{K})$ | $\leq$0.005 T | 0.5 T |
| $J_c(0\text{ T}, 4.5\text{ K})$ | $1.6\times10^5$ A/cm$^2$ | $3.2\times10^6$ A/cm$^2$ |
| | Derived parameters | |
| $H_{c2}(0)$ | 140 T | 29 T |
| $\xi(0)$ | $\xi_z = 7$ Å | $\xi_0 = 34$ Å |
| $H_c(0)$ | 2.7 T | |
| $\lambda_{GL}(0)$ | $\lambda_z = 1250$ Å | $\lambda_0 = 260$ Å |
| $\kappa$ | $\kappa_z = 37$ | $\kappa_0 = 7.6$ |

We next consider to what extent the anisotropic properties of $Y_1Ba_2Cu_3O_{7-x}$ can be understood in terms of existing theories. Above 78 K, the linearity of our data indicates agreement with anisotropic Ginzburg-Landau theory. Our experimental results indicate $H_{c2}$ anisotropies of 5:1 near $T_c$ and $H_{c1}$ anisotropies of at least 1:10 at low temperatures. Existing theories cannot account for the greater anisotropy measured in $H_{c1}$. Lawrence and Doniach's results[10] for $H_{c1}$ anisotropy according to both an anisotropic Ginzburg-Landau formulation and a Josephson-coupled layered superconductor model indicate that the anisotropy of $H_{c1}$ should be reciprocal to that of $H_{c2}$ and smaller in magnitude. Kogan and Clem[14] and Kogan[15] and, recently, Balatskii, Burlachkov, and Gor'kov[16] calculate that the anisotropy in $H_{c1}$ should be exactly reciprocal to the $H_{c2}$ anisotropy. If these relationships remain valid down to low temperatures, the larger anisotropy we observe for $H_{c1}$ at low temperatures indicates that the $H_{c2}$ anisotropy at low temperature must be larger than it is near $T_c$. The Klemm-Luther-Beasley[11] extensions of the Josephson-coupled layer model indicate that pronounced upward curvature in $H_{c2}^{\parallel}$ (and therefore an increase in anisotropy) can occur in layered systems when the coherence length, $\xi_z$, becomes small enough that vortex cores fit between the layers. This behavior has been seen in a number of intercalated layered superconductors. While this theory does provide a mechanisms to explain an increase of anisotropy with lowering temperature, our estimates indicate that the vortex core size does not shrink small enough with decreasing temperature to force a crossover to two-dimensional behavior and thus an increase in anisotropy. Some other mechanism is necessary to cause an increase of $H_{c2}^{\parallel}$ and anisotropy. A break in the temperature dependence of $H_{c2}^{\perp}$, like that at 78 K, is not predicted by either the anisotropic Ginzburg-Landau theory

or the Josephson-coupled layered theory. One possible cause for this behavior could be a complicated Fermi surface as described by Dalrymple and Prober[7] for $Nb_{1-x}Ta_xSe_2$. Another possible explanation could be a transition from *d*-wave coupling to a combination of *s*- and *d*-wave coupling as has been suggested by Kotliar.[17]

In conclusion, we have established from upper-critical-field data that the high-temperature superconductivity in $Y_1Ba_2Cu_3O_{7-x}$ is three dimensional in nature and in accord with the expectations of anisotropic Ginzburg-Landau theory. The strong anisotropy (5:1) is associated with the Cu-O planes. The larger anisotropy measured for the lower critical field and the temperature dependence of the upper critical field at lower temperatures indicate that, at least, elaborations of the simplest theoretical models for anisotropic superconductors are needed to describe $Y_1Ba_2Cu_3O_{7-x}$ at lower temperatures.

This work was supported in part by the U.S. Office of Naval Research under Contract No. N00014-85-C-0361. We thank S. J. LaPlaca, P. M. Horn, and D. Keane for single-crystal x-ray results, K. F. Etzold for help with the high-frequency measurements, T. P. Smith and J. J. Nocera for help with the high-field measurements, R. L. Greene for helpful discussions, and S. Foner for advise on high-field measurements.

[1]J. G. Bednorz and K. A. Müller, Z. Phys. B **64**, 189 (1986).

[2]Y. Hidaka, Y. Enomoto, M. Suzuki, M. Oda, and T. Murakami, Jpn. J. Appl. Phys. Part 2 **26**, L377 (1987).

[3]T. R. Dinger, T. K. Worthington, W. J. Gallagher, and R. L. Sandstrom, Phys. Rev. Lett. **58**, 2687 (1987).

[4]S. Shamoto, M. Onoda, and M. Sato, to be published.

[5]Y. Hidaka, Y. Enomoto, M. Suzuki, M. Oda, A. Katsui, and T. Murakami, Jpn. J. Appl. Phys. Part 2 **26**, L726 (1987).

[6]Y. Iye, T. Tamegai, H. Takeya, and H. Takei, Jpn. J. Appl. Phys. Part 2 **26**, L1057 (1987).

[7]B. J. Dalrymple and D. E. Prober, J. Low Temp. Phys. **56**, 545 (1984).

[8]H. H. Sample, B. L. Brant, and L. G. Rubin, Rev. Sci. Instrum. **53**, 1129 (1982).

[9]N. R. Werthamer, E. Helfand, and P. C. Hohenberg, Phys. Rev. **147**, 295 (1966).

[10]W. E. Lawrence and S. Doniach, in *Proceedings of the Twelfth International Conference on Low Temperature Physics, Kyoto, 1970,* edited by E. Kanda (Keigaku, Tokyo, 1971), p. 361.

[11]R. A. Klemm, A. Luther, and M. R. Beasley, Phys. Rev. B **12**, 877 (1975).

[12]P. P. Freitas, C. C. Tsuei, and T. S. Plaskett, Phys. Rev. B **36**, 833 (1987).

[13]P. deTrey, S. Gygax, and J.-P. Jan, J. Low Temp. Phys. **11**, 421 (1973).

[14]V. G. Kogan and J. R. Clem, Phys. Rev. B **24**, 2497 (1981).

[15]V. G. Kogan, Phys. Rev. B **24**, 1572 (1981).

[16]A. V. Balatskii, L. I. Burlachkov, and L. P. Gor'kov, Zh. Eksp. Teor. Fiz. **90**, 111 (1986) [Sov. Phys. JETP **63**, 866 (1986)].

[17]G. Kotliar, to be published.

# Field-effect conductance of $YBa_2Cu_3O_6$

A. Levy, J. P. Falck, and M. A. Kastner
*Department of Physics, Massachusetts Institute of Technology, Cambridge, Massachusetts 02139*

W. J. Gallagher, A. Gupta, and A. W. Kleinsasser
*IBM Thomas J. Watson Research Center, Yorktown Heights, New York 10598*

8

(Received 15 October 1990; accepted for publication 14 January 1991)

Metal-insulator-semiconductor field effect transistors have been fabricated using laser ablation to deposit YBaCuO thin films onto $SrTiO_3$, MgO, $LaAlO_3$, and $LaGaO_3$ substrates. The substrates were used as gate insulators. The conductivity of two films on $SrTiO_3$ could be modulated, while for other samples the conductivity was independent of the gate voltage. The field-effect mobility was extracted and found to be of magnitude comparable to the mobility of metallic $YBa_2Cu_3O_7$.

The high $T_c$ superconductors can be viewed as degenerately doped versions of progenitors that are antiferromagnetic semiconductors.[1] The high charge carrier density required for superconductivity is usually achieved by doping, but one might hope to induce this density with an electric field, as is done in field effect transistors for conventional semiconductors like Si. Indeed, because the latter method induces the carriers without the concomitant disorder due to charged impurities, the density of carriers required for superconductivity may be lower when induced electronically rather than chemically.[2]

A three terminal metal-insulator-semiconductor field effect transistor (MISFET) that is superconducting in its high conductance state might be valuable technologically. Fabrication and measurement of such a MISFET was first reported using the In/InO system.[3] Recently a measurement of a MIS capacitor using MgO as the insulator and YBaCuO as the semiconductor was reported.[4] We describe here the characteristics of a MISFET in which the semiconductor is $YBa_2Cu_3O_6$. As the insulator we have tested $SrTiO_3$, MgO, $LaAlO_3$, and $LaGaO_3$. We find evidence that, as for conventional semiconductors, the properties of the MISFET are sensitive to the nature of the insulator-semiconductor interface.

Figure 1 shows a schematic diagram of the structure used for these studies. Epitaxial thin films of $YBa_2Cu_3O_7$ 3000 Å thick were deposited on (100)-oriented insulators using the laser ablation technique.[5] The latter yields smooth films with the $c$-axis oriented perpendicular to the interface, which display a sharp superconducting transition at 90 K. Before the deposition of the film the substrates were rinsed in acetone and methanol. Ar ion milling was used to define isolated rectangles of $YBa_2Cu_3O_7$ with dimensions $1\times0.7$ mm. Sputtered gold contacts were then patterned by standard photolithographic techniques. On top of each substrate typically 20 structures were thus prepared. The final fabrication step was to anneal the sample at 500 °C in an Ar flow for 2 h. After annealing the YBaCuO film was semiconducting, presumably having composition $YBa_2Cu_3O_{5.85}$.[6] Applying silver paint to the back of the substrate allowed the oxide substrates to be used as gate insulators.

The sample was placed in a variable temperature cryostat, and the conductivity was measured as a function of the gate voltage at various temperatures. For several samples the leakage current between the gate electrode and the four resistance probes was large at the higher temperatures, so the resistance was measured with an ac technique while the dc voltage on the gate was swept continuously. An ac voltage at 100 Hz was applied between two of the electrodes and the current was determined by measuring the voltage across a load resistor in series with these electrodes. The resistance was determined by dividing the voltage across the other two electrodes by the current, as indicated in Fig. 1. Both voltages were measured with a lock-in amplifier. We found that when the contacts were blocking, large phase shifts appeared between the voltage and current in such a measurement. For the data presented here such phase shifts were very small, indicating that the contact resistance was smaller than that of the sample. The applied voltage was kept low enough that the four-probe current was proportional to the four-probe voltage.

For most samples the conductivity of the YBaCuO film was independent of gate voltage indicating a high density of interface or bulk localized states. However two films, for which $SrTiO_3$ was used as gate insulator, displayed a modulation of the conductivity when a gate voltage was applied. In the following we discuss results for these samples.

The voltages required by the large thickness, 0.635 mm, of the insulator are somewhat reduced by its large dielectric constant, $\varepsilon = 330$ at 300 K. However, $SrTiO_3$ undergoes a variety of structural phase transitions and exhibits ferroelectricity below 110 K, making the field-effect experiments more complicated at these temperatures. Therefore, most of the measurements were made between 130 and 300 K.

Results of the measurements for one of our field-effect structures are presented in Fig. 2. The conductance per square is given in units of the quantum of conductance, $e^2/h$. At room temperature, the conductance increases for both polarities of the gate voltage. This result is not fully understood, but most likely is due to the high leakage currents discussed above. On the other hand, below 250 K the leakage current is smaller than the measuring current, and

 0021-8979/91/084439-03$03.00  

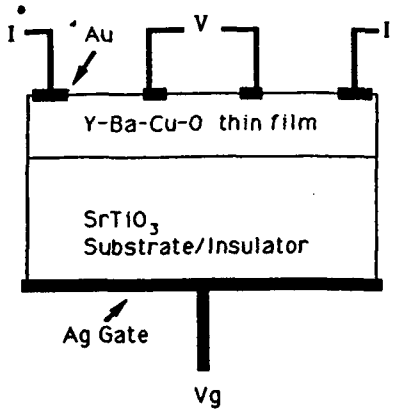


FIG. 1. Schematic cross section of the metal-insulator-semiconductor field effect transistor. The YBaCuO film was reduced to make it a semiconductor.

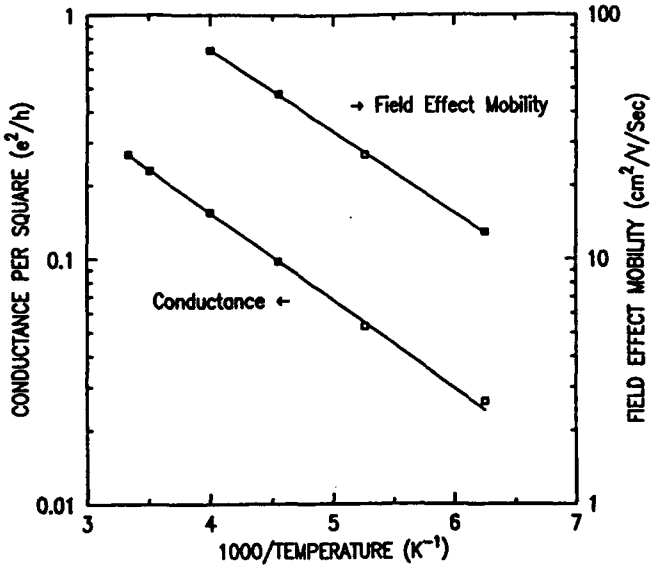


FIG. 3. The logarithm of the zero bias conductance and the field-effect mobility as functions of temperature.

the behavior is quite asymmetric. When holes are added to the semiconductor the conductance increases dramatically, whereas, when electrons are added the conductance is constant to within experimental error. This is consistent with the hole-type conduction characteristic of YBaCuO.

It is clear from Fig. 2 that both the field induced excess conductance and the zero-gate-voltage conductance increase with increasing temperature. To compare the dependencies of these two quantities in a meaningful way, we have calculated the field-effect mobility at the gate voltage for which $1.1\times10^{12}$ cm$^{-2}$ holes are accumulated ($V_g = 200$ V at 250 K) for each temperature. We have used literature values of the temperature-dependent dielectric constant of $SrTiO_3$ to calculate the field induced carrier density.[7] The field-effect mobility and the $V_g = 0$ conductance are plotted logarithmically against $T^{-1}$ in Fig. 3.

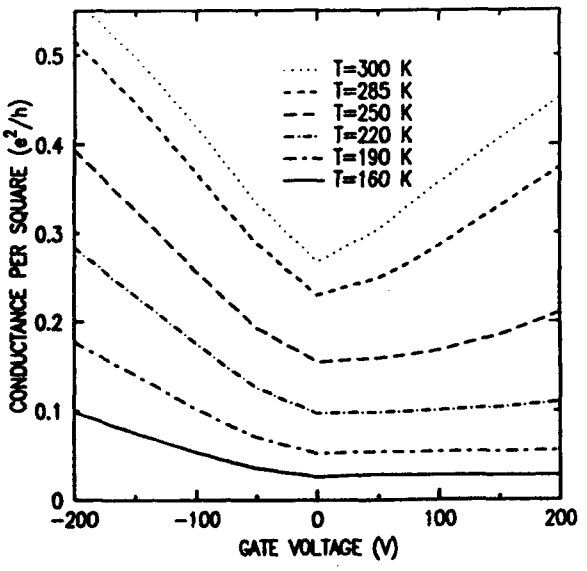


FIG. 2. Conductance per square in units of $e^2/h$ as function of gate voltage for different temperatures.

Two encouraging observations can be made from Figs. 2 and 3. The first is that the field-effect mobility is very large. At 250 K we find $\mu_{FE} = 70$ cm$^2$/V s. This is very high, considering that it is a lower bound on the true carrier mobility, because carriers trapped in surface or bulk localized states do not contribute to the mobility. Despite this, the mobility is nearly as large as values found in the normal state of superconducting $YBa_2Cu_3O_7$ from field effect[8] and Hall measurements.[9]

The second promising feature is that the induced conductance per square is close to $e^2/h$. Experiments on $La_{2-x}Sr_xCuO_{4+y}$ with hole concentrations from $5\times10^{-4}$ to 0.2 of the Cu atom density[1] and thin metal films[10] show that when the conductance per square per CuO layer exceeds a few $e^2/h$, superconductivity appears. Since the accumulation layer is expected to be only a few $CuO_2$ layers thick, our transistors have nearly the carrier density necessary for superconductivity.

However, the temperature-dependent field effect shows that our accumulation layers are not metallic but semiconducting. Indeed, the temperature dependence in Fig. 3 requires further explanation. Fitting the data in Fig. 3 to straight lines one finds activation energies of 71 meV for the zero-gate-voltage conductance and 67 meV for the mobility. Such behavior is often found when the Fermi level $E_F$ lies in a high density of localized states, as in, for example, amorphous semiconductors.[11,12] Indeed, the behavior of our samples is consistent with there being a high density of localized states at $E_F$, as we now elaborate.

For ease of discussion, we discuss the case of electrons rather then holes. If $E_F$ lies in a high density of localized states, additional electrons induced by the gate will, for the most part, occupy those states. The Fermi level will rise because of this extra charge, by $\Delta E_F$, but at zero temperature this will give no increase in conductance because the

extra carriers are localized. However, at finite temperature, a small fraction of the carriers will be thermally excited to the mobility edge $E_C$ in the conduction band. This fraction is proportional to $\exp[-(E_C - E_F)/kT]$ and the increase of $\Delta E_F$ will therefore cause a fractional increase in the conductivity $(\Delta G/G)$ of $[\exp(\Delta E_F/kT) - 1]$.

If the bands are flat at zero bias, the increase in $E_F$ occurs only in the accumulation region, of width $x$ much less than the film thickness $d$, and one predicts a change in the film conductance $G$ (proportional to $\mu_{FE}$) given by:

$$\frac{\Delta G}{G} \approx \frac{x}{d}[\exp(\Delta E_f/kT) - 1]. \quad (1)$$

If $\Delta E_F < kT$ then $\Delta G$ has almost the same temperature dependence as $G$. In this case, $\Delta G/G \ll 1$ because $x/d \ll 1$. However, we observe the same temperature dependence for $\Delta G$ and $G$ even though $\Delta G \approx G$. One explanation is that, for those films that show the field effect, the surface is already in accumulation for zero gate voltage. In that case the conductance at zero bias is dominated by the accumulation layer and the factor $x/d$ does not appear in Eq. (1).

To explain why the bias that gives depletion does not *reduce* the conductance (see Fig. 2) one must then postulate a high density of states just below $E_F$. We estimate that a density of bulk states greater than $10^{19}\ \mathrm{cm}^{-3}\ \mathrm{eV}^{-1}$ or of surface states greater than $10^{13}\ \mathrm{cm}^{-2}\ \mathrm{eV}^{-1}$ would be necessary to explain the observation. If such a high density of bulk states were present one would probably not observe a field effect in any film. That we see the effect only for a subset of samples is consistent with the idea that there is a high density of surface states which is sometimes chemically compensated.

In summary, we have fabricated metal-insulator-YBCuO field-effect transistors, and in two of the samples for which SrTiO was used as the insulator we have been able to modulate the conductivity. We have found that the field-effect mobility is temperature dependent, and we have concluded that in the reduced YBaCuO film the Fermi energy was located near a high density of localized states, probably surface states, that prevent easy depletion.

One of us (M.A.K) acknowledges stimulating discussions with R. J. Birgeneau. This work was conducted under the auspices of the Consortium for Superconducting Electronics with partial support by the Defence Advanced Research Projects Agency (Contract No. MDA972-90-C-0021). The work at IBM was also supported in part by ONR Contract No. N00014-85-C-0361.

[1] N. W. Preyer, R. J. Birgeneau, C. Y. Chen, D. R. Gabbe, H. P. Jenssen, M. A. Kastner, P. J. Picone, and T. Thio, Phys. Rev. B 39, 11563 (1989); N. W. Preyer, R. J. Birgeneau, A. Cassanho, C. Y. Chen, D. R. Gabbe, H. P. Jenssen, M. A. Kastner, P. J. Picone, and T. Thio, Physica C 162, 1003 (1989).
[2] S. A. Brazovski and V. Yakovenko, Phys. Lett. A 132, 290 (1988).
[3] A. T. Fiory and A. F. Hebard, Physica 135B, 124 (1985).
[4] U. Kabasawa, K. Asano, and T. Kobayashi, J. Appl. Phys. 29, L86 (1990).
[5] G. Koren, A. Gupta, E. Giess, A. Segmuller, and R. B. Laibowitz, Appl. Phys. Lett. 54, 1054 (1989).
[6] G. Koren, A. Gupta, and A. Segmuller, Physica C 162-164, 1021 (1989).
[7] R. C. Neville, B. Hoeneisen, and C. A. Mead, J. Appl. Phys. 5, 2124 (1972).
[8] A. T. Fiory, A. F. Hebard, P. M. Mankiewich, R. Howard, and M. L. O'Malley, Bull. Am. Phys. Soc. 35, 786 (1990).
[9] H. L. Stormer, A. F. J. Levi, K. W. Baldwin, M. Anzlowar, and G. S. Boebinger, Phys. Rev. B 38, 2472 (1988).
[10] H. M. Jager, D. B. Haviland, B. G. Orr, and A. M. Goldman, Phys. Rev. B 40, 182 (1989).
[11] M. A. Kastner and H. Fritzsche, Mater. Res. Bull. 5, 631 (1970).
[12] G. W. Neudeck and A. K. Malhotra, J. Appl. Phys. 46, 2662 (1975).

# Chemical and electrical properties of interfaces between deposited insulators and $La_2CuO_4$

A. Levy, M. J. Lercel, J. P. Falck, and M. A. Kastner
*Department of Physics, Massachusetts Institute of Technology, Cambridge, Massachusetts 02139*

A. A. Bright and A. W. Kleinsasser
*IBM Thomas J. Watson Research Center, Yorktown Heights, New York 10598*

(Received 22 August 1991; accepted for publication 11 November 1991)

Metal-insulator-semiconductor capacitors have been fabricated using plasma enhanced chemical vapor deposition of $Si_3N_4$ and $SiO_2$ insulators on $La_2CuO_4$ semiconducting single crystals. Auger electron spectroscopy was used to characterize the insulator-semiconductor interface after annealing at several temperatures. Copper segregation and oxygen out-diffusion were observed and the $Si_3N_4$-semiconductor interface was found to be more stable than the $SiO_2$-semiconductor one.

## I. INTRODUCTION

An unusual feature of the high-temperature copper-oxide superconductors is the proximity of the superconducting phase to an antiferromagnetic insulating phase.[1] One reaches this insulating state in $YBa_2Cu_3O_7$, for example, by reducing the material, thus lowering the charge carrier (hole) density. This has led to the suggestion that an externally applied electric field might be used instead of chemical modification to change the hole concentration.[2] Several groups[3–6] have attempted to drive YBaCuO from the superconducting to the insulating state. We previously reported[7] efforts to do the opposite. Such a superconducting field effect transistor (SUFET) might be technologically valuable, and it would certainly open new avenues of scientific inquiry.

The efficacy of this approach depends sensitively on the properties of the interface between the superconductor and the insulator across which the field is applied. In this article we report results of a study of the interface between $La_2CuO_4$, which becomes a superconductor with $T_c \sim 40$ K when doped with Sr, and two insulators that are used in conventional semiconductor processing, $Si_3N_4$ and $SiO_2$. While crucial to assessing the feasibility of SUFETs, such studies are expected to be valuable, as well, for the future fabrication of multilayer superconductor-insulator-superconductor structures and integrated superconductor-semiconductor devices.

We have fabricated metal-insulator-semiconductor structures by depositing $Si_3N_4$ and $SiO_2$ insulators on semiconducting $La_2CuO_4$ single crystals using plasma enhanced chemical vapor deposition (PECVD). These structures have been annealed at temperatures between 200 °C and 900 °C in vacuum or Ar gas. After each annealing step, an Auger depth profile was taken to characterize the interface between the $La_2CuO_4$ crystal and the insulator. We found that even at very low annealing temperatures the interface is oxygen poor and copper rich. At higher annealing temperatures (above 800 °C) the lanthanum oxide phase separates near the interface. These effects are much more severe for the $SiO_2$ insulator than for $Si_3N_4$.

## II. EXPERIMENT

The single crystals of $La_2CuO_4$ used in this study were grown by the top seeded solution method in CuO flux. Laue x-ray diffraction was used to align the surface of the crystals parallel to the copper oxide planes (perpendicular to the $b$ axis in orthorhombic notation, space group Cmca). Details of the crystal growth technique have been previously published.[8]

In order to minimize the carrier density the $La_2CuO_{4+\delta}$ crystals were annealed in vacuum at 900 °C for 30 min. Magnetic susceptibility measurements showed that the Néel temperature was 322 K, verifying that the carrier density is less than $\sim 10^{18}$ cm$^{-3}$ or 0.01% of the Cu atom density.[1] After annealing, the crystals were polished to an optically smooth surface and then etched with a solution of 1% Br in methanol for 10 min to remove surface damage resulting from the annealing and polishing.

The $SiO_2$ and $Si_3N_4$ layers were deposited by PECVD to a thickness of approximately 700 Å as measured by ellipsometry. The PECVD parameters are shown in Table I. The dielectric constants for $La_2CuO_{4+\delta}$ have been found[9] to be $\epsilon_1 = 5$ and $\epsilon_2 = 2$ at the wavelength of 6238 Å, used for the ellipsometry. A zero-bias capacitance measurement of the $Si_3N_4$ sample indicates an insulator thickness of 750 Å using low frequency $\epsilon_l = 6$. The 50 Å difference between the ellipsometry and the capacitance thickness estimates may be due to effects of the excess oxygen in the sample of Ref. 9 on the dielectric constant.

Various surface treatments before the insulator deposition were tested in addition to the Br etching discussed above, including ion milling and helium plasma precleaning. These did not alter the results significantly. Annealing of the insulator-semiconductor structures in either vacuum, at a pressure of roughly $1 \times 10^{-6}$ Torr, or in 1500 sccm argon flow, gave the same results.

The Auger electron spectroscopy (AES) was done using a Physical Electronics model 660 Auger spectrometer with a primary beam energy of 5 keV, a primary beam current of 60 nA, and a beam raster of 2 $\mu$m $\times$ 2 $\mu$m. An incident $AR^+$ beam was used for ion milling. The ion-milling time was related to depth using a Dektak profilo-

 0021-8979/92/041764-04$04.00  

TABLE I. PECVD deposition parameters of $SiO_2$ and $Si_3N_4$.

| | |
|---|---|
| (a) $SiO_2$ | |
| Equipment | |
| $SiH_4$/He (2%) flow | 200 sccm |
| NO flow | 1000 sccm |
| He flow | 1400 sccm |
| Power | 200 W |
| Pressure | 500 mTorr |
| (b) $Si_3N_4$ | |
| $SiH_4$/He (2%) flow | 400 sccm |
| $N_2$ flow | 800 sccm |
| He flow | 1400 sccm |
| Power | 200 W |
| Pressure | 1.0 Torr |

meter to determine the milling rate of 250 Å/min for $La_2CuO_4$ and 700 Å/min for $SiO_2$ and $Si_3N_4$.

## III. RESULTS AND DISCUSSION

### A. Silicon dioxide

As a control sample, an Auger depth profile was taken for a $La_2CuO_4$ crystal after it had been reduced, polished, and etched in bromine, with no deposited insulator. This sample displayed an abrupt surface for which the concentrations of La, Cu, and O are constant for depths greater than about 20 Å. Since the depositions of the $SiO_2$ and $Si_3N_4$ were done at temperatures of 200 °C and 350 °C we will refer to such samples, which underwent no further annealing, as though the crystal were annealed at the deposition temperatures. In Fig. 1 we show the AES atomic concentration profiles of interfaces of $La_2CuO_4$-$SiO_2$ annealed at temperatures from 200 °C to 900 °C.

For the 200 °C anneal, the concentrations of copper and lanthanum rise monotonically at the insulator-crystal interface and there is no sign of chemical inhomogeneity. The copper signal rises about 10 Å ahead of the lanthanum, as expected, due to the higher energy of the copper Auger electrons. However, at higher annealing temperatures, a peak in the copper concentration starts to develop beneath the interface. The height of this peak (corresponding to the segregating copper) increases with increasing annealing temperature, and the peak is pushed backward from the $SiO_2$ interface (Table II).

For annealing temperatures of 800 °C and lower, the peak is approximately at the interface. However, for the 900 °C anneal, the copper peak is pushed back from the interface by approximately 400 Å (Table II). In this case, lanthanum oxide is formed at the interface, probably in the form of $La_2O_3$, as indicated by the relative intensities of the La and O Auger peaks. The copper peak is also very broad. This may result from surface roughness caused by the phase separation.

The AES spectra, in addition to the profiles, can be used to further characterize the interface. In Fig. 2 we present the Auger electron energy spectra, in the vicinity of the oxygen peak, as a function of the ion-milling cycle for the 900 °C annealed sample. When the sample is annealed at temperatures lower than 800 °C (not shown) the oxygen

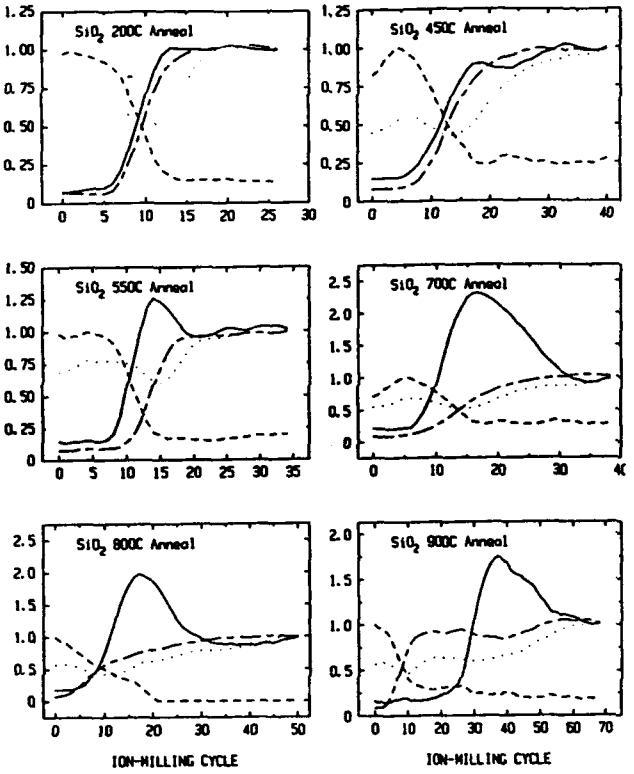


FIG. 1. AES atomic concentration (arbitrary units) as function of the ion-milling cycle number of $SiO_2$-$La_2CuO_4$ interfaces at several annealing temperatures for copper(——), lanthanum(— · —), oxygen(·····), and silicon (– – –).

peak shifts in energy by 7.0±0.3 eV in going from the environment of the $SiO_2$ layer to the $La_2CuO_4$. In the samples annealed at higher temperatures, the oxygen shows two shifts as seen in Fig. 2. First, the shift is 5.8±0.5 eV for the transition from the $SiO_2$ to the $La_2O_3$, and second, the shift is 1.2±0.5 eV from the $La_2O_3$ to the $La_2CuO_4$. The total shift in this sample is then 7.0±0.5 eV which matches the shift in the lower-temperature annealed sample. In addition, the lower-temperature samples display a rapid change in oxygen peak position compared to the very gradual transition (which indicates a smeared interface) from $SiO_2$ to $La_2O_3$ and then to $La_2CuO_4$ seen in the higher-temperature annealed samples.

In all the samples, the oxygen is depleted at the surface. This is seen, in Fig. 1, as a dip in the oxygen concen-

TABLE II. Copper peak width and depth relative to the $SiO_2$/$La_2CuO_4$ interface.

| Annealing temp (°C) | Peak width (Å) | Peak decrease from $SiO_2$/$La_2CuO_4$ interface (Å) |
|---|---|---|
| 200 | 130 | 30 |
| 450 | 230 | 31 |
| 550 | 180 | 39 |
| 700 | 315 | 37 |
| 800 | 400 | 70 |
| 900 | 1580 | 400 |

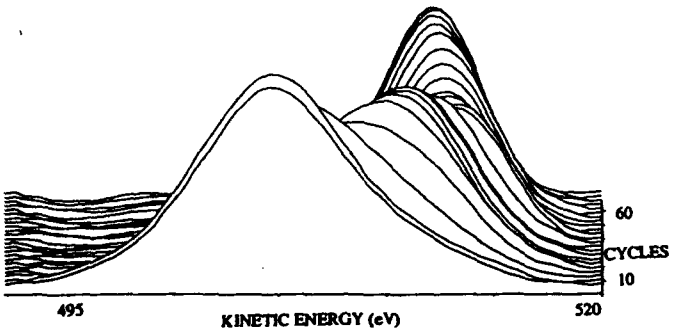


FIG. 2. Oxygen AES as function of the ion-milling cycle for the 900 °C annealed sample.

tration near the interface. Since the crystal was fully reduced before processing (there was no excess oxygen), a probable explanation for the oxygen depletion is that during the deposition process, oxygen was pulled out of the crystal by excess silicon in the insulator layer. This loss of oxygen may destabilize the crystal chemically; this, in turn, may be the reason why the material separates into other components, probably $La_2O_3$ and oxides of Cu at high temperature. Grain boundary diffusion, as was seen in other studies[10,11] on $YBa_2Cu_3O_7$ films, is most likely not the cause for the loss of oxygen near the surface of $La_2CuO_4$ single crystals. A different explanation, preferential ion milling of oxygen in the $La_2CuO_4$, was ruled out using the control sample.

### B. Silicon nitride

The AES atomic concentration profiles of the $La_2CuO_4$-$Si_3N_4$ interfaces are shown in Fig. 3. Again, the copper and lanthanum concentrations rise monotonically for the low-temperature annealed samples. The sample annealed at 500 °C shows a copper peak similar to that seen in the $SiO_2$-coated samples but much smaller in both height and depth.

As for the $SiO_2$ covered sample, the oxygen concentration is depleted at the surface, as seen especially in the sample annealed at 500 °C. Again, the silicon in the $Si_3N_4$ layer may extract oxygen, and this might cause instability at high temperature. However, the interface is more abrupt than with $SiO_2$ and there is less oxygen diffusion out of the $La_2CuO_4$ and less copper segregation on the surface. In general, it seems that the $Si_3N_4$-$La_2CuO_4$ interface is more thermally stable than the $SiO_2$-$La_2CuO_4$ interface.

The nitride-coated sample annealed at 500 °C showed significant asymmetry in capacitance versus voltage ($C$-$V$) measurements, indicating charge depletion in the $La_2CuO_4$ crystal. This signal was reproducible for different frequencies and sweep directions and displayed no hysteresis. Figure 4 shows the 1 kHz $C$-$V$ curve for this sample at room temperature. Fitting this graph with the usual Schottky screening model gives an acceptor density of $N=4\times10^{17}$ $cm^{-3}$. Previous measurements of $La_2CuO_4$ charge carrier densities using Hall effect give a density of about $8\times10^{18}$

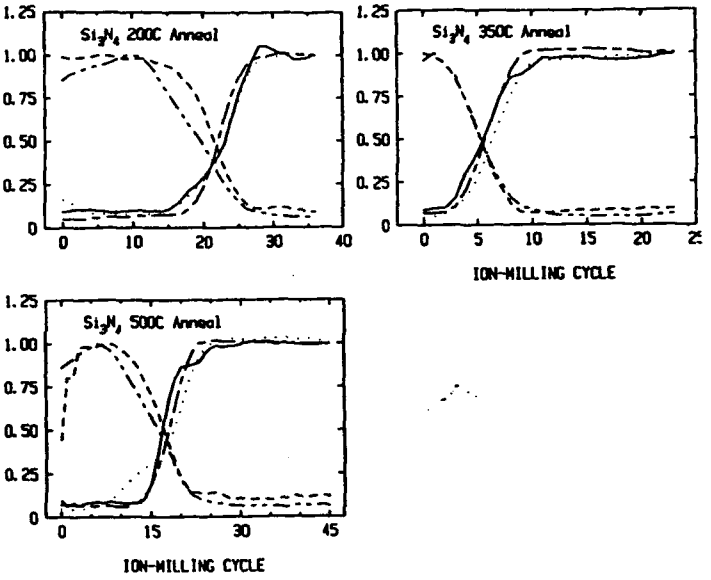


FIG. 3. AES atomic concentration (arbitrary units) as function of the ion-milling cycle number of $Si_3N_4$-$La_2CuO_4$ interfaces at several annealing temperatures for copper(——), lanthanum(— - —), nitrogen(- - -), oxygen(·····), and silicon(——).

$cm^{-1}$ for a crystal with a 310 K Néel temperature. For the fully reduced crystal ($T_N=322$ K) the carrier density should be lower, consistent with the capacitance measurement. Since the depth of the depletion layer is much larger than the surface damage caused by annealing we conclude that most of the depleted carriers are in an approximately stoichiometric $La_2CuO_4$ crystal.

The effective resistance of the coated sample displayed a significant asymmetry as well, which cannot be explained by a standard Schottky depletion. This asymmetry may be due to states in the band gap of the insulator. These states can be attributed to dopants of $Si_3N_4$ such as oxygen dif-

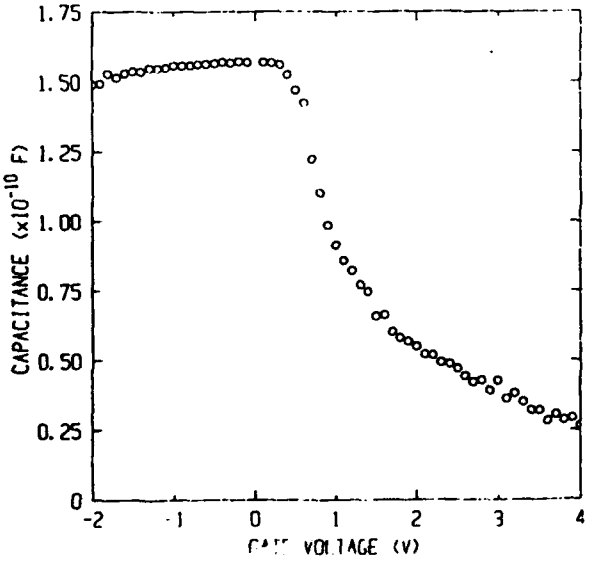


FIG. 4. Capacitance as a function of gate voltage for the $Si_3N_4$-coated, 500 °C annealed sample.

fusing out of the $La_2CuO_4$ crystal or hydrogen ions which are present during deposition. The presence of ions in the insulator may shift the *C-V* curve as a function of gate voltage thus preventing us from estimating the difference in work function of the gate metal and the semiconductor ($La_2CuO_4$). However, since there was no frequency or sweeping rate dependence of the *C-V* curve the rough estimate of the acceptor density should still be valid.

In summary, the change in $La_2CuO_4$ at the interface, when $SiO_2$ or $Si_3N_4$ insulators are deposited, makes producing an effective field-effect device difficult. Most semiconductor fabrication procedures require annealing at high temperatures in order to improve this interface and reduce the number of interface states that hide the field effect. Obviously, such an annealing step destroys the crystal structure at the $La_2CuO_4$ surface where the field effect is most sensitive. Future attempts at improving the $La_2CuO_4$-insulator interface will require annealing at low temperatures (below roughly 400 °C) and silicon nitride seems to be a better choice than silicon dioxide.

## ACKNOWLEDGMENTS

We acknowledge assistance in the Auger data acquisition by E. L. Shaw. This work was conducted under the auspices of the Consortium for Superconducting Electronics with partial support by the Defence Advanced Research Projects Agency (Contract No. MDA972-90-C-0021). The work at IBM was also supported in part by ONR contract No. N00014-85-C-0361.

[1] N. W. Preyer, R. J. Birgeneau, C. Y. Chen, D. R. Gabbe, H. P. Jenssen, M. A. Kastner, P. J. Picone, and T. Thio, Phys. Rev. B 39, 11 563 (1989).
[2] S. A. Brazovski and V. Yakovenko, Phys. Lett. A 132, 290 (1988).
[3] U. Kabasawa, K. Asano, and T. Kobayashi, Jpn. J. Appl. Phys. 29, L86 (1990).
[4] A. T. Fior, A. F. Hebard, R. H. Eick, P. M. Mankiewich, R. E. Howard, and M. L. O'Malley, Phys. Rev. Lett. 65, 3441 (1990).
[5] J. Mannhart, J. G. Bednorz, K. A. Muller, and D. G. Schlom (unpublished).
[6] X. X. Xi, Q. Li, C. Doughty, C. Kwon, S. Bhattacharya, A. T. Findikoglu, and T. Venkatesan, Appl. Phys. Lett. (to be published).
[7] A. Levy, J. P. Falck, M. A. Kastner, W. J. Gallaher, A. Gupta, and A. W. Kleinsasser, J. Appl. Phys. 69, 4439 (1991).
[8] P. J. Picone, H. P. Jenssen, and D. R. Gabbe, J. Cryst. Growth 85, 576 (1987).
[9] S. Etemad, D. E. Aspens, M. K. Kelley, R. Thompson, J. M. Tarascon, and G. W. Hull, Phys. Rev. B 37, 3396 (1988).
[10] T. Venkatesan, E. W. Chase, X. D. Wu, A. Inam, C. C. Change, and F. K. Shokoohi, Appl. Phys. Lett. 53, 243 (1988).
[11] Y. Ichikawa, H. Adachi, T. Mitsuyu, and K. Wasa, Jpn. J. Appl. Phys. 27, L381 (1988).

Physica C 194 (1992) 92–96
North-Holland

PHYSICA C

(10)

# $SrTiO_3/YBa_2Cu_3O_{7-\delta}$ bilayers: fabrication and characterization

W. Eidelloth [a], A. Levy [b], B.P. Chang [c], W.J. Gallagher [a]

[a] *IBM Research Division, Thomas J. Watson Research Center, Yorktown Heights, NY 10598-0218, USA*
[b] *Department of Physics, Massachussetts Institute of Technology, Cambridge, MA 02139, USA*
[c] *Department of Materials Science and Engineering, Massachussetts Institute of Technology, Cambridge, MA 02139, USA*

Received 27 January 1992

We report on the deposition and characterization of $SrTiO_3/YBa_2Cu_3O_{7-\delta}$ bilayers with $SrTiO_3$ thickness up to 0.7 μm. The films were grown by laser ablation onto $NdGaO_3$ and also onto Nb-doped $SrTiO_3$ substrates. Investigations by X-ray diffraction revealed very good crystallinity and (100) orientation of the $SrTiO_3$ films. The relative permittivity was found to increase from 320 at room temperature to 780 at 65 K. The dielectric breakdown of a 4500 Å thick $SrTiO_3$ film at 4.2 K occurred asymmetrically at $6.2\times10^4$ V/cm and $2.2\times10^5$ V/cm. The highly oriented $YBa_2Cu_3O_{7-\delta}$ films deposited on top of these insulating layers had $T_c(R=0)>90$ K and $J_c(77\text{ K})\gtrsim 2.7\times10^6$ A/cm$^2$.

## 1. Introduction

Much progress has been made during the last several years on the deposition of highly oriented high-$T_c$ superconducting thin films. Many groups have reported on the fabrication nd characterization of high quality films, in particular $YBa_2Cu_3O_{7-\delta}$ (YBCO) films. $SrTiO_3$ (STO) has been identified very early as a preferred substrate for YBCO films because it has an excellent lattice match and also because its thermal expansion properties are similar to those of YBCO [1]. Several groups have reported on the successful fabrication of multilayer devices which comprise superconducting and insulating layers using laser ablated STO films as insulators [2–8]. The basic requirements for insulating layers are similar to those for substrates, namely a good lattice match and a good thermal expansion match to the superconductor. For structures such as cross-overs in superconducting transformers the quality of the insulator is not crucial as long as some degree of epitaxy is preserved and electrical shorts are avoided (e.g. the density can be low). For other devices (e.g. FET-like structures), however, it may be necessary to have insulators of very high quality which are also relatively thick ($\simeq 0.5$ μm). It is necessary to preserve epitaxy to facilitate the subsequent growth of highly oriented superconducting layers. Recently the fabrication of FET-like structures has been reported [7,8] using YBCO and STO. For such devices the insulator should have a high permittivity and a large breakdown field. Good crystallinity must be preserved to allow the deposition of high quality YBCO on top. Here we report on the fabrication and characterization of high quality STO which fulfils the above requirements.

We have fabricated bilayers of STO and YBCO (fig. 1) with excellent quality STO layers having a thickness up to 0.7 μm. X-ray diffraction patterns of the STO film show excellent epitaxy and crystallinity. The top YBCO films showed electrical properties comparable to single layer films deposited directly onto single crystal STO substrates. This indicates a highly oriented growth of the STO films because high quality YBCO films do not grow on polycrystalline substrates. The electrical performance

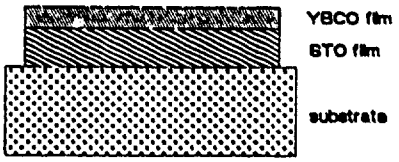


Fig. 1. Schematic view of the bilayers.

(relative permittivity, dielectric break-down) of the STO films was measured between 4.2 K and 300 K.

## 2. Fabrication

The STO thin films were deposited by layer ablation from a 2.5 cm diameter single crystal target using a frequency- tripled Nd:YAG laser (355 nm). The laser was operated at a repetition rate of 10 Hz. The laser beam was incident on the target at a 45° angle, thus yielding an elliptical spot size. The beam was scanned over an area of 19 mm × 11 mm. The substrates were thermally anchored to a Haynes alloy heater block using a thin layer of silver paint. The heater was positioned at a distance of 54 mm from the target with the substrate parallel to the target surface. The heater block was kept at 700°C during the deposition. The laser beam energy was 115 mJ/pulse and the background oxygen pressure was 150 mTorr. This beam energy corresponded to an average energy density of 4.6 J/cm$^2$.

For subsequent YBCO deposition the heater block temperature was increased to 745°C, the oxygen pressure was adjusted to 250 mTorr, and the incident laser beam energy was 100 mJ/pulse (i.e. 4 J/cm$^2$). These parameters yield a deposition rate of about 470 Å/ min for YBCO. After the ablation process oxygen was backfilled to 610 Torr within 5 min and the heater was cooled to room temperature at a rate of 20°C/min.

To investigate the deposition rate of STO we first deposited STO films only (no YBCO) on (110) $NdGaO_3$ substrates using the above described deposition parameters. After removal from the deposition system photoresist patterns were defined on these films using standard photolithography. The films were then etched in 5% HF in deionized water under modest ultrasonic agitation [4]. This method yielded etch rates of about 800 Å/min both for STO films and for (100) STO substrates. As reported earlier [4], this etchant does not attack $NdGaO_3$. The thickness was then measured with a mechanical stylus which had a resolution of about 30 Å. We found that the above deposition parameters yield a deposition rate of about 250 Å/min for STO.

## 3. Characterization

Some STO films were characterized by X-ray diffraction. Figure 2(a) shows a $\theta$–$2\theta$ scan for a 5000 Å thick STO film on $NdGaO_3$. The thin, plain lines indicate the theoretical locations for polycrystalline STO peaks. In fig. 2(b) the results for the substrate alone are shown (we simply flipped over the chip). It can be seen in fig. 2(a) that besides the substrate peaks there are only three STO peaks. These are the (100), the (200) and the (300) reflections. The absence of signals other than for the ($i$00) directions imply that this film has a very high degree of orientation in the (100) direction. A rocking curve of the (100) peak revealed a full width at half maximum (FWHM) of less than 0.1°, confirming both the excellent crystalline quality and the high degree of orientation of this film.

Figure 3 shows a typical result for the electrical resistance of a YBCO film in a STO/YBCO bilayer measured as function of temperature. The shape of this $R$–$T$ curve resembles closely those of YBCO films deposited directly onto STO substrates. The resistivity of the YBCO films on top of STO films, however, was found to increase with STO film thickness. This point is further discussed below. The YBCO films of two bilayers deposited on (110) $NdGaO_3$ substrates were patterned into 20 μm wide lines (350 μm long) for measurements of the critical currents. As an etchant we used EDTA (ethylenediaminetetraacetic acid) [9] which does not attack the underlying STO film. Bilayer A consisted of 0.46 μm thick STO and 0.25 μm YBCO, bilayer B was a 0.7 μm thick STO film with 0.26 μm YBCO film on top. Silver was sputtered onto the contact pads of these structures through a lift-off stencil. After lift-off and annealing at 450°C in oxygen the devices on each chip were contacted by wire bonding. Measuring the four point resistance of these structures allowed us to calculate the room temperature resistivities. For bilayer A we found $\rho(300\ \mathrm{K}) \simeq 300\ \mu\Omega\,\mathrm{cm}$, the devices on bilayer B had resistivities $\rho(300\ \mathrm{K}) \simeq 460\ \mu\Omega\,\mathrm{cm}$. To measure the critical currents the bilayers were immersed into liquid nitrogen. For chip A we found a critical current density $J_c(77\ \mathrm{K}) = 4.5\times10^6\ \mathrm{A/cm^2}$, chip B yielded $J_c(77\ \mathrm{K}) = 2.7\times10^6\ \mathrm{A/cm^2}$.

To further investigate the quality of the STO films we deposited a 4500 Å thick STO layer followed by

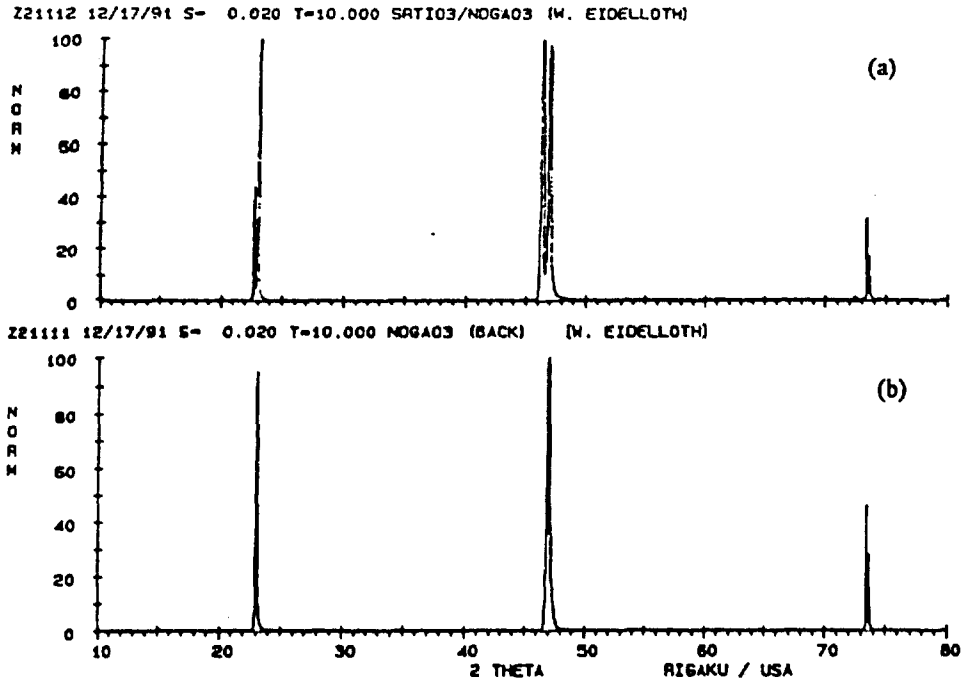


Fig. 2. X-ray diffraction pattern (a) of a 0.5 μm thick STO film on $NdGaO_3$, (b) of the $NdGaO_3$ substrate.

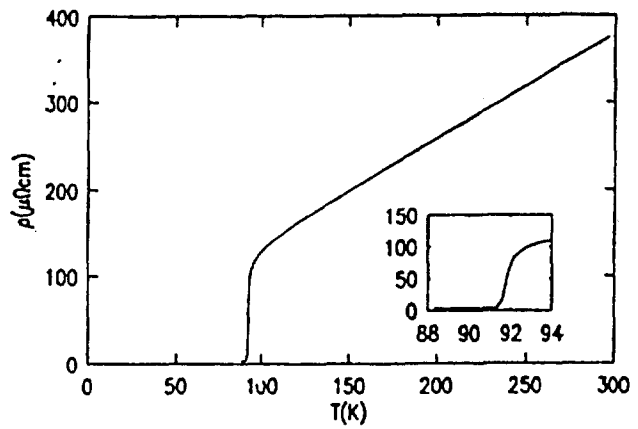


Fig. 3. Resistivity vs. temperature for a 2500 Å thick YBCO film on top of 4500 Å thick STO film on $NdGaO_3$.

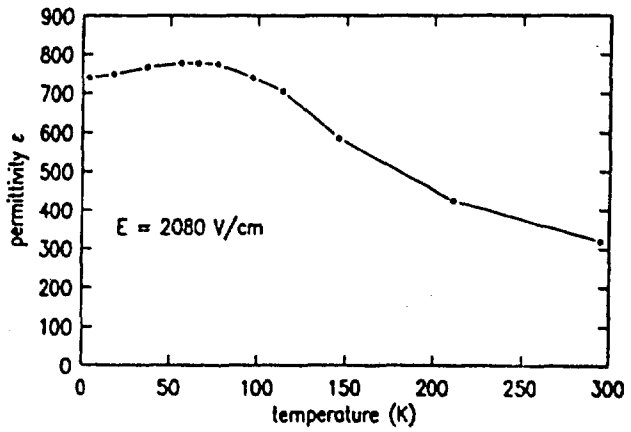


Fig. 4. Relative permittivity vs. temperature for a 4500 Å thick STO film deposited on Nb-doped STO.

a 2500 Å thick YBCO layer onto a Nb-doped STO substrate. After patterning of the YBCO both the superconductor and the conducting substrate were electrically contacted. Capacitance measurements were made to deduce the permittivity ($\epsilon$) for the STO film. The applied field was 2.08 kV/cm. Figure 4 shows $\epsilon$ as a function of temperature. The room temperature value of about 320 increases with decreasing temperature and peaks at 65 K with a value of 780. This peak is expected [10] for single crystal STO. The thickness of the STO film is accurate to within 10%. Therefore the absolute values of the permittivity are also only accurate to about 10%.

We also measured the dielectric breakdown of this bilayer at room temperature, at 93 K, and at 4.2. Figure 5 shows the current through the STO film versus voltage applied between the substrate and the superconductor at these three temperatures. The pos-

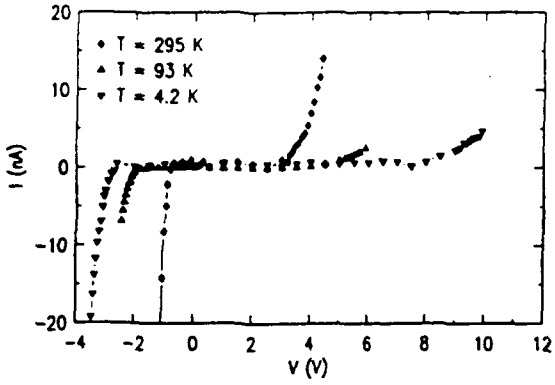


Fig. 5. Dielectric breakdown of a 4500 Å thick STO film on a Nb-doped STO substrate.

itive electrode was at the substrate. Taking the breakdown voltage as the voltage at which the current first exceeds 5 nA, we find the breakdown at 4.2 K to occur at fields $E_{bd} \simeq 6.2\times10^4$ V/cm and $2.2\times10^5$ V/cm. Mannhart et al. [7] pointed out that the product $\epsilon\times E_{bd}$ must exceed $10^8$ V/cm for the insulator to be technologically useful in FET-like structures. For these devices we find $\epsilon\times E_{bd} \simeq 4.6\times10^7$ V/cm/ $1.6\times10^8$ V/cm at 4.2 K, and $4.0\times10^7$ V/cm/ $0.99\times10^8$ V/cm at 93 K.

## 4. Discussion

As mentioned above, the chemical etch rate of the STO films was found to be the same as for (100) STO substrates. This indicates that the density of the STO thin films is comparable to that of single crystals. We expect that denser insulating films have better dielectric properties. X-ray measurements revealed that these films are highly crystalline and that they are oriented in the (100) direction.

Comparing the performance of the YBCO in chip A and B it can be seen that both the resistivity and the critical current density deteriorate as the STO film thickness increases. For YBCO films on STO *substrates* we typically obtain $J_c(77\ \mathrm{K}) = 2\text{–}5\times10^6$ A/cm$^2$, and $\rho(300\ \mathrm{K}) \simeq 200\text{–}300\ \mu\Omega$ cm. These numbers are similar to those of the YBCO film on bilayer A. In the case of chip B, however, a distinct degradation is observed. We attribute the decay in electrical quality to an increasing surface roughness of the STO film. To confirm this we scanned the STO surface (after YBCO removal) of both chips with a mechanical stylus. We found that the thicker STO layer (chip B) had a rougher surface. The surface height varied by as much as 1000 Å whereas in the case of chip A only a 500 Å variation was observed. This roughness appears to be caused mainly by particulates which are commonly observed in laser ablated thin films. The total number of such "boulders" increases with deposition time and therefore there are significantly more particulates on the thicker STO film. In fig. 6 two optical micrographs of the STO surfaces of the two chips are shown. It can be seen that there are more particulates on chips B. Such "boulders" are likely to cause a reduction of the breakdown field. They also prevent the deposition of smooth YBCO layers on top.

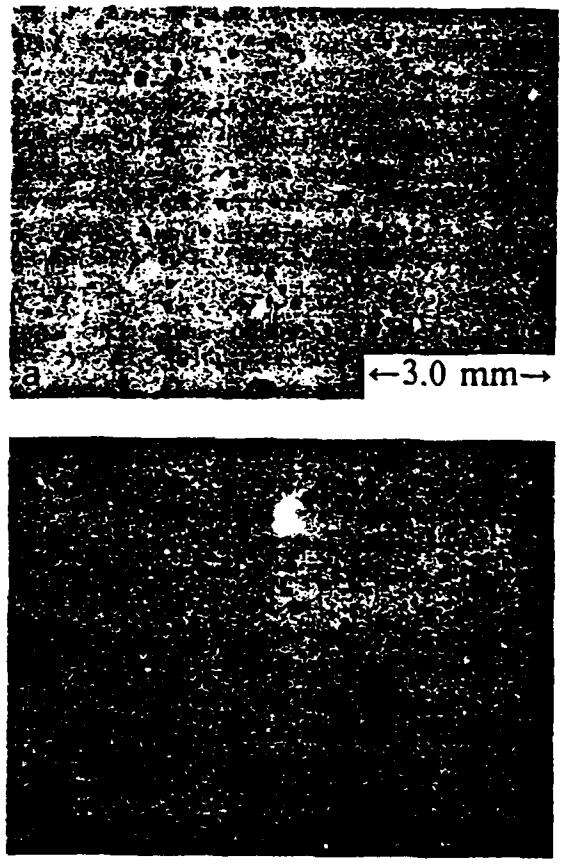


Fig. 6. Optical micrographs of (a) a 0.46 μm thick STO film and of (b) a 0.7 μm thick STO film.

Mannhart et al. [7] fabricated structures similar to ours by sputtering. The insulator thickness reported was 1600 Å and the deduced room temperature permittivity was 36. This is much less than expected. The breakdown fields, however, were $2\times10^5$ V/cm and $4\times10^6$ V/cm at room temperature. These values are impressive and result in $\epsilon\times E_{bd}$ values similar to ours. Xi et al. reported on the electric field effect in ultra thin YBCO films [8]. These researchers deposited a very thin layer of YBCO on an insulating substrate and grew STO on top of the YBCO. Both YBCO and STO were deposited by laser ablation. Using a top electrode of gold they obtained breakdown fields of $7.4\times10^4$ V/cm and $6\times10^5$ V/cm at 50 K, indicating very high quality STO layers.

## 5. Summary and conclusions

We have fabricated STO/YBCO bilayers with STO films as thick as 0.7 μm. The STO films were found to grow in the (100) direction and had excellent dielectric properties. One problem, however, is the occurrence of particulates during deposition, which seem to limit the electrical properties of both the insulator and the superconductor deposited on top. Improvements in film deposition may lead to a reduction of such particulates resulting in further improvement of the dielectric performance of the insulating layers. This should also facilitate the deposition of better YBCO films on top of STO films thicker than 0.7 μm. These results are significant for the fabrication of devices which rely on thin but high quality insulating layers such as FETs.

## Acknowledgements

We are grateful to R.L. Sandstrom for helpful suggestions. Clarifying discussions with A. Kleinsasser are highly appreciated. This work was partially supported by the US Office of Naval research under contract number N00014-88-C-0439.

## References

[1] See for example E.A. Giess, R.I. Sandstrom, W.J. Gallagher, A. Gupta, S.L. Shinde, R.F. Cook, E.I. Cooper, E.J.M. O'Sullivan, J.M. Roldan, A.P. Segmüller and J. Angilello, IBM J. Res. Dev. 34 (1990) 916, and references therein.
[2] F.C. Wellstood, J.J. Kingston, M.J. Ferrari and J. Clarke, Appl. Phys. Lett. 57 (1990) 1930.
[3] B. Oh, R.H. Koch, W.J. Gallagher, R.P. Robertazzi and W. Eidelloth, Appl. Phys. Lett. 59 (1991) 123.
[4] W. Eidelloth, W.J. Gallagher, R.P. Robertazzi, R.H. Koch, B. Oh and R.L. Sandstrom, Appl. Phys. Lett. 59 (1991) 1257.
[5] K. Char, M.S. Colclough, L.P. lee and G. Zaharchuk, Appl. Phys. Lett. 59 (1991) 2177.
[6] W. Eidelloth, B. Oh, R.P. Robertazzi, W.J. Gallagher and R.H. Koch, Appl. Phys. Lett. 59 (1991) 3473.
[7] J.J. Mannhart, J.G. Bednorz, K.A. Müller and D.G. Schlom, Z. Phys. B 83 (1991) 307.
[8] X.X. Xi, Q. Li, C. Doughty, C. Kwon, S. Bhattacharya, A.T. Findikoglu and T. Venkatesan, Appl. Phys. Lett. 59 (1991) 3470.
[9] F.K. Shokoohi, L.M. Schiavone, C.T. Rogers, A. Inam, X.D. Wu, L. Nazar and T. Venkatesan, Appl. Phys. Lett. 55 (1990) 2661.
[10] R.C. Neville, B. Hoeneisen and C.A. Mead, J. Appl. Phys. 43 (1972) 2124.

# Field and Hall effects in semiconducting $YBa_2Cu_3O_{6+\delta}$

A. Levy, J. P. Falck, M. A. Kastner, and R. J. Birgeneau
*Department of Physics, Massachusetts Institute of Technology, Cambridge, Massachusetts 02139*

A. T. Fiory and A. F. Hebard
*AT&T Bell Laboratories, Murray Hill, New Jersey 07974*

W. J. Gallagher and A. W. Kleinsasser
*IBM Thomas J. Watson Research Center, Yorktown Heights, New York 10598*

A. C. Anderson
*Lincoln Laboratories, Lexington, Massachusetts 02173*
(Received 10 February 1992)

The field-effect mobility, Hall coefficient, and conductivity as functions of the oxygen concentration and temperature are reported for $YBa_2Cu_3O_{6+\delta}$ films on the insulating side of the insulator-to-metal transition. The temperature dependence of the conductivity and Hall coefficient indicate that for small $\delta$ the excess oxygen introduces acceptor states at about 30 meV above the valence-band edge. The field effect reveals a space-charge layer in which carriers are depleted at the air-$YBa_2Cu_3O_{6+\delta}$ interface. The size of the field effect is limited by localized states at the interface.

One of the common characteristics of the high-$T_c$ copper oxide superconductors is the existence of an antiferromagnetic semiconducting phase near the superconducting one.[1] In contrast to other copper oxides, $YBa_2Cu_3O_{6+\delta}$ can be easily doped in oxygen, converting it chemically from one phase to the other.[2] Since the primary role of doping is to increase the charge concentration, it has been suggested[3] that charge carriers might be induced by an external electric field rather than by doping to drive the material across the phase boundary. The feasibility of this approach is determined by the density of states in the band gap of the semiconductor. If the density of states is too high, the external electric field required to shift the Fermi level will be inaccessible.

In order to characterize the bulk and surface localized states in semiconducting $YBa_2Cu_3O_6$ and those introduced by adding oxygen, we have measured the conductivity, Hall coefficient, and field-effect mobility as functions of temperature and oxygen content in thin films of $YBa_2Cu_3O_{6+\delta}$. We find that for small $\delta$ the material behaves like a somewhat compensated $p$-type semiconductor with a depletion region near the air-$YBa_2Cu_3O_{6+\delta}$ interface. Although we find evidence for a high density of localized interface states on some films, this density varies greatly with the structure of the interface. Thus, interfaces may exist for which the electric-field-driven transformation to the superconducting phase is possible.

Two $YBa_2Cu_3O_{6+\delta}$ films were grown on $LaAlO_3$ substrates using the *in situ* ff-axis rf magnetron sputtering method. A detailed description of the growth method was reported elsewhere.[4] As grown, the films displayed a sharp superconducting transition at 88 K. Samples 1–3 were cut from one film, and samples 4 and 5 originated from the other. To vary the oxygen concentration the films were then annealed in Ar containing a low partial pressure of oxygen.

Field-effect experiments were made using the method of Fiory *et al.*[5] at temperatures from 4 to 300 K with applied gate voltages between $-1$ and $+1$ kV. Repetitive Br etching[5,6] consistently produced the same field effect on these air-$YBa_2Cu_3O_{6+\delta}$ interfaces. Hall bars were subsequently lithographically patterned, and the Hall effect was measured at fields from $-0.65$ to $+0.65$ T, over which range the Hall voltage was found to be linear with applied magnetic field.

In the top half if Fig. 1 we present the conductance as a function of temperature for all of the films studied. The conductance of samples 2–5 can be fitted by the sum of two contributions: The component that is dominant at high $T$ is thermally activated, that is, $g = g_0 \exp(-E_a/kT)$ where $E_a$ is the activation energy and $k$ is the Boltzmann constant. The best fit to the experimental results yields $E_a = 20\pm3$, $40\pm6$, $40\pm6$, and $140\pm15$ meV for samples 2–5, respectively. The second component behaves like that which arises from variable range hopping between localized states near the Fermi energy and is given by $g = g_1 \exp(-(T_0/T)^n)$. The best fit gives $n = \frac{1}{4}$ although lower-temperature data are required to rule out other exponents. Sample 1 has a very weak temperature dependence, indicating that it is close to the crossover from strong localization to nearly metallic conductance. The gradual decrease of $E_a$ as the carrier density is decreased from sample 2 to 4 is typical of doped semiconductors near the insulator-to-metal transition.[1] The abrupt increase of $E_a$ (for sample 5) signals the elimination of the shallow impurities.

 

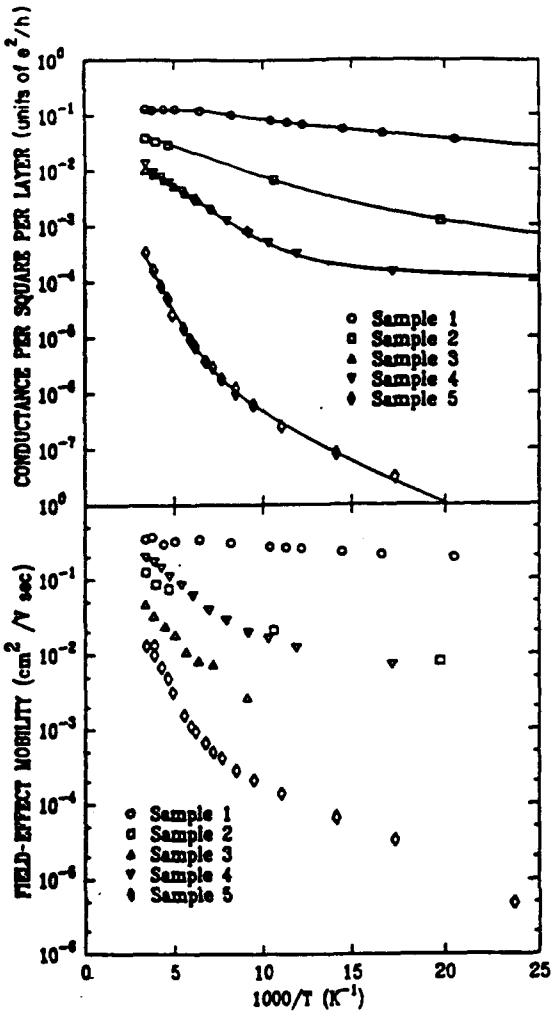


FIG. 1. Conductance per square per layer, and field-effect mobility as functions of the temperature for $YBa_2Cu_3O_{6+\delta}$. Solid lines are least-squares fits to the sum of a simply activated component and a variable-range-hopping component.

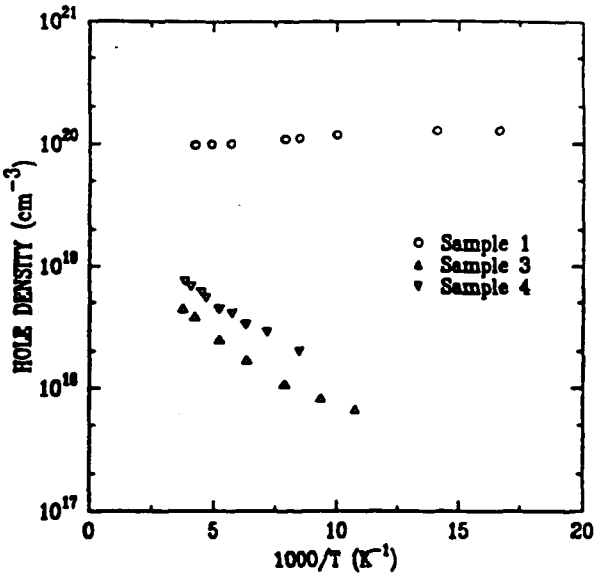


FIG. 2. Charge-carrier (hole) density extracted from Hall-effect experiments on $YBa_2Cu_3O_{6+\delta}$ vs temperature.

The Hall coefficient also displays a behavior typical of doped semiconductors. Hall charge-carrier densities are plotted as a function of temperature in Fig. 2. The Hall coefficient is always positive, indicating that the charge carriers are holes. The most conducting sample (1) displays an almost constant charge density, indicating once again that this film is nearly metallic. For samples 3 and 4 the mobile hole density, like the conductivity, is thermally activated. The activation energy is $E_a = 30 \pm 5$ meV, which is close to the activation energy (40 meV) of the conductance for these two samples, showing that the primary temperature dependence of the conductivity comes from the $T$ dependence of the hole density.

The defects or impurity states that determine the position of the Fermi energy once the shallow acceptors are removed partially compensate the acceptors. Whereas the activation energy in an uncompensated doped semiconductor is half the binding energy of the hole to the impurity, it is equal to the binding energy in the compensated case.[7] Thus, the 30-meV activation energy provides a measurement of the binding energy of the hole to the oxygen acceptor in $YBa_2Cu_3O_{6+\delta}$. This agrees within the reported errors with the value 34 meV found[1] for the binding energy of the oxygen acceptor in $La_2CuO_{4+y}$.

For samples 3 and 4 there is no evidence in Fig. 2 for saturation of the carrier density up to room temperature. Thus we can only place a lower bound of $\sim 10^{19}$ cm$^{-3}$ on the carrier densities. It is clear, however, by comparing the behavior of sample 1 with that of samples 3 and 4 that the transition from strong localization to nearly metallic behavior occurs near $10^{20}$ cm$^{-3}$, approximately 1% of the copper atom concentration. Superconductivity is seen[8] only above $\sim 2\%$ of holes within the $CuO_2$ planes.

The Hall mobility, shown in Fig. 3, is nearly independent of doping and has magnitude $\mu_H \sim 2$ cm$^2$/V sec. This is quite close to the value $\sim 3$ cm$^2$/V sec found for

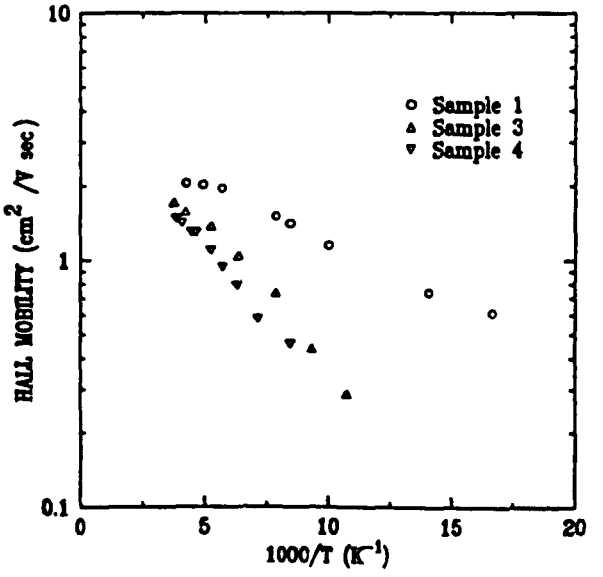


FIG. 3. Hall mobility vs temperature for $YBa_2Cu_3O_{6+\delta}$.

$La_{2-x}Sr_xCuO_{4+y}$. Using the free-electron mass one finds from these mobilities that the scattering time at room temperature is comparable to that in the highest-$T_c$ superconductors. The decrease of the mobility as $T$ decreases is probably caused by the transition from simply activated conductance to variable range hopping.[1]

In the field-effect experiment the applied voltage induces a charge per unit area $\delta Q$ near the surface of the sample. As a result, the conductance per square of the film changes to $\delta G$. The field-effect mobility is given by $\mu_{FE}=dG/dQ$. For all our measurements $\delta G$ is found to be proportional to $\delta Q$. The field-effect mobility is plotted versus $1/T$ in the lower half of Fig. 1. It is seen that $\mu_{FE}$ has roughly the same temperature dependence as the conductance.

Comparing samples 3 and 4 we find that, whereas their conductances and Hall coefficients are nearly the same, their field-effect mobilities differ appreciably. Using scanning electron microscopy we detected inclusions of the $a$-axis $YBa_2Cu_3O_{6+\delta}$ phase on the surface of the film from which samples 1–3 were taken. Inclusions of the $a$-axis oriented phase have been observed in the past,[9] and are known to increase with the thickness of the film; the samples that show the $a$-axis phase are from the thicker of the two films. The nearly identical conductivities and Hall coefficients of samples 3 and 4 show that grain boundaries do not have a significant influence on the transport properties. The lower values of $\mu_{FE}$ for sample 3 therefore suggest that, for samples 1–3 most of the added charge is localized in surface states and that the $a$ axis has a higher density of surface states than the $c$ axis.

The high density of surface states fixes the position of the Fermi energy $E_F$ in the band gap at the surface. We show next that the similarity of the temperature dependences of $\mu_{FE}$ and the conductance is consistent with the assumption that the charge carriers are depleted near the semiconductor surface.

In general, the conductance of the film is given by

$$G=\int \sigma(x)dx=\int_0^W \sigma(x)dx+\sigma(d-W)\,, \qquad (1)$$

where $W$ is the width of the space-charge region, in which the conductivity depends on the charge density and thereby on position $x$, $d$ is the film thickness, and $\sigma$ is the conductivity in the interior of the film. In depletion $G$ is dominated by the second term, and the change in $G$ results from the change in $W$. In addition, $W$ is simply related to the charge added per unit area to the bulk of the semiconductor $Q_B$ by $dW/dQ_B=[e(N_A-N_D)]^{-1}$, where $N_A$ and $N_D$ are the densities of acceptors and compensating donors, respectively. Consequently, the field effect mobility is given by

$$\mu_{FE}=dG/dQ=-\sigma(dQ_B/dQ)[e(N_A-N_D)]^{-1}\,, \qquad (2)$$

where $dQ_B/dQ$ is the fraction of added charge that ionizes shallow impurities; the balance is trapped in surface states and localized states in the depletion region. From Eq. (2) one predicts that the ratio $\sigma/\mu_{FE}$ is independent of temperature. As seen in Fig. 4, $\sigma/\mu_{FE}$ is, indeed, constant between ~100 and 300 K for all but the most resistive sample.

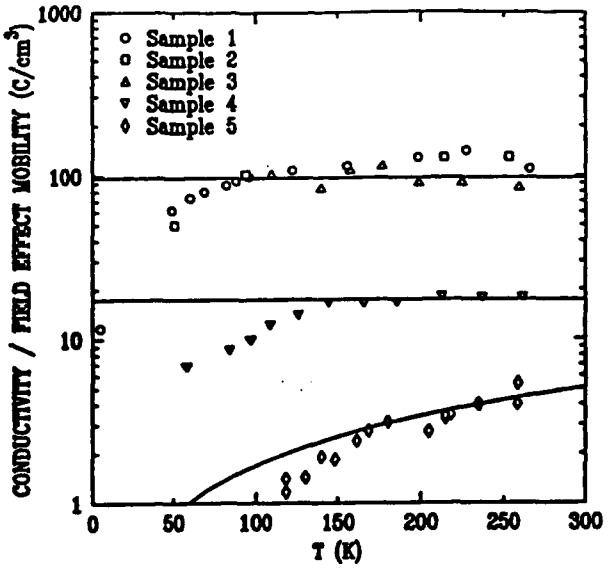


FIG. 4. Ratio of the conductivity to the field-effect mobility as a function of the temperature for $YBa_2Cu_3O_{6+\delta}$. The solid lines for samples 1–4 represent a constant. The curve for sample 5 is the best fit of the data to $\sigma/\mu_{FE}\propto T$. Note that the values for samples 1–3 are high because the high density of interface states make $\mu_{FE}$ small.

Note that $\sigma/\mu_{FE}$ is nearly the same for samples 1–3, consistent with the idea that all of these, which come from the same film with $a$-axis inclusions, have the same high density of surface states, which gives a large value of $dQ/dQ_B$. For this sample we estimate that the surface density of states is $\sim 10^{14}$–$10^{15}/\mathrm{cm}^2\,\mathrm{eV}$, which is very high.

From the data for sample 4 in Fig. 4 one finds $(N_A-N_D)=dQ_B/dQ\times 10^{20}\ \mathrm{cm}^{-3}$. As discussed above, the density of holes that can be ionized from acceptors $N_A-N_D$ is larger than $10^{19}\ \mathrm{cm}^{-3}$ for sample 4. Thus the fraction of charge added to the bulk of the semiconductor is larger than $\frac{1}{10}$. The same observation can be made directly by noting that $\mu_{FE}$ for sample 4 (Fig. 1) is about ten times smaller than the Hall mobility (Fig. 3) at ~300 K. This means that for sample 4 the surface states do not overwhelmingly dominate the field effect as they do for samples 1–3.

The decrease of $\sigma/\mu_{FE}$ at low $T$ for samples 1–4 may result from conduction in the surface states or the space-charge region when the conductivity mechanism changes to hopping. Because the latter mechanism depends exponentially on the density of states at the Fermi energy, and because the density of states may vary nonmonotonically in the space-charge region, the contribution from the latter region is difficult to estimate.

The field effect for sample 5 has a rather stronger temperature dependence than that of the other films. This is consistent with the idea that all shallow acceptors are eliminated in this sample, and that the screening of external fields is, therefore, different. The temperature dependence seen in Fig. 4 may be understood[10] by assuming that the field is screened by a high density of localized states in the band gap in which the band bending is small.

A simple argument leads then to $\sigma/\mu_{FE} \sim T$. The data for sample 5 are in reasonable agreement with this prediction as seen in Fig. 4.

In summary, we have shown that the temperature and doping dependence of the conductance and Hall coefficient are consistent with a model in which $YBa_2Cu_3O_{6+\delta}$ is a doped semiconductor with some compensation. In fact, the properties of this material are remarkably similar to those of $La_{2-x}Sr_xCuO_{4+y}$. In particular, the Hall coefficient provides a good measure of the free carrier density, a property that appears to hold well into the superconducting phase. The activation energy of the hole density shows that the binding energy of the hole to the oxygen acceptor is ~30 meV in $YBa_2Cu_3O_{6+\delta}$, close to the value found for $La_2CuO_{4+y}$. We note that this is a measurement of the binding energy in single crystals of $YBa_2Cu_3O_{6+\delta}$.

Chen *et al.*[11] showed that the small binding energy in $La_2CuO_{4+y}$ comes about because of coupling of the charge carriers to optical phonons. The screening of the Coulomb field by the static dielectric constant, which is $\epsilon \sim 30$ in $La_2CuO_4$, reduces the binding energy from the value ~0.5 eV it would have if screening were only by the electronic contribution (~5) to the dielectric constant. From the small value of the binding energy we find in $YBa_2Cu_3O_{6+\delta}$ we infer that coupling of the holes to the optical phonons is important in this material as well.

From the field-effect measurements we conclude that there is a depletion region at the air-$YBa_2Cu_3O_{6+\delta}$ interface and that the density of states at this interface is relatively high. However, there is now much evidence that the density of states depends on detail on the structure of the interface. In addition to the dependence on surface orientation reported here, it is possible to achieve a lower density of states and a concomitantly higher field-effect mobility at the interface of $YBa_2Cu_3O_6$ and $SrTiO_3$.[12] Thus, there is reason to believe that much higher field effects can be realized. Alternatively, higher field effects can be achieved using thinner and larger-dielectric-constant gate insulators.[13–15]

This work was conducted as part of the Consortium for Superconducting Electronics with partial support by the Defense Advanced Research Projects Agency (Contract No. MDA972-90-C-0021) and National Science Foundation (Grant No. DMR 9022933).

[1]N. W. Preyer *et al.*, Phys. Rev. B 39, 11 563 (1989); Physica C 162, 1003 (1989).
[2]G. Koren, A. Gupta, and A. Segmuller, Physica C 162-164, 1021 (1989).
[3]S. A. Brazovski and V. Yakovenko, Phys. Lett. A 132, 290 (1988).
[4]A. C. Westerheim *et al.*, IEEE Trans. Magn. 27, 1001 (1991).
[5]A. T. Fiory *et al.*, Phys. Rev. Lett. 65, 3441 (1990).
[6]R. P. Vasquez, B. D. Hunt, and M. C. Foote, Appl. Phys. Lett. 53, 2692 (1988).
[7]J. S. Blakemore, *Solid State Physics* (W. B. Saunders, Philadelphia, 1969).
[8]N. P. Ong, in *Physical Properties of High-Temperature Superconductors II*, edited by D. M. Ginsburg (World Scientific, Singapore, 1990).
[9]B. M. Clemens *et al.*, Appl. Phys. Lett. 53, 1871 (1988).
[10]M. Kastner and H. Fritzsche, Mater. Res. Bull. 5, 631 (1970).
[11]C. Y. Chen *et al.*, Phys. Rev. B 43, 392 (1991).
[12]A. Levy *et al.*, J. Appl. Phys. 69, 4439 (1991).
[13]J. Manhart, J. G. Bednorz, K. A. Müller, and D. G. Schlom, Z. Phys. B 83, 307 (1991).
[14]X. X. Xi *et al.*, Appl. Phys. Lett. 59, 3470 (1991).
[15]W. Eidelloth, A. Levy, B. P. Chang, and W. J. Gallagher (unpublished).

# SUPERCONDUCTING DEVICES

*Edited by*

**Steven T. Ruggiero**

Department of Physics
University of Notre Dame
Notre Dame, Indiana

**David A. Rudman**

Department of Materials Science and Engineering
Massachusetts Institute of Technology
Cambridge, Massachusetts

ACADEMIC PRESS, INC.
*Harcourt Brace Jovanovich, Publishers*
Boston San Diego New York
Berkeley London Sydney
Tokyo Toronto

## CHAPTER 9

# Three-Terminal Devices

A.W. KLEINSASSER
and
W.J. GALLAGHER
*IBM Research Division*
*T.J. Watson Research Center*
*Yorktown Heights, New York*



## 1. Introduction

Over the last three decades, superconductive electronics has developed along two lines: digital applications based on high switching speed and low power dissipation, and analog applications based on extremely high sensitivity and/or frequency response extending into the far infrared. Virtually all of superconductive electronics depends on the use of tunneling and/or the Josephson effect in two-terminal devices. Without a three-terminal transistor-like device, superconductive electronics will undoubtedly remain relegated to specialized niches. There has been no lack of proposals for three-terminal devices. Some of these devices are not truly transistor-like, and none have yet

 

been developed to a practical stage. Progress has been made, however, in a number of areas since the last general review of this subject [1]. This chapter will discuss the subject of three-terminal superconducting devices with an emphasis on recent progress.

The discovery of superconductivity at temperatures exceeding 100 K in copper oxide-based materials broadens the scope of potential superconducting device applications considerably. There is a convergence of semiconductor technology, with its growing focus on low temperatures (particularly 77 K) for advanced computer applications, and superconductor technology [2,3]. Although the most obvious application might be to use superconducting interconnects in advanced semiconductor circuits, there is considerable interest in using the unique aspects of superconducting devices at higher temperatures, or in looking for new devices that take advantage of, for example, a larger superconducting energy gap. To date, there has been little work on high temperature three-terminal superconducting devices, with most thinking aimed at extending old ideas to a new temperature range. This article will therefore focus on low (helium) temperature three-terminal devices, extrapolating to higher temperatures where possible. Of course, it is possible that truly novel high temperature applications will emerge in the future.

Research on three-terminal superconducting devices has been aimed at demonstrating basic operating principles and is not focused on specific applications, although digital devices appear to be the most common aim. The discussion in this chapter is thus intended to be fairly general, with a slant towards digital applications. The basic function of a transistor-like device can be understood through use of Landauer's simple fluid-actuated valve analogy [4], illustrated in Fig. 1. A piston, actuated by a "control" fluid in one pipe, is used to control the flow of fluid in another pipe. The two fluids must be separate, with little mixing. Three-terminal devices such as vacuum tubes, junction transistors, and FETs can be described by this model, making it a useful guide for evaluating new device ideas. For example, the deficiencies of some proposed non-equilibrium superconducting devices can be clearly illustrated using this fluid analogy [1]. For actual applications, of course, there is an additional list of desirable properties for three-terminal devices. In digital applications, for example, one needs current and voltage gain, high speed, compatibility with line impedances, and manufacturability, among other properties [5].

For applications involving high levels of circuit integration, removal of the heat dissipated by device operation is a particular concern, especially for low operating temperatures. The product of power dissipated per switching cycle

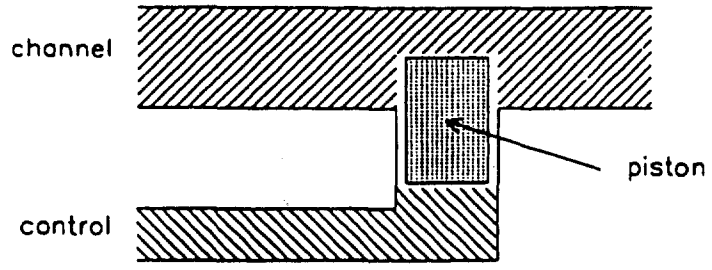


Fig. 1. Schematic of a simple fluid model for a three-terminal device. The fluid in one (gate) pipe controls a piston that varies the flow of fluid in a second pipe. Separation of the two fluids is important. Three-terminal devices such as vacuum tubes, junction transistors, and FETs can be described by this model.

and switching delay is thus an important figure of merit for digital devices. This power-delay product is orders of magnitude smaller in Josephson devices than in competing semiconductor devices, a much-touted advantage of Josephson technology. This is often illustrated with plots of power versus gate delay [2], in which Josephson devices are far removed from semiconductor devices. However, the ability to remove heat from a wafer scales linearly with temperature [6], and device power dissipation must be reduced along with the operating temperature. The standard plots of power versus delay should really be replaced by plots in which power is scaled by $kT$, and the comfortable margin enjoyed by Josephson technology is actually much smaller than is generally appreciated. Clearly, low temperature digital devices must operate at low voltages. Conventional semiconductor devices dissipate too much power to be of interest for dense circuits at low ($\sim 10$ K) temperatures. The superconducting energy gap ($<5$ meV for conventional superconductors) sets a suitably small voltage scale for dense low temperature circuits. However, many potential applications for low temperature devices, both analog and digital, do not require high circuit density, so the requirement of low operating voltage is not a general one.

In this chapter, we discuss devices that are intended to act like transistors. The major subject will be hybrid superconductor–semiconductor devices, which are discussed in Section 2. This has been the most active research area in recent years. Section 3 deals with devices based on nonequilibrium superconductivity. Such devices have received considerable attention, but the prospects for useful devices appear to be narrowing, with the remaining interest focused on low carrier density materials. A brief discussion of magnetic and other devices is included in Section 4, and Section 5 contains concluding remarks.

## 2. Hybrid Superconductors–Semiconductor Devices

### 2.1. *Introduction*

In stark contrast to the situation with superconducting devices, there are several entrenched classes of three-terminal semiconductor devices, the most significant being bipolar and field effect transistors. It is reasonable to take working device principles from semiconductor technology and apply them in hybrid superconductor–semiconductor devices; indeed, several such devices have been proposed. In this section, we discuss these devices in the context of the familiar types of semiconductor devices, addressing the questions of what advantages the incorporation of superconductivity into a device can offer and whether any new device principles result.

Semiconductor transistors are by themselves interesting for low temperature applications. This is becoming particularly evident at 77 K, but is also true down to helium temperatures. A comprehensive review of low temperature semiconductor electronics is clearly beyond the scope of this article. The interested reader is referred to the literature, which includes compilations of recent articles on low temperature electronics [7,8], a review of high speed semiconductor electronics [9], a comparison of semiconductor and Josephson technologies [10], and two short reviews of hybrid superconductor–semiconductor device work [11,12].

For our purposes, existing semiconductor devices can be placed into two categories, junction transistors and field effect transistors (FETs). Junction transistors include both bipolar (BJT) and unipolar (UJT) devices, the latter being hot electron (majority carrier) devices which are similar in concept and structure to bipolar devices. FETs are also unipolar (current is carried by one type of carrier, in contrast to bipolar transistors, in which both electrons and holes are important). BJTs and FETs are familiar in semiconductor technology, while UJTs remain in an exploratory stage. Most hybrid superconductor–semiconductor device work has been in these categories. Numerous other novel devices such as tunneling transistors [13,14], resonant tunneling transistors [15,16], and devices based on real space charge transfer [17,18] have been proposed. Such devices are of current research interest, but no attempts have been made to consider superconducting versions.

The scale of operating voltages in superconducting devices is usually of the order of the superconducting energy gap, which is a few meV or less for conventional superconductors and, being proportional to $T_c$, is expected to be a few tens of meV for the new oxide materials (i.e., in a material with $T_c \approx$ 90–120 K). Typical voltages required for semiconductor device operation

are of order 1 V, but scaling down of device dimensions in order to allow denser circuits requires a reduction of device voltages. This scaling is most successful with MOS devices, Si CMOS [19] for example, leading to voltages of the order of a few hundred mV in 0.25 $\mu$m circuits, and tending to force a reduction of the operating temperature for CMOS circuits. This may lead to some convergence of the voltage scales for superconducting and semiconducting technologies, although they are at present still an order of magnitude or so apart. As will emerge in the following discussion, the operating voltages of hybrid devices may or may not be determined by the same physics that applies to the related semiconductor devices.

### 2.2. *Junction Transistors*

Junction transistors have three active regions: emitter, collector, and base. Device operation consists of the injection of charge carriers from emitter to base, transit across the base, and collection [20]. The injected carriers are energetically separate from the charge carriers in the base, conforming to the fluid analogy described earlier. In an npn (pnp) bipolar transistor, electrons (holes), which are majority carriers in the emitter, are injected into the base, where they are minority carriers, the majority carriers in the base being the control fluid. In order for the device to have gain, the transport of the injected carriers must be controlled with only a small base current.

Typical Si bipolar transistors do not work at low temperatures [9], although this is not a fundamental limitation. However, at low voltages no current can flow until the emitter–base bias exceeds a voltage that is essentially the band gap of the base. Bipolar devices are thus not competitive for applications that require low power dissipation (even in small gap materials, this voltage is several hundred mV). For the purposes of the present discussion, we need only note that the bipolar transistor is a purely semiconductor device, and there is no obvious way to incorporate superconductivity into a hybrid device. However other devices of interest were inspired by the bipolar transistor concept.

#### 2.2.1. Hot Electron Transistors

The speed of bipolar devices is limited by the time it takes minority carriers to diffuse across the base. The use of a thinner base reduces this time, but this is of limited use because of the resulting increase in base resistance. In 1960, Mead [21] proposed the metal base transistor (MBT), a unipolar analog of the

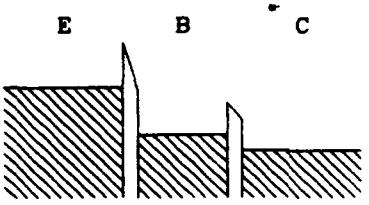


Fig. 2. Schematic band diagram of a MIMIM hot electron transistor. Carriers from the emitter (E) are injected by tunneling into the base (B) (alternatively, thermionic emission over the top of a barrier can be used). Under certain conditions, these "hot" carriers must be collected over the top of the collector (C) barrier before relaxing down to the base Fermi energy and contributing to the base current.

bipolar transistor. Such a device is shown schematically in Fig. 2. The device is based on the injection of majority carriers (electrons) into the base film; these carriers have a large kinetic energy in the base (i.e., they are "hot") and are thus energetically separate from the equilibrium carriers in the base. The control and controlled fluids in Landauer's model are the majority equilibrium and minority hot carriers in the base (in analogy to majority holes and minority electrons in the base of an npn bipolar transistor). These hot carriers must be collected before they lose so much energy or normal component of momentum that they cannot surmount the base–collector barrier, in which case they scatter and become mixed with the controlling equilibrium carriers. A number of versions of this basic device have been introduced [20]. For example, it is possible to use a semiconductor as the collector, with the base–collector barrier formed by the Schottky barrier existing at the interface. Thus, NININ, NINSm, and SmNSm are among the possible structures.* Hot carrier injection into the base can be accomplished by tunneling through, or thermionic emission over, a barrier. All of these devices are "hot electron transistors" (HETs). The ultimate goal in an HET device is ballistic transport, in which electrons traverse the base region without scattering, and emerge from the base with their full injection energy, since this promises the ultimate in device speed (or at least base transit time) and current gain. For a thorough

* A comment on notation: In describing the various device structures of interest here, N denotes a (normal) metal, M a metal which can be either normal or superconducting, Su a superconductor, Sm a semiconductor, and I an insulator. Thus, normal and superconducting oxide tunnel junction structures are NIN and SuISu, while the general case is MIM. A Schottky contact is NSm. In Sections 3 and 4, S will be used to denote a superconductor since it is unambiguous in absence of semiconductors in the device structure.

discussion of HETs, the interested reader is referred to the literature, accessible through various recent reviews [22–25].

The early interest in hot electron transistors waned, due to fundamental problems with achieving current gain. The common-base current transfer ratio $\alpha$ (the ratio of collector current to emitter current) must approach unity if the device is to have a useful current gain $\beta = \alpha/(1 - \alpha)$, the ratio of collector to base current in the common-emitter configuration. Losses in the base and quantum mechanical reflections at the base–collector barrier tend to limit $\alpha$ to rather small values in MBTs. Large $\alpha$ values were occasionally reported, but such results were usually attributed to pinholes; measurement of $\alpha$ alone is of limited value. The permeable base transistor (PBT) [26], a device of substantial current interest for high frequency applications, uses intentional pinholes in the base to achieve a vertical FET with many parallel channels.

Interest in hot electron transistors has revived in recent years, with impressive progress due largely to technological advances that make it possible to form an entire multilayer device structure from epitaxial, lattice-matched heterojunctions, allowing a reduction of interfacial scattering, electron–electron scattering in the base, and quantum mechanical reflections. A version of Mead's tunnel injection device can be made using doped GaAs for the metal layers and undoped AlGaAs (which has a larger bandgap) for the insulating barriers [22]. Injection via thermionic emission over a barrier is used in planar doped barrier (PDB) device [27]. Experimental demonstrations of these devices have been made, as described in recent reviews [23,24,25]. In particular, ballistic operation in devices with significant current gain has been demonstrated. In vertical pseudomorphic devices [28], $\beta$ values of 27 and 41 have been reported at 77 and 4.2 K, while $\beta$'s in excess of 100 have been obtained in lateral 2DEG devices [29] at 4.2 K.

Much of the interest in ballistic devices has centered on the extremely short ($< 1$ ps) base transit time that should be possible. The response of a real device is limited by the time required to charge the device capacitance, which depends upon base resistance. Estimates of the ultimate switching time of these devices range from less than a picosecond [24] to several picoseconds [23].

Large base resistance, due to the limitations imposed by the trade-off between base doping and base thickness, is a significant potential problem in these devices. Two possible solutions are the use of materials that have long ballistic mean free paths [30], and the use of a high mobility two-dimensional electron gas (2DEG) in the base to improve conductivity [31] and reduce impurity scattering. The recent work of Levy and Chiu [32] on a device structure aimed at room temperature operation has a number of features that

make it interesting for this discussion. The device consists of a $AlSb_{0.92}As_{0.08}$ emitter, a thin InAs (2DEG) base, and a GaSb collector on a GaSb substrate. The use of a wide gap emitter allows room temperature operation. Non-alloyed barrier-free ohmic contacts are made to the InAs base. In principle, scattering rates for hot electrons are low in InAs [30], although scattering for the case of transport normal to a 2DEG is not presently understood.

Quantum mechanical reflections at the base–collector interface represent a fundamental problem for hot electron devices [31,33]. The problem is much larger with a metal than with a semiconductor base, due to the large value of the Fermi energy in a metal. The ratio of barrier height to electron energy is the important parameter in a simple analysis [31]; this ratio must be small to minimize reflections. The point is that these energies are measured from the bottom of the conduction band, and the large value of the Fermi level makes the ratio large. The use of a collector material having a small effective mass (compared with that of the base material) can greatly reduce the reflection problem [34], as originally indicated by Crowell and Sze [35]. In fact, a simple analysis indicates that reflections can be virtually eliminated by matching the hot electron velocities in the base and collector layers [32] by a proper choice of materials (effective masses). Grading of the base–collector barrier, a straightforward matter with heterojunction devices, can also help in minimizing reflections. If, however, carriers are largely unscattered in traversing the base, the effect of reflections on current gain should be drastically reduced anyway [25], because the reflected electrons will also be largely unscattered, either re-entering the emitter or making another pass through the base (in neither case do they contribute to losses in the base). In many cases, this amounts to allowing reflections to be virtually ignored. If this prediction is correct, it is very important in that it removes a major objection to hot electron transistors in general, and metal base transistors in particular. This may be key to the operation of a superconducting version of the metal base transistor.

### 2.2.2. Superconducting-Metal Base Transistor

The fact that base resistance has always been an issue with junction transistors leads to consideration of a superconducting base, which would eliminate base resistance althogether (making base inductance an important parameter). Aside from considerations of operating temperature, this is an obvious step forward for metal base transistors. However, it is backward step along the path that hot electron device work has followed in recent years, in that the tendency has been to use low carrier densities, or even a 2DEG, in the base to minimize

both electron–electron and impurity scattering. The mean free path for ballistic motion should be very short in a metal due to the large carrier density, and the presence of superconductivity does nothing to alter this fact. In fact, mean free paths in high-$T_c$ oxide materials are extremely short, a significant drawback for higher temperature devices. Of course, it is the ratio of base thickness to effective mean free path that matters, and zero base resistance should allow the base layer to be extremely thin, down to tens of angstroms.

Tonouchi *et al.* have studied a metal base device, which they named Super-HET, both theoretically [34] and experimentally [36]. The device has a SmSuSm structure. Referring to Fig. 2, the emitter is a degenerate semiconductor (GaAs), the emitter–base insulator is a depletion region (GaAs–Nb Schottky barrier), the base is a superconductor (Nb or NbN), the base–collector barrier is a second depletion region (Nb–InSb Schottky barrier), and the collector is a second degenerate semiconductor (InSb). The device has an inverted structure: InSb, which forms low Schottky barriers to metals, is deposited in polycrystalline form on the base film; GaAs is the substrate.

Electrical measurements of the common-base characteristics of Nb (20–40-nm thick) and NbN (60-nm thick) based devices at 4.2 K were consistent with $\alpha$ values of $\approx 0.6$–$0.8$ and $\approx 0.6$, respectively. Assuming that $\alpha \propto \exp(-d/\lambda)$, where $d$ is the base thickness, the effective hot electron mean free path $\lambda$ was inferred to be 70 nm or greater in the Nb case (and even larger for NbN). This hot electron mean free path was measured to be 110 nm in Nb at 4.2 K in a separate set of related experiments [37]. Of course, a simple measurement of common-base characteristic does not differentiate between ballistic electrons and electrons that have undergone scattering but which still have sufficient forward momentum to surmount the collector barrier (thus, the claim of a measurement of a ballistic mean free path, implied by the title of reference [36], was later withdrawn [34]. For Nb, the same group calculated a ballistic mean free path [34] of $\approx 14$ nm at low temperatures, limited by phonon emission (the component due to electron–electron scattering was estimated to be exceed of 200 nm for all energies of interest).

It is difficult to establish the absence of pinholes that may allow PBT action. A similar situation exists in the case of epitaxial Si–$CoSi_2$–Si devices [38], and analysis of electrical measurements in conjunction with careful electron microscopy studies allows some light to be shed on the pinhole question. It is clear that this sort of analysis or, even better, hot electron spectroscopic experiments [24], are needed on the Super-HET structure to eliminate the possibility of pinholes, and more experimental work is needed to establish reliable values for both ballistic and non-ballistic mean free paths.

The behavior of Nb-polycrystalline InSb–Au structures used to study the base–collector interface was non-ideal, although this was blamed on alloying at the interface with the Au contact and not the Nb. The emphasis of recent experimental work [39] has been on epitaxial growth of Nb on the GaAs emitter. A decrease of Nb film quality with decreasing film thickness for non-epitaxial Nb causes a degradation of performance in thin base devices [37]. However, much earlier hot electron transistor work emphasized the base–collector interface as being most important.

The work described above used an inverted SmSuSm structure with the emitter on the bottom. The device can also be made with the collector as the bottom layer. It is also possible to use a NISu emitter–base structure-[40]. With this structure, the emitter, emitter–base barrier, and base can be polycrystalline or amorphous layers deposited on the single-crystal semiconductor collector (alternatively, the base film could be grown epitaxially on the collector). Techniques for making well-controlled barriers and thin superconducting films are readily available from Josephson technology. The emitter can even be superconducting. The collector can then be any suitable semiconductor, either the substrate itself or a lattice-matched or strained (pseudomorphic) layer [41]. Heterojunction collector structures are then possible, allowing low voltage devices and hot electron spectroscopy. The possibility of studying ballistic transport in metals is interesting even if these transistors do not prove to have practical applications.

The operating voltage of heterojunction devices can be quite small, far below the intrinsic voltage scale of bipolar devices, making them interesting from the point of view of low power dissipation. The voltage scale is set by barrier heights, which are controlled by composition and doping. In principle, arbitrarily low barriers are possible. Experimental explorations of low barriers have been made [14,42,43]; however, the question of fundamental limits is still open. Control of barrier heights, doping uniformity (including random density variations), quantum mechanical reflections, and base resistance represent significant problems.

The voltage scale for a semiconductor–collector metal base devices is determined by the Schottky barrier height of the base–collector contact, typically hundreds of meV. This is far larger than the characteristic voltage associated with superconductivity, the energy gap. It is a limitation for low temperature applications, where a meV (or few tens of meV) scale is more appropriate. The base–collector barrier height is a more or less intrinsic property of the particular metal–semiconductor system used. With most III–V semiconductors, Schottky barrier heights do not vary much for dif-

ferent metals. They are fixed by the pinning position of the Fermi level at surfaces or interfaces with metals. This pinning usually occurs at about midgap; however, it varies widely with composition. In some materials, such as InAs, pinning occurs in the conduction band, resulting in a negative Schottky barrier (accumulation layer) to n-type material. In ternary system, such as $In_xGa_{1-x}As$, the Schottky barrier height varies with composition $x$, from roughly 0.7 to $-0.2$ eV. Thus, ternary materials are of interest for structures in which low barrier heights are desirable.

### 2.2.3. SUBSIT

Even prior to the work discussed above, Frank *et al.* [44] proposed SUBSIT (SUperconducting-Base Semiconductor-Isolated Transistor), a superconducting metal base transistor that avoids the difficulties of ballistic mean free path and quantum mechanical reflections and actually resembles a bipolar transistor. The device structure is illustrated in Fig. 3a. The device has a MISuSm structure, with the MISu being the emitter–base section (the emitter can be superconducting). Quasiparticles (essentially unpaired electrons) are injected into the base film by tunneling. Unlike the usual metal base transistor, these quasiparticles do not need to be "hot". They can be injected with energies just above the superconducting energy gap in the base, or they can relax down to this level by scattering. The injected quasiparticles diffuse across the base, and gain in the device depends upon their being collected before they recombine into pairs. Unlike hot electron transistors, however, they do not have to enter the collector on the first attempt. This improves the collection

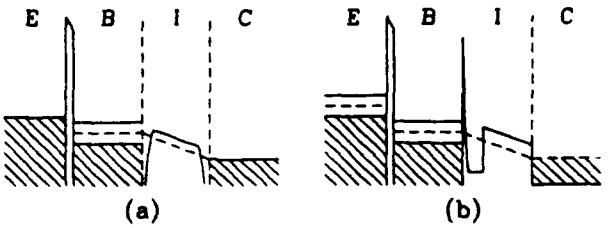


Fig. 3. (a) Schematic diagram of SUBSIT [44]. Single electron tunneling is used to inject electrons into the superconducting base. The injected quasiparticles diffuse across the base and are collected before they can recombine into pairs that contribute a base current. The isolator (I) allows a collector bias without imposing a barrier between base and collector that would tend to trap carriers in the base. (b) Schematic of recent realization of SUBSIT [47]. The emitter and base are Nb, with an Al oxide barrier. The isolator and collector are an $n^+$InGaAs–InAlGaAs–$n^+$InGaAs heterostructure. The barrier between base and isolator is very thin in order to minimize its role in current transport.

efficiency, but increases the base transit time (it is not a ballistic device). However, as mentioned above in connection with hot electron transistors, this time is not the dominant one in determining device speed in the picosecond regime, and simulations that include transport and charging time indicate that SUBSIT should be a fast device [44], with response in the 10 ps range. In contrast to the Super-HET, the operating voltage scale for SUBSIT is set by the base energy gap voltage. Current gain depends on the base transit time, the effective base quasiparticle recombination time, and a transmission factor. Rough estimates indicate that this gain can be large [44].

The two "fluids" in the base are the pairs (majority carriers) and quasiparticles (minority carriers) in the superconductor, in close analogy to the bipolar transistor. This device is unique in that it is consistent with an old suggestion by Landauer [4] that that analogy might somehow be exploited, and it is probably as close as one can get to having a superconducting bioplar transistor, that is, one in which the base "fluid" has no electrical resistance. Complementary devices (i.e., both hole and electron based) are possible.

As in other metal base transistors, the key to SUBSIT operation is the base–collector contact, the realization of which will be key to making the proposed device work. Frank *et al.* [44] refer to the semiconductor layer in contact with the base as the "isolator", the collector being the metal (or heavily doped semiconductor) contact to this layer. Contacts to the isolator must not only be ohmic, but barrierless (on the scale of the superconducting energy gap), since the presence of a barrier would tend to trap quasiparticles in the base, decreasing the current gain and slowing down the device. The isolator also serves the function of preventing direct pair-breaking tunneling between base and collector; this process represents a potential leakage current. The isolator must be frozen out since thermally generated carriers also represent a source of leakage. Of course, the operating temperature must be low enough that thermally generated quasiparticles in the base do not contribute a significant leakage current or source of quasiparticles for recombination.

A metal (superconducting base)–semiconductor (isolator) contact having a barrier height smaller than the superconducting energy gap has yet to be realized. A material in which the Fermi level pinning position is in the conduction band (or valence band for p-type material) forms contacts with negative barriers, so that an accumulation layer forms between base and collector (this type of contact was assumed by Frank *et al.* [44]). However, the effect of such a layer, which may act as a two-dimensional proximity effect superconductor, has not been explored. A contact having no barrier (either

positive or negative) is possible in principle using ternary semiconductors [45], such as $In_xGa_{1-x}As$ (see above discussion). However, the barrier height change with composition $x$ is of order 10 meV/at.%, so that requirements on the ability to control composition (spatial distribution on a wafer and between fabrication runs) are stringent. Also, given the discrete nature of dopants and the relatively large local variations of potential on the meV scale of the superconducting gap, it is not really permissible to use the usual continuum picture for the spatial variation in semiconductor bands. High-$T_c$ superconductors allow some relaxation of requirements, due to the presumed order of magnitude or so increase in the gap, but the problem is still present.

Tamura *et al.* [46] proposed a similar structure and made several experimental attempts at realizing an operating device. Their original structure consisted of Nb–$Al_2O_3$–Nb–nInSb (note the use of a superconducting emitter) and had a common base current transfer factor $\alpha$ of order $10^{-4}$. There was no reference to an isolator in their original proposal. (The energy band diagram which appears in [46] should include a substantial Schottky barrier, much larger than the superconducting energy gap, between base and collector.) A later design [47] that included an isolator replaced the InSb collector with a heterostructure based on nInGaAs and InAlGaAs, lattice-matched to an InP substrate. The structure is shown schematically in Fig. 3b. An $\alpha$ of $\approx 0.3$ was reported for this device in a preliminary experiment.

The philosophy followed by this group has been to accept a small, and therefore very transmissive, barrier at the base–collector interface, rather than to aim for a barrierless contact. (Note that there are no ternary compounds that give barrierless contacts and also lattice-match to reasonable substrates, such as GaAs and InP, so that pseudomorphic structures would have to be used [41].) As mentioned above, the barrier should affect speed and current gain, which will presumably be studied in future experiments. This group has also done modeling of the device [48] and has predicted large achievable gain and $\approx 10$ ps response.

In summary, the present situation for superconducting junction transistors is as follows: There are two devices, one (Super-HET) simply substitutes a superconductor for the normal layer in a well-known device (MBT) and the other (SUBSIT) involves a novel control principle. For the SUBSIT, it is the case that the operating voltage is set by the superconducting energy gap, but this is also the more difficult device to realize, the principal problem being the very low barrier metal–semiconductor contact for the base–isolator junction. In fact, no convincing demonstration has been made to date.

## *2.3. Field Effect Transistors*

### 2.3.1. Josephson Field Effect Transistors

Field effect transistors are pervasive in low temperature semiconductor electronics because their power dissipation is small (relative to bipolar devices), making them attractive for high circuit density applications. Lowering the operating temperature (at least down to 77 K) results in improved performance [8], particularly in such devices as high electron mobility transistors. A number of years ago, a field effect transistor with superconducting source and drain electrodes was independently proposed by Silver *et al.* [49] and Clark *et al.* [50]. The device is a gate-controlled Josephson weak link (JOFET), illustrated schematically in Fig. 4. The weak link is SuNSu-like (often denoted SNS [51]), with a semiconductor as the normal material [52] (i.e., the structure is SuSmSu). The link (channel) is superconducting due to the proximity effect [53]. Cooper pairs leak from the superconducting source and drain electrodes into the semiconductor (the semiconductor must contain mobile carriers at the operating temperature, which can be achieved by using heavy doping or an inversion layer). Overlap of the proximity effect regions of the electrodes results in Josephson coupling in a suitably short link, with a coupling strength (i.e., critical supercurrent) that depends on the carrier density in the link region. Use of the field effect to control carrier concentration is one means of controlling both super and normal currents in the device.

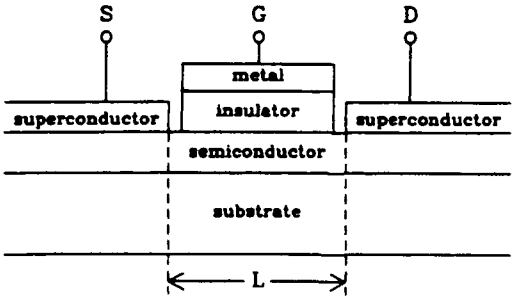


Fig. 4. Schematic diagram of a Josephson FET (JOFET). Superconductivity is induced in the semiconductor by the superconducting source (S) and drain (D) electrodes. A supercurrent is possible if the separation $L$ of these electrodes is no more than a few coherence lengths in the semiconductor. The gate (G) controls both super and normal currents in the device by modulating the properties of the semiconductor channel. Although a metal–insulator–semiconductor (MIS or MOS) FET is illustrated, other types of gates are suitable as well.

Although a MISm gate structure (MISFET) is illustrated in Fig. 4, pn junction (JFET), metal–semiconductor (MESFET), high electron mobility (HEMT), and other devices are also possible. The JOFET represents a limiting case of conventional (nonsuperconducting) FETs. Any FET with superconducting source and drain metallizations should, in principle, exhibit a supercurrent (at low enough temperature), although it will be trivially small unless the channel is quite short and the contacts carefully made. The basic physics and expected device properties from JOFETs have been discussed in a number of papers [11,50,54,55,56]. We review here the experimental results to date and then discuss the relevant physics and device properties.

The first experimental demonstrations of gate-controlled supercurrents were made on MISFET structures. Nishino *et al.* [57,58] used an Al gate and thermal oxide on the back of a heavily doped Si membrane that had a Pb-alloy weak link formed on top (the Si membrane acted as the link material). Although the normal conductance was negligibly affected by the gate, the critical current was varied by more than an order of magnitude with a gate voltage swing of $\sim 100$ mV. The membrane structure was not well enough characterized to model it in detail; however, the large response to a gate voltage that only slightly perturbed the channel carrier density was quite surprising [59] (the device would not be expected to function as an inverted-gate FET with even several volts applied to the gate), and the experiment has evidently not been reproduced.

In another MISFET experiment at about the same time, Takayanagi and Kawakami [60,61] used deposited gate dielectrics and Nb electrodes in both n- and p-type InAs weak links. Unfortunately, it is not presently possible to fabricate high quality gates on InAs, and the devices responded only weakly to rather large gate voltages, a major drawback.

InAs does have two attractive features for JOFET applications. The first is a low effective electron mass, which means that the coherence length can be larger than in a higher mass material, allowing a larger spacing between source and drain electrodes and/or a larger supercurrent, as discussed below (other III–V materials, such as GaAs and InGaAs, also have relatively small electron masses). The second is strong pinning of the Fermi level in the conduction band at interfaces, which makes barrier-free metal–InAs contacts possible, a major advantage. Unfortunately, this same pinning severely limits the effectiveness of NISm gates. Also, a conducting layer is present over the entire surface of an InAs wafer, making it difficult to isolate devices from each other. This difficulty was avoided by Kleinsasser *et al.* [62], who used an insulating GaAs substrate and obtained excellent characteristics for mesa-isolated weak

links in unstrained InAs layers grown by MBE. It was intended to extend this structure to FETs using pseudomorphic heterostructure gates, with InGaAs or InAlAs as the dielectric, allowing the problem of Fermi level pinning at the interface between InAs and the gate insulator to be circumvented. Unfortunately, although initial results were promising, MISm capacitors of sufficiently high quality to be of real interest for gate dielectrics were not produced [63], and it is not known whether or not this approach is really viable. Future use of InAs as an FET material depends on the development of an adequate gate structure. One possibility based on the unique properties of InAs [49], an InAs JFET, has been proposed [64] that would eliminate the need for an insulated gate.

More recently, what might be called the first superconducting FET, in which both normal and super currents exhibited a significant response to a gate, was reported by Ivanov and Claeson [65]. The device was a GaAs–AlGaAs HEMT with Nb electrodes. This materials system, like Si–$SiO_2$, is widely used for semiconductor devices, and the device behaved qualitatively as expected, although only a single device was reported. A serious problem with this type of structure is the Su–Sm contact. The JOFET requires a strong proximity effect coupling between the superconducting electrodes and the 2DEG channel, and the alloy contact scheme that was used appeared to seriously limit the output voltage range. This issue is discussed in more detail below.

Subsequent to this initial work, a self-aligned coplanar Si-coupled weak link structure was introduced [66] that featured a direct contact between the superconductor and the channel and which should be applicable to coplanar FET devices. This promised to be a major improvement on the original Si membrane device; however, the work was never extended to FETs. On the other hand, channel lengths in more normal FET structures have been pushed to sub-100 nm dimensions. The use of a self-aligned structure in which superconducting source and drain metallizations are as close as possible to the gate does indeed yield devices that act as JOFETs, as demonstrated by Nishino *et al.* [67], who recently reported n-channel Si MOSFETs with 100-nm gate lengths (and source–drain metallization spacings). Nb electrodes contacted implanted source and drain regions, which in turn contacted the 2DEG, which was produced by application of a gate bias in excess of a 0.3 V threshold. Further increases in gate bias increased both the supercurrent and normal conductance in accordance with qualitative expectations.

The materials system that has the lowest Schottky barrier heights and smallest effective mass with which high quality FETs have been produced is

$In_{.53}Ga_{.47}As$, grown epitaxially on InP substrates. Recently, superconducting junction FETs with Nb electrodes that exhibit gate-controlled supercurrent and normal conductance have been demonstrated by Kleinsasser *et al.* [68] with this material. The structure is intended as a model for investigations of physics and device properties. The pn junction gate is below the thin epitaxial channel layer, allowing exploration of the effect of the superconductor–semiconductor contact properties on device performance without affecting gate quality.

### 2.3.2. Semiconductor-Coupled Weak Links

A JOFET is basically a gate-controlled SuSmSu weak link. Much of the relevant physics can be studied using ungated links, for which there is a considerable body of literature. While there has long been work on both SuISu and SuNSu-like sandwich structures [69], which are one-dimensional (1D) in the sense that the superconducting order parameter varies in only one direction, we are principally concerned with SuNSu-like bridge (2D) structures such as that of Fig. 4 (without a gate). Virtually all experimental work on bridges has been on Si [52,58,66,70–73], with two experiments on InAs bridges [62,74] and none on other materials. The focus has been on studying the critical current, which depends on device length, temperature, carrier concentration, magnetic field, and contact properties.

There is no lack of theoretical work in this area. Again, almost all attention has focused on the critical current. The critical current of SuNSu junctions was first worked out by de Gennes [75] for long junctions near $T_c$. Subsequently, Likharev [51,76] worked out a theory for a class of SuSmSu junctions for all lengths and temperatures. Seto and Van Duzer [70] explicitly discussed SuSmSu structures; their result is consistent with de Gennes, except for an unspecified constant prefactor that arises from tunneling through the Schottky barriers at the SuSm interfaces. The problems stemming from the fact that all of the early theoretical work assumed a one-dimensional (1D) device geometry was discussed by van Dover *et al.* [77], who also considered arbitrary boundary conditions in SuNSu structures. It has been argued that this result can be extended to SuSmSu devices [78]. A nice feature of this approach is that a hard to calculate prefactor in the expression for the critical current, which is related to the transmission probability for carriers at the SuSm contacts, can be obtained from independent experiments. In the past ten years, there has also been a significant effort in the Soviet Union on SuSmSu theory, which has been virtually ignored by experimentalists in the West. Both

1D [79] and 2D [80] device geometries have been considered. Finally, there has been significant interest recently in devices in which the Sm layer is a 2DEG, although only 1D device geometries have been considered [81]. (Note that there are a number of differences between various theoretical papers which we do not discuss here: the full temperature range may be covered or only that near $T_c$, Schottky barriers may or may not be included, the treatment may assume the clean or dirty limit, etc.)

The experimental results can be said to agree with theory only in a very limited sense. Virtually nothing in the experiments performed on SuNSu-like SuSmSu junctions to date tests any theory that goes beyond the original work of de Gennes. There is general agreement that the critical current of a long link is exponential in device length scaled by the (temperature-dependent) coherence length in the semiconductor. Little else has been clearly established. For example, the absolute magnitude of the critical current (i.e., the critical current–resistance product) is not understood. This is due in part to a lack of definitive experiments on well-characterized device structures and basic studies of the proximity effect in semiconductors, a situation which has been improving in the past several years. Nevertheless, the size of the critical current (and critical current–resistance product) in SuSmSu weak links [78] and the magnitude of the proximity effect in SuSm structures (as indicated by the reduction of transition temperature [82]) are too large to be consistent with existing theory, which thus appears to be inadequate even though experiments have so far made contact with only the most basic theoretical predictions.

What emerges clearly from the literature on this subject is that the properties of SuSmSu weak links and JOFETs depend critically on two major factors, the SuSm contact and the coherence length in the semiconductor. It is the former factor which has received inadequate attention. We will concentrate on the SuSm contact issue first, followed by a discussion of the length scale.

### 2.3.3. Superconductor–Semiconductor Contacts

SuSmSu and SuNSu devices are often pictured as being equivalent; however, the presence of (insulating) Schottky barriers at the SuSm contacts invalidates this simple picture, making SuSmSu equivalent to SuINISu, and not SuNSu. The penetration of Cooper pairs into the neutral (conducting) region of the semiconductor is limited by the requirement that they must tunnel through these barriers [70], drastically reducing the proximity effect. This implies that SuSmSu weak links should have very small critical currents (this was

recognized in the early FET proposals [49,50], which emphasized the use of materials such as InAs that do not form Schottky barriers at metal contacts).

It has been well established that the proximity effect can be observed in SuSm contacts, through the experiments involving SuSmSu weak links. However, the simplest demonstration of the effect is the depression of the Su transition temperature of SuSm bilayers due to leakage of Cooper pairs into into the Sm layer; this is a widely used technique in SuN systems [53]. Leakage of pairs out of the superconductor into a normal material can cause an observable lowering of $T_c$ if the superconductor is only a few coherence lengths thick. For SuSm systems, such measurements have been reported for Nb on p-Si [82], for which a value for the coherence length was extracted, directly verifying the proximity effect in an SuSm system. However, it is the number of pairs that penetrate into the normal layer, rather than how far they penetrate, that is most important for the proximity effect [83], a point which is generally ignored.

Study of the $T_c$ dependence of thin superconductor films on thick semiconductor layers with varying doping can directly study the boundary conditions for the pair amplitude (the variation of barrier thickness or tunnel probability with doping is inherently more important than the variation of normal coherence length). This is qualitatively evident in the experiment of Hatano *et al.* [82], which showed $T_c$ reductions (from the bulk value) of 7–23% for 40 nm Nb films on $4.5-30 \times 10^{18}\,\mathrm{cm}^{-3}$ pSi. The tunneling probability through a Schottky barrier for a particle of mass $m$ and charge $q$ is (in the WKB approximation) [84] $P \sim \exp(-E_B/E_{00})$, where $E_B$ is the barrier height and $E_{00} = (q\hbar/2)(N_D/\varepsilon_s m)$. Here $N_D$, $\varepsilon_s$, and $m$ are dopant density, dielectric constant, and effective mass, respectively. Using a value of $E_B = 0.41$ eV for the Schottky barrier height of Nb on p-Si [85], $\mu = 100\,\mathrm{cm}^2/\mathrm{V\text{-}s}$, and $m = 0.16\,m_e$, one obtains $E_{00} = 0.074$ eV and $P$ ranges from $2 \times 10^{-7}-2 \times 10^{-3}$ in these samples. This implies a significant and sample-dependent reduction of the pair amplitude in crossing the SuSm boundary, which is inconsistent with the large observed changes in $T_c$. Thus, Cooper pairs appear to penetrate more easily into the semiconductor than expected. It may well be that what is being tested in all of these experiments is the breakdown of the simple tunneling theory for Schottky contacts. Recent theoretical work [86] suggests that the zero bias conductance of a Schottky contact may be significantly higher at large dopings than is generally believed [87]. One potentially important effect is the breakdown of the continuum band picture for the barrier, due to the discrete nature of the charged dopants that are responsible for the depletion region; this is important for thin barriers. Experimental measurements of

contact resistances are difficult in the high doping limit and proximity effect-related measurements are more sensitive, making them rather interesting in this context.

In a second direct demonstration of the proximity effect in SuSm contacts, Nishino *et al.* [88] used tunneling spectroscopy to study SuSm bilayers, observing both the induced gap in the semiconductor and the dependence of the gap in the superconductor on changes in carrier concentration in the semiconductor (due to changes in dopant density and applied gate voltages). Again, the size of the effects is surprising, given the expectation that the pair potential in the semiconductor should be reduced by tunneling, making these effects negligibly small. This type of bilayer $T_c$ experiment can also be used to study contact processes, for example, chemical or sputter etching to remove oxides, since the $T_c$ reduction rapidly disappears if an oxide (or. other insulating) layer exists at the SuSm contact. Also, the sensitivity to Schottky barrier thickness makes this a potentially interesting probe of ohmic contacts (limited, of course, to superconducting metals).

The critical current $I_c$ and the critical current–resistance product $I_cR_n$ should be reduced by a factor of order $P^2$ from the values expected from a perfectly transmissive barrier [78]. Yet the observed $I_cR_n$ products [52,58,68] are not much smaller than the value expected for ideal Josephson junctions [89], consistent with the above discussion. Experiments on Super-Schottky diodes [90] demonstrate that SuSm interfaces act as SuIN tunnel junctions. For example, both SuSmSu Josephson junctions and Super-Schottky diodes have been made with Pb (or Nb) on p-Si on the same device structure [72,85]. In this light, the observation of a crossover between SuINISu and SuNSu behavior with increasing channel doping (increasing barrier transmittance), observed in nInGaAs JOFETs [68] with Nb electrodes, is significant. What is needed in the future is more quantitative experiments that relate a measured or inferred barrier transmittance to the JOFET (or weak link) critical currents, or to the strength of the proximity effect (e.g., $T_c$ depression). Such work should lead to understanding of the role of Schottky barrier tunneling in the SuSm proximity effect.

To conclude our discussion of SuSm contacts, we mention some recent work on achieving good superconducting contacts to conventional semiconductors. The role of damage produced by sputter "cleaning" in reducing the barrier height in Nb–Si contacts [91], while not explaining why a proximity effect is seen at all, points up the need for further process studies. In the case of GaAs, Au–Ge contacts with an Nb overlayer have been demonstrated [92]. This, along with the above-mentioned GaAs/AlGaAs MODFET experiment

[65], raises the question of how thick a normal layer between the Su and Sm layers can be tolerated before a significant reduction of the critical current results. Finally, we mention the recent work on InGaAs [68], which takes advantage of reduced effective mass and barrier height to increase the expected tunneling probability by orders of magnitude.

### 2.3.4. Normal Coherence Length

We now discuss the issue of length scale. Near an Su–N (or Su–Sm) interface, the Cooper pair amplitude falls off exponentially with distance into the N (or Sm) layer with a characteristic length [53] which is the distance an electron travels in time $\hbar/kT$. We will refer to this decay length as the normal coherence length $\xi_n$. In the clean limit ($l \gg \xi_n$), $\xi_{nc} = \hbar v_F/2\pi kT$, while in the dirty limit ($l \ll \xi_n$), $\xi_{nd} = (\hbar D/2\pi kT)^{1/2}$, where $l$, $v_F$, and $D$ are the electron elastic mean free path, Fermi velocity, and diffusion constant ($D = v_F l/d$ in a $d$-dimensional material), respectively. In general [83], $\xi_n \approx (\xi_{nc}^{-2} + \xi_{nd}^{-2})^{-1/2}$. In the case of extreme disorder, localization corrections to $\xi_{nd}$ are predicted [93]. The critical current of a proximity effect Josephson weak link (SuNSu, SuINISu, SuSmSu) of length $L$ is exponential in $L/\xi_n$ (for $L \gg \xi_n$ and temperature not too close to $T_c$ or 0), which provides a means for determining the normal coherence length in weak link experiments.

All experiments performed to date have been in the dirty limit. For a three-dimensional semiconductor with carrier density $n$, effective mass $m^*$, and mobility $\mu$ is

$$\xi_{nd} = \left(\frac{\hbar^3 \mu}{6\pi m^* e k T}\right)^{1/2} (3\pi^2 n)^{1/3}. \tag{2.1}$$

High mobility and low effective mass are desirable since a given coherence length can be obtained at a low carrier density, which is desirable if the FET is to be sensitive to gate voltage. The dependence of normal coherence length on temperature is illustrated in Fig. 5 for $n = 10^{19}\,\mathrm{cm}^{-3}$ in n-Si ($m^* = 0.26\,m_e$) and n-InAs ($m^* = 0.023\,m_e$), which were chosen because they are materials of experimental interest with widely differing values of effective mass, and therefore of $\xi_n$. For each material, the solid (upper) curve represents the clean or large mobility limit and gives the upper limit for $\xi_n$ (this limit is not valid for any experiments reported to date). The dashed (lower) curves are for reasonable lower bounds for $\mu$. The shaded region between the two curves indicates the range of possible coherence lengths for the material. $\xi_n$ is significantly smaller in Si than in InAs because of the order of magnitude

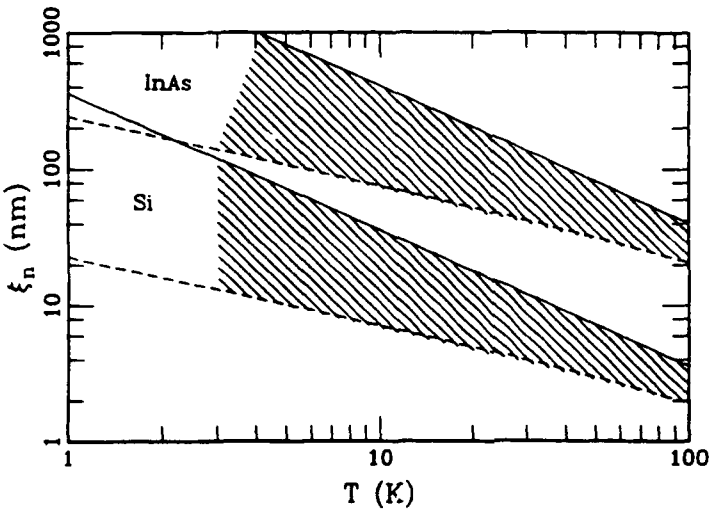


Fig. 5. Temperature dependence of normal coherence length in n-type Si and InAs for $n = 10^{19}$ cm$^{-3}$ (coherence length varies as $n^{1/3}$). The shaded areas indicate ranges of values corresponding to low and high mobility material. Although high mobility is important, the major difference between the materials is the carrier effective mass. This plot is roughly correct for 2DEG materials at mid-$10^{12}$ cm$^{-2}$ densities (the dependence is $N_s^{1/2}$ in the 2D case).

difference in effective mass. Of course, $\xi_n \propto n^{1/3}$. This favors materials that allow the greatest channel carrier density, but increasing $n$ means increasing gate voltage, which, as will be shown below, limits voltage gain, which is already a serious problem.

At 4.2 K, the values for $\xi_n$ in n-Si are in the range 10–100 nm. Useful weak links cannot be longer than a few coherence lengths, so that Si device lengths have an upper limit of a few hundred mm for a high-mobility 2DEG. (The dirty limit curves in Fig. 5 are valid for the 2D case with $N_s = 4.6 \times 10^{12}$ cm$^{-2}$. The clean limit curves are too large by 23%.) Significantly longer devices are possible using low mass materials. For InAs, $\xi_n \approx 0.1$–$1$ $\mu$m (the effective mass used is that corresponding to the conduction band minimum; this is not correct for large carrier densities in such a low mass material, making the InAs $\xi_n$ values optimistic). At 77 K, $\xi_n$ in Si is smaller than $\approx 5$ nm, ruling out FET devices for practical purposes at present. In contrast, the value for InAs is still several tens of nm, so that devices up to $\approx 100$ nm long are possible. Thus, only III–V or other small effective mass materials appear to be interesting for nitrogen temperature operation in the foreseeable future.

Experimental and theoretical coherence lengths are reasonably consistent [52,58,62,70–74], although careful measurements of $\mu$, $m$, and $n$, the parameters needed to calculate the length, are generally lacking. Effects such as the increase of effective mass with carrier concentration due to the breakdown of the parabolic band approximation (particularly significant in low effective mass materials such as InAs) and crossover between dirty and clean limits may account for discrepancies between theoretical and experimental results.

Two-dimensional (2DEG) systems are of interest, and the above coherence length discussion is roughly correct in 2D if $n^{1/3}$ is replaced by $N_s^{1/2}$, $N_s$ being the sheet carrier density. For example, Silver *et al.* [49] were interested in p-InAs, in which the Schottky barrier height exceeds the band gap due to the pinning of the Fermi level in the conduction band, forming a "complete Schottky barrier" and resulting in an electron-rich inverted surface (2DEG) that is in direct contact with the metal. This was evidently the case in one of the early JOFET experiments [60] and should be relevant to MODFETs [65] and MISFETs [67], which are 2DEG devices. There have been no predictions of qualitatively different behavior between 2DEG and 3DEG weak links, and no clear experimental proof of two-dimensional behavior in weak links.

### 2.3.5. Gate-Dependent Critical Current

Recent results of Nishino *et al.* [67] provide, for the first time, data on the gate dependence of JOFET critical currents that can be straightforwardly interpreted. We plot their data, for an n-channel Si MOSFET with Nb electrodes at 4.2 K, in Fig.6 (solid dots). The form

$$I_c \propto \xi_n^{-1} e^{-L/\xi_n} \tag{2.2}$$

for the critical current, derived by Seto and Van Duzer [70], shown by the solid curve, gives an excellent fit. A value of $L/\xi_n = 2.5$ for $V_G = 2$ V was used and the curve was matched to the data at that gate voltage. The gate voltage dependence was assumed to be contained in the coherence length, which, for a 2DEG, is given by

$$\xi_n = \left(\frac{\hbar^3 \mu N_s}{2m^* ekT}\right)^{1/2}, \tag{2.3}$$

where the carrier concentration $N_s = C_G(V_G - V_T)/e$, where $C_G$ is the gate capacitance and $V_G$ and $V_T$ are the gate and threshold voltages. This result is

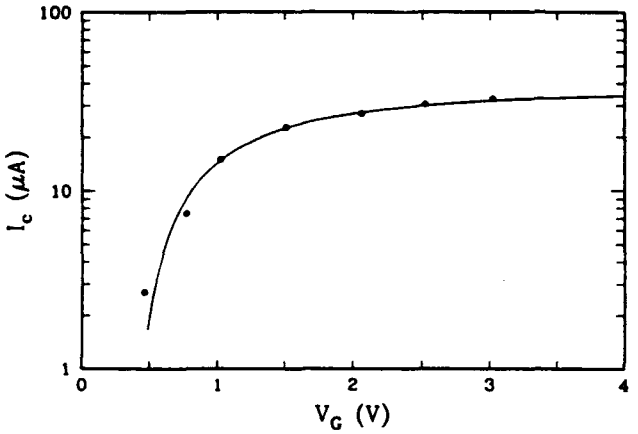


Fig. 6. Dependence of critical current on gate voltage for a n-channel MOSFET with Nb electrodes at 4.2 K [67]. The channel length is less than 100 nm.

important because the data cannot be fit to the form for the critical current derived by Likharev [67]:

$$I_c = R_n^{-1} \frac{4\Delta^2(T)}{\pi e k T_c} \frac{L}{\xi_n} e^{-L/\xi_n}, \tag{2.4}$$

which applies to SuNSu weak links, but is often used for SuSmSu devices. This expression contains an additional gate voltage-dependent factor $R_n^{-1} = eN_s\mu W/L$, where $W$ and $L$ are the device width and length.

The crucial prefactor in Equation (2.2), which is related to the Schottky barrier tunneling probability, is absent; however, it is not likely to depend strongly on gate voltage. A more complete expression, inspired by earlier SuNSu work [75,77] that dealt with varying boundary conditions was obtained by Kleinsasser [11,78]:

$$I_c = R_n^{-1} \frac{\pi\Delta^2}{2ekT_c} \frac{\rho_n m_s}{\rho_s m_n} A^2 f^2 \frac{L}{\xi_n} e^{-L/\xi_n}(1 + 2r). \tag{2.5}$$

In this expression, the resistivities and effective masses in Su and Sm are $\rho_s$, $\rho_n$, $m_s$, and $m_n$, respectively. $f^2 \sim 1$ is the ratio of the value of the order parameter in Su at the interface to its bulk value (we expect $f \approx 1$), and $A$ is the factor by which the order parameter changes in crossing the SuSm interface. $A$ is related to the Schottky barrier tunneling probability and can be independently determined by experiments such as $T_c$ depression in SuSm bilayers. The last

factor in Equation (2.5) is due to the contact resistance, with $r$ the ratio of the resistance of a contact to the channel resistance (assumed to be small in this discussion). The boundary conditions in an SuSmSu bridge and in the SuNSu structure studied by Likharev are different; in the latter case, a cancellation occurs ($A^2 \approx \rho_s m_n/\rho_n m_s$) that causes $I_c R_n$, rather than $I_c$, to have the dependence given by Equation (2.2). This type of experiment is important because it provides a new means of studying the boundary conditions. Note that the Likharev expression may apply in the case of SuNSu-like SuSmSu structures, i.e., those with barrier-free contacts, as indicated by one experiment on InAs weak links [62]. Equation (2.5) should be valid in SuINISu and SuNSu-like structures, and should be a reasonable basis for future work until a more complete result is obtained.

The effective channel length in this MOSFET is unknown, although it is less than 100 nm. We do know the oxide thickness and the gate bias dependence of $I_c$ and $R_n$. We can rewrite the expression (2.3) for $\xi_n$ as $\xi_n = (\hbar^3\sigma/2m^*e^2kT)^{1/2}$, where $\sigma = L/R_n W$ is the conductivity. For $V_G = 2$ V, with $m^* = 0.19\, m_e$, $W = 60\,\mu$m, and using $R_n = 8.9\,\Omega$ (obtained from Fig. 3 of Ref. [70]), the above value of 2.5 for $L/\xi_n$ means that $L = 26.7$ nm, and therefore $\xi_n = 10.7$ nm with a 2 V gate bias. Using $C_G = 0.345\,\mu$F/cm$^2$ and $V_T = 0.3$ V, a mobility value of 85 cm$^2$/V-s is obtained from $R_n = L/C_G(V_G - V_T)\mu W$. The published resistance and critical current data are all consistent with these parameter values. The channel length inferred is rather short, perhaps due to diffusion of the source and drain implants under the gate.

### 2.3.6. JOFET Device Properties

Although JOFETs are Josephson junctions, device speed and power dissipation are not the same as for digital Josephson technology. The control mechanism is identical to that in conventional FETs, with the same gate voltage swing required in both cases to produce a given change in channel carrier concentration. Switching the device on and off requires the same $CV^2$ energy per cycle in both cases. Also, making the channel superconducting does not change carrier transit time, which represents a limit to the speed of FET devices. The role of superconductivity in a superconducting FET is to change the device characteristics, allowing a zero on-state resistance.

Analysis of the prospects for JOFETs as digital devices by Kleinsasser and Jackson [54] concluded that large-signal voltage gain is the major issue. Using a simple model of Si JOFETs, Glasser [56] analyzed the small signal response,

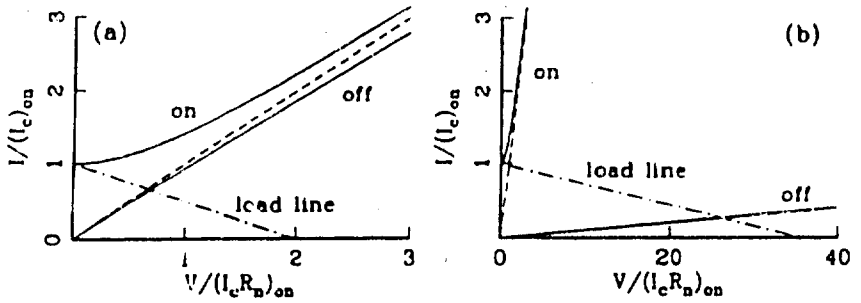


Fig. 7. Schematic IV characteristics of a superconducting FET. (a) If the supercurrent is much more sensitive to the gate field than is the normal conductance, then the resistance change is small between the "on" (large $I_c$) and "off" (small $I_c$) states. The dashed line represents the "on" state in the same device in the absence of superconductivity. Output voltage is limited by the device $I_cR_n$ product, which is much smaller than the gate voltage swing. (b) When both normal and supercurrents are greatly altered by the gate field, the resistance change is large between "on" and "off". Then the output voltage can be made arbitrarily large (i.e., the device can have significant large-signal voltage gain).

also concluding that voltage gain is a problem. The natural output voltage scale of these devices is set by the $I_cR_n$ product of the weak link, and thus limited by the superconducting energy gap, while the input (gate) voltage is orders of magnitude larger. Large-signal voltage gain is possible, but it originates from control of channel resistance, as in an ordinary FET [54], rather than from superconducting properties. This is illustrated in Fig. 7. We define "on" and "off" states corresponding to large and negligible critical current. $I_c$ responds exponentially to gate voltage ($I_c \sim \exp(-L/\xi_n)$, $\xi_n \propto n^{1/2}$, $\Delta n \propto \Delta V_{gate}$), so a large change in $I_c$ can be made with only a small change in $R_n$, as experimentally observed [57]. The "off" output voltage is of order $I_cR_n$ of the weak link in the "on" state, as shown in Fig. 7a, and the voltage gain is $\ll 1$. However, an optimal link is of order one coherence length long, in which case the critical current response is linear, not exponential. In a well-designed device, the output resistance switches between small and large values, and large voltage gain is possible, as shown in Fig. 7b. Note, however, that the difference between the IV characteristics in the "on" state for superconducting and nonsuperconducting electrodes (solid and dashed curves) is not nearly as dramatic in the latter case (i.e., superconductivity makes little difference in the characteristics).

Experimental IV curves of JOFETs [65,67,68] are similar to those in Fig. 7b. Superconductivity affects the source–drain characteristics only at low (mV) voltages, so that the normal resistance for a given gate voltage is constant. The condition $I_cR_n \ll \Delta V_G$ (the gate voltage in excess of threshold)

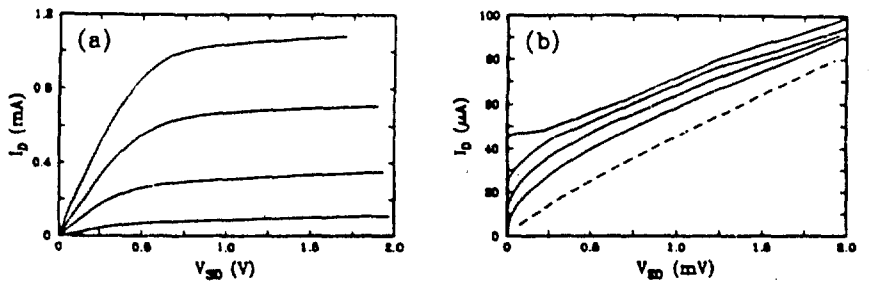


Fig. 8. Current–voltage characteristics of InGaAs JFETs [68]. (a) On a large voltage scale, the devices behave as normal FETs. (b) On a small voltage scale, superconducting effects, such as gate-controlled supercurrent, are evident (the dashed curve was obtained with the electrodes normal).

is equivalent to the condition $I_c \ll I_{sat}$, the saturated source–drain current [54]. Thus, the region of interest for JOFETs is the linear region of the characteristics of a normal FET. Figure 8 shows source–drain current–voltage characteristics for the Nb–InGaAs JFETs of Kleinsasser *et al.* [68], which illustrate these points. On a coarse voltage scale (Fig. 8a), the JOFET exhibits the familiar saturation of current that is characteristic of semiconductor transistors. On a much finer scale (Fig. 8b), the effects of the superconducting electrodes become evident (e.g., the gate-controlled supercurrent).

The small scale of voltages for which superconductivity is significant in the device characteristics makes it vital that the gate voltage swing be as small as possible; this is limited by the ability to control the inversion threshold (or equivalent threshold voltage) and by the gate capacitance (the number of carriers introduced by a given gate voltage). It is difficult to conceive of mV gate voltages, but tens of mV should be possible. Operation at source–drain and gate voltages corresponding to the energy gap of a conventional superconductor is not feasible, so operation at larger voltages using high-$T_c$ superconductors, which offer the possibility of gap voltages of tens of mV, is potentially very important. Since the size of the $I_c R_n$ product is very important for any potential JOFET applications, the origin of the basic lack of agreement between experiment and theory needs to be understood through experiments on well-defined and characterized device structures. At present, we can say that the ratio of the maximum value of the $I_c R_n$ product to the gate voltage swing required to switch off the device is a figure of merit which should be as large as possible if these devices are to be of significance (values well exceeding $\sim 0.1$ would be suitable); this may be possible with thin gates and high $T_c$ materials.

### 2.3.7. Gate-Controlled Superconductivity

Is it possible to make a FET having a superconductor as the channel (rather than depending on the proximity effect)? An insulated gate FET is basically a capacitor having a current flowing along one of the plates (the channel). Changing the voltage between the capacitor plates (the gate voltage) changes the number of carriers in the plate, thereby changing channel properties. Although the idea of using the field effect to vary the surface properties of a superconductor is not new [94], its possibilities are still being explored [95,96]. The most obvious device would have a metal channel and use the gate to change (either increase or decrease) $T_c$ and/or resistivity. Alternatively, one might use an insulating material and use the gate to induce a superconducting channel [96,97].

The large carrier density in a metal makes it difficult to produce a significant change in carrier density with an attainable gate electric field. Using a ferroelectric gate insulator (high dielectric constant), it may be possible to produce a few percent change in a 1-nm thick metal film with $10^{22}$ $cm^{-3}$ carriers [96]. For potential applications, low carrier density metals would be important [95]. For low voltage (low power) applications, however, the limitations of devices of this sort are obvious. Using rather aggressive numbers, a relative dielectric constant of 10 and a gate electric field of $10^7$ V/cm, a change in sheet carrier density of $5 \times 10^{13}$ $cm^{-2}$ is possible, representing a change in carrier density of $10^{20}$ $cm^{-3}$ in a 5 nm metal film. This may be large enough for some interesting physics experiments, but hardly represents an effect that is likely to find practical applications. Considering the possibility of inducing a superconducting surface layer, $5 \times 10^{13}$ carriers/$cm^{-2}$ implies a resistivity of order 10 kΩ/□ (using a mobility of 10 $cm^2$/V-s), making the possibility of inducing even a metallic surface rather marginal. The fact that 5 V is required to produce a field of $10^7$ V/cm, even using a 5-nm thick dielectric, indicates that a metal FET will not be a low voltage device.

## *2.4. Summary*

We have described two distinct types of superconductor–semiconductor hybrid devices that are clearly related to well-known semiconductor devices, namely metal base transistors and FETs. Of the two metal base devices, one (Super-HET) is clearly an extension of existing devices and the other (SUBSIT) embodies new device physics. The field effect device (JOFET) may offer some improvement on conventional FETs, although it may be best viewed as a unique type of controlled Josephson junction with possible

applications completely different from those associated with ordinary FETs [56]. The voltage scale for operation of the Super-HET is determined by metal–insulator barrier heights, and not by the characteristic superconducting scale (the gap). The JOFET voltage scale is determined by the required gate voltage swing, which is also unrelated to the energy scale associated with superconductivity. However, the superconducting gap does sets the voltage range over which superconductivity makes a significant difference in device characteristics. In the SUBSIT case, the operating voltage is determined by the superconducting energy gap, independent of other parameters, giving it a low natural operating voltage. The principal difficulty with this device is realizing a very low barrier metal–semiconductor contact for the base–isolator junction.

These devices tend to rely on narrow gap III–V semiconductors and/or heterostructures based on ternary III–V alloys, materials that are significant in exploratory device research. The hybrid devices we have discussed tend to emphasize low resistance non-alloyed contacts, low barrier heights (even at metal interfaces), high mobility, and low effective mass, and thus tend to rely on materials such as InAs and InGaAs, rather than GaAs, AlAs, and InP. There has been much more success with the rather familiar device material InGaAs than with the more exotic InAs. The materials problems associated with these devices are closely related, so that study of one device should shed light on the others.

Finally, the study of devices like SUBSIT or JOFET, along with related experiments such as those we discussed, are of basic interest because of their relevance to the fundamental physics of semiconductor contacts on the meV scale, particularly superconductor–semiconductor contacts, and because they probe the proximity effect in new regimes, i.e., in situations in which there is a large mismatch between the Su and N materials or in which there is a fairly transmissive tunnel barrier present.

## 3. Nonequilibrium Superconducting Devices

### *3.1. Introduction*

Electronic devices inherently operate out of thermodynamic equilibrium. Some devices, such as the Josephson junction, operate very close to equilibrium, the nonequilibrium aspect in this case being very low energy gradients in the phase of the superconducting order parameter (and negligible deviations of quasiparticle densities from their equilibrium values). Other devices, such as bipolar transistors, involve substantial nonequilibrium carrier

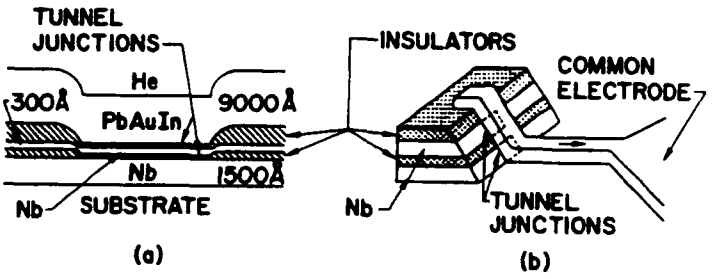


Fig. 9. Schematic representations of nonequilibrium superconducting devices. Planar (a) and edge (b) stacked junction structures. Materials indicated in (a) are those of the quiterons studied in Refs. [1,101], while those indicated for the stacked edge junction structure (b) were used by Buhrman and collaborators [103].

densities. In this section, we focus on attempts to use nonequilibrium superconducting phenomena as the basis for three-terminal devices.

The most commonly investigated nonequilibrium superconducting device structure is stacked back-to-back tunnel junctions, depicted in Fig. 9a. Stacked edge junctions, shown in Fig. 9b, are a variation on this structure that has also been explored. Proposals for stacked-junction superconducting transistor proposals date back to a superconducting gap tunneling device originally proposed by Giaever [98,99], and include a device based on quasiparticle recirculation in the output junction, due to Gray [100], and a gap suppression device called the quiteron, proposed by Faris [101]. Only Giaever's device is based on a microscopic principle that works like the fluid-actuated valve of Fig. 1, which is prototypical of true transistor operation. Consideration of the microscopic mechanism will, however, lead us to propose a second type of stacked junction device that is truly transistor-like.

The other nonequilibrium superconducting device concept that has been investigated is the injection-controlled superconducting link [102]. Planar and edge structures for this device are shown in Fig. 10a,b. These have little microscopic or functional analogy with semiconducting transistors, but have been investigated because devices with substantial gains are easily realized.

We will concentrate here on developments in these classes of nonequilibrium devices that have occurred since the earlier reviews by Gallagher [1] and Buhrman [103]. Thus, we emphasize recent work on quiteron-like devices and injection-controlled links, as well as some new device concepts. The reader is referred to these reviews for more details about earlier work on nonequilibrium superconducting devices. We will have little to say about nonequilibrium devices made with the new high temperature superconduc-

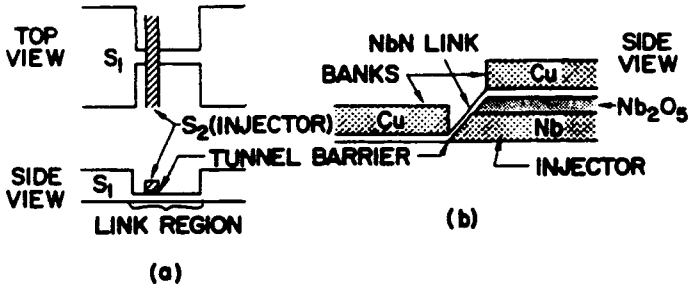


Fig. 10. Planar (a) and edge (b) injection-controlled link structures. The materials for the edge structure are those used by Sprik *et al.* [119].

tors. There has been no investigation of nonequilibrium superconductivity in these materials yet; neither have there been any convincing realizations of tunnel junctions of reasonable quality, which are elements of all known low-$T_c$ devices.

### *3.2. Stacked-Junction Devices*

#### 3.2.1. Tunneling through the Gap of a Superconductor

The first proposal for a stacked-junction superconducting transistor dates back to Giaever's patent on the superconductor tunnel junction itself [98]. Giaever proposed biasing a normal metal–insulator–superconductor–insulator–normal metal (NISIN) sandwich such that no filled energy states in the outer electrodes line up with empty states in the middle electrode, but filled states in one of the outer electrodes do line up with empty states in the other outer electrode. Ideally in such a situation at low temperatures, no current should flow into the middle electrode, but current can flow between the outer electrodes. The superconducting energy gap forms part of the tunnel barrier between the outer electrodes. By varying the location of the energy gap with a bias on the superconductor, the tunnel current between the outer electrodes should be adjustable . Among the device proposals that we consider in this section, this is the one that could operate closest to equilibrium.

There appears to be no published experimental work directed at observing tunneling through the superconducting gap, which is the phenomenon at the heart of this device. In principle, though, there is no reason to believe the effect will not occur. The technology available at the time of Giaever's original proposal, however, would not have been adequate for observing the effect. The

main technological challenge is making the probability of tunneling through the combination of tunnel barriers sufficiently high to pass practical currents while keeping subgap leakage currents through the individual junctions negligibly small. Detailed calculations [99] for ideal quality Nb and NbN junctions indicate that it should be possible to observe the gap tunneling effect at low temperatures (possibly at 1–2 K with NbN), which would be interesting in and of itself.

### 3.2.2. Gray's Superconducting Transistor

The first demonstration of a stacked-junction superconducting device with some transistor-like properties was made by Gray in 1978 [100]. Gray studied a superconductor–insulator–superconductor–insulator–superconductor (SISIS) stack in which the gain mechanism was based on a novel nonequilibrium superconducting effect involving the admixing of electrons and holes in superconductors and their recirculation in the output, or collector, junction. His device consisted of three stacked 300-Å thick superconducting Al layers, with tunnel junctions separating the layers. One junction, called the injector, had high resistance and was operated with bias voltages above its sum gap. It served to inject excess quasiparticles into the middle film. The other junction, the collector, was biased below its sum gap so as to pass only current due to quasiparticles between its two electrodes. It had a low resistance so that the excess quasiparticle density injected into the middle film was readily shared with the collector film. Due to the dual part hole-like and part electron-like nature of superconducting excitations, it is possible for long-lived excitations to tunnel many times back and forth in the collector junction. Loosely speaking, one can think of electron-like tunneling in one direction and of hole-like tunneling in the other direction. The currents due to these processes add, and the result is that each quasiparticle injected through the injector results in several recirculations through the collector, and thus there is current gain. Gray observed a temperature-dependent current multiplication, which was as large as 4 at the lowest temperature he operated the device, $\sim 0.6$ K. There was a large signal voltage loss accompanying this, as the injection was above the $\sim 0.35$ mV sum gap voltage while the collection voltage was below. (A lower gap outer electrode material in the injector could improve the large-signal voltage gain situation.)

Although the electrical characteristics of this device were reminiscent of transistor characteristics, this device, which relies on the quasiparticle recirculation in the output electrodes for gain, has no analog in Landauer's

fluid-actuated valve model (Fig. 1). It is not possible to identify separate control and moving charge. As Gray himself pointed out, the device has a common base gain $\alpha > 1$, whereas transistors have $\alpha \leq 1$. Common base gains $\alpha > 1$ result in the possibility of negative current gain in the common emitter and common collector configurations (negative resistance) and these in turn lead to circuit design difficulties, as pointed out by Gallagher [1]. Gain-bandwidth product estimates of only $10^9$ Hz by Gray [104] and Frank *et al.* [105] for devices with Nb electrodes also lead to the conclusion that this device could not be competitive for high performance digital applications. There has been little new work on this sort of device over the last few years, save for a comment that the recirculation effect could enhance the gain of a quasiparticle trapping and multiplying device proposed by Booth [106].

### 3.2.3. The Quiteron

Faris [101] proposed a SISIS stacked junction device with an operating principle based on nonequilibrium gap suppression in the middle electrode. The gap suppression is caused by injection above the sum gap voltage in one junction, the injector. This modulates the conductivity of the output junction, the acceptor, and its characteristics are expected, at least ideally, to evolve from SIS-like to SIN-like with increasing injection. According to Faris's proposal, there is current gain (over the voltage range at which the output junction modulates) if the output junction can be made to carry substantially more current than the input junction.

Three groups have fabricated and studied quiteron devices, including dc and switching speed measurements [1,101,107,108]. Earlier work [1] had identified isolation as a fundamental problem of this device, symptomatic of the fact that it does not truly function like the fluid actuated valve that is the basis of the transistor. Referring back to the fluid analogy, the lack of isolation of the quiteron device can be seen to stem from the fact that the controlling fluid and the controlled fluid are really the same: the device makes use of only one type of fluid. Whether the source of the fluid is from the injector or the acceptor junction, the gap suppression effects are the same once the fluid is in the middle electrode. The isolation, or nonreciprocity, of a device can be quantified in terms of the ratio of forward to reverse transfer functions. In the only explicit experimental report on this issue, Gallagher [1] measured a 3 : 1 transresistance ratio for the Nb/I/Nb/I/PbInAu quiterons. This asymmetry was higher than expected and was thought to be due to asymmetric cooling of the outer electrodes of the devices. Unfortunately,

this outer electrode response, as we shall discuss in more detail below, is a slow and therefore undesirable part of the device output response.

Recent experimental work has not affected the conclusion that the quiteron lacks isolation, but dynamical studies have confirmed that there is indeed a long time scale associated with a substantial part of the output response. In fact, a fairly consistent picture of the switching performance of quiteron devices emerged from studies of quiteron structures made with three sets of materials: Nb/I/Nb/I/PbInAu studied at IBM [1,101], Sn/I/Sn/I/Sn studied at the University of Tsukuba [107], and NbN/I/PbInAu/I/PbAu studied at Hitachi [108]. The Nb/I/Nb/I/PbInAu quiterons made by IBM, when injected with a $\sim 2$ ns pulse with a $\sim 300$ ps rise time, showed a response with a 1 ns rise time and a 1.7 ns fall time [101]. In other measurements [1], these devices when subjected to a step input signal with a 40 ps rise time displayed an output response on two time scales, with about 50% of the response occurring in less than 100 ps and the other 50% of the response occurring over 10 ns [1]. Measurements of the Sn/I/Sn/I/Sn quiterons were made with 2–3 ns time resolution, but showed rise times of $\sim 15$ ns and decay times of several tens of nanoseconds [107]. The NbN/I/PbInAu/I/PbAu quiterons measured with a Josephson sampler showed a 300 ps turn-on delay, a 300 ps rise time for $\sim 50$–$70\%$ of the output response, and a slow saturation over several nanoseconds [108]. The response times have been discussed in terms of models for coupled nonequilibrium superconductors. Generally the faster response is due to nonequilibrium effects in the middle electrode, while the slower response reflects heating of the entire structure [109,110,111]. In particular, Iguchi's calculations [111] showed that the first 50% of the response could be quite fast.

One way to eliminate the slow response is by efficiently cooling the two outer electrodes by quasiparticle diffusion, as demonstrated in Hunt and Buhrman's double edge structure [112,113]. On the other hand, the improved cooling in their structure eliminated the negative resistance and precluded the large power gains. Another common suggestion is to make the middle electrode out of a very low carrier density material, such as certain oxide superconductors, which could be driven out of equilibrium with far fewer excess quasiparticles than are necessary to heavily perturb the other electrodes. In either case however, one is still left with a device with a bidirectional response, i.e., a device that lacks isolation, a conclusion that Hunt *et al.* [113] have independently reached. Buhrman [103] proposed using injection from one NIS junction to switch from the supercurrent state of a

second junction to the normal state to get a latching device, but one that at least avoided some of the effects the output has on the input of devices operated in the quiteron mode. This particular proposal does not appear to have been pursued experimentally, but it bears some similarities to injection-controlled links, which are discussed below.

### 3.2.4. Superconducting Metal Base Tunneling Transistor

Neither Gray's device nor the quiteron truly functions like a transistor, but one can imagine a purely superconducting, nonballistic, SISIS analog of SUBSIT (which was discussed earlier) that does. The base and collector are separated in this case by a highly transmissive, but low leakage SIS tunnel junction, instead of a special superconductor–semiconductor contact. Gain is possible if quasiparticles injected into the base tunnel into the collector before they have a chance to recombine in the base. Transport through the base need not be ballistic, but the injected quasiparticles must not recombine before they tunnel into the collector if the device is to have gain. The principal difficulty is that as injection is made heavier and heavier, recombination, which is a binary process, becomes more likely, and thus gain becomes more difficult to achieve. It is for this reason that a highly transmissive, yet nonleaky, barrier into the collector is needed. Unfortunately, it is more or less universally observed [114] that as tunnel junction specific resistances go below about $10^{-7}$ $\Omega$-cm$^2$ (current densities above $\sim 10^4$ A/cm$^2$ at 1 mV), junction leakage starts to increase rapidly. Whether the degradation mechanism is universal (for example a higher order tunneling process) or is a materials-related problem is not clear.

One variation of this device [115] that could ease the high current density requirements would use spin-polarized quasiparticle injection [116]. In superconductors with low spin-orbit scattering, the injected quasiparticles should stay spin polarized and be long lived. Even under heavy injection, there would be no opposite spin quasiparticles with which they could recombine. Indeed, the nonequilibrium superconducting properties of spin-polarized quasiparticles have never been explored experimentally, and the observation of an enhanced lifetime would be very interesting and could lead to a new way of measuring spin-orbit scattering rates. Recently demonstrated EuS tunnel barriers with substantially different tunneling rates for spin-up and spin-down electrons [117] might lead to a convenient, low field means of inducing spin polarization.

### 3.3. *Injection-Controlled Links*

By now it should be clear that there is considerable difficulty in realizing a nonequilibrium superconducting device that truly works like a transistor. Considering the fact that, even including the Josephson device, there is no available high gain digital superconducting device, it is worthwhile asking whether or not there are nonequilibrium devices that, while not possessing all the attributes of transistors, possess high gain or some other property that makes their use attractive. There is indeed one such superconducting device that has demonstrated large power gain, the quasiparticle injection-controlled link operated in a latching mode in which quasiparticle injection through a tunnel junction triggers a superconducting-to-normal transition in a current carrying superconducting line. Wong *et al.* [102] first demonstrated such a device in which 1.2 mA of quasiparticle current injected at a few millivolts was able to trigger the switching of a 20-fold greater supercurrent in a long line. The line eventually developed up to a 200 mV voltage drop. The voltage gain can be made arbitrarily large by increasing device length, but the response time governed by "hot spot" propagation increases proportionally. The main early interest in this device was to use injection to produce a controlled Josephson element. That is not our concern here. Rather, we will focus on operating these devices in the regime in which large gains are possible. One conclusion of the reviews of both Gallagher [1] and Buhrman [103] was that this class of devices merited more research because of its high gain potential and structural simplicity. To obtain high speed and low power, a very small microbridge was required [1,103], and, even so, the bridge should best be a low carrier density superconductor [103]. In recent years, Takeuchi and Okabe [118] and Sprik *et al.* [119] have reported on injection-controlled link devices operated in this large signal mode. We will review the results of Sprik *et al.*, which were on submicron devices and included switching speed measurements.

Sprik *et al.* studied small injection-controlled NbN-links made with an edge junction structure (see Fig. 10b). This structure yielded links with very small dimensions using only optical photolithography. NbN was chosen as the link material because it possesses both high critical supercurrent densities and high normal state resistivities. The combination gives the link both favorable on-state and off-state properties and should lead to considerable Joule heating during switching, which, in turn, it was hoped would enhance the speed of the switching process. The NbN link reported on was 0.3 $\mu$m in length, 6 $\mu$m in width, and $\sim 350$ Å thick and carried a critical supercurrent current density of $3 \times 10^5$ A/cm$^2$ at 4.2 K. The quasiparticles were injected from a Nb-injector

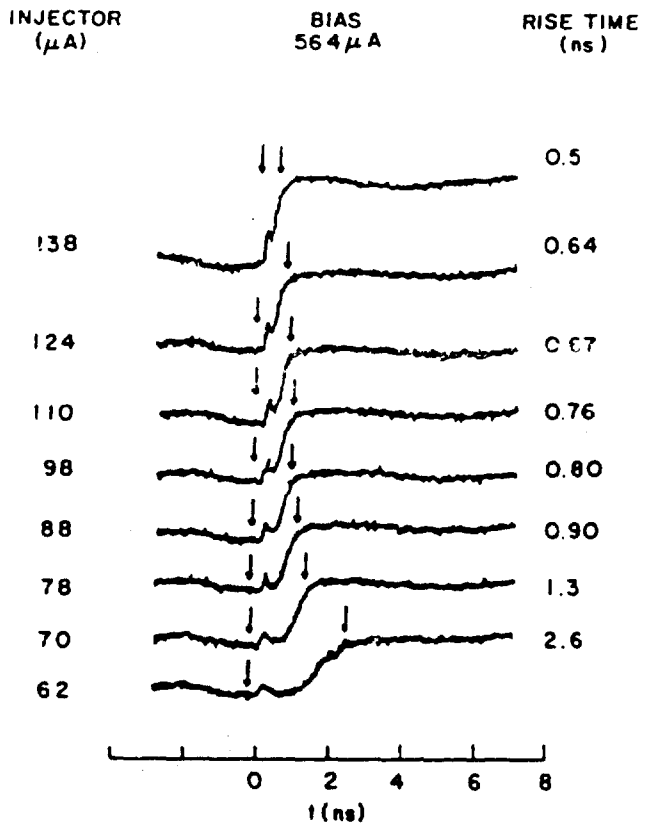


Fig. 11. Observed transient response of the edge injection-controlled link of Sprik *et al.* [119] shown in Fig. 10b. The indicated injector levels are the amplitude of a step pulse applied with a rise time of ~70 ps. The rise times are the delay between the initial spike and the time at which the voltage reaches 80% of the normal state value.

into the NbN-link through a $Nb_2O_5$ tunnel barrier. The dc-characteristics of the link displayed a critical current of 600 μA, which was reduced to zero by an injection current of 55 μA, for a dc current gain of about 10.

Sprik *et al.* tested the switching speed of devices incorporated in on-chip ~50Ω coplanar transmission-line structures using a cryogenic probe and standard sampling techniques with a time resolution of ~70 ps. Figure 11 shows their data for the development of output voltage across links biased in the superconducting state and triggered by a injection current pulse stepped on with a fast (40–70 ps) rise-time pulse. For low injection amplitudes, the link remained superconducting. When the injector amplitude increased, the link switched into the normal state and a voltage developed. Since the leading edge of the injector pulse was much faster than the response of the output, the latter

was a direct measure of the transient response of the device. The leading edge displayed three features: a fast spike followed by a somewhat slower rise over 0.5 to ~2.5 ns followed, in turn, by the final 10–20% of the turn-on that developed rather slowly over several nanoseconds. The overall rise time depended strongly on the injector current and increased when the sum of the injector current and the bias current approached the critical current of the link. The short spike was not due to electrical cross-talk.

Sprik *et al.* interpreted their results using an extension of a phenomenological model introduced by Tinkham [120] for such supercritical microbridges. Microbridges driven by step-wise supercritical currents display superconducting-to-resistive transitions that are similar in both the overall rise time and in the presence of the initial spike, which was due to a kinetic inductance effect. Tinkham's model combined a time-dependent Ginzburg–Landau equation with an effective temperature description of the quasiparticles, and Sprik *et al.* added a direct injection term. The predictions for the injection-driven microbridge at least qualitatively described the switching data. The overall time dependence was similar to that of supercurrent-driven microbridges, but the magnitude of the predicted spike was somewhat smaller for the case of quasiparticle injection. Extensive overdrive of the injection enhances speed, but at the expense of current gain. Sprik *et al.* concluded that the observed switching behavior was governed by condensate dynamics, which in turn was driven by the direct injection of quasiparticles. There was no evidence for a hoped-for enhancement of switching speed due to the large amount of Joule heating that eventually developed in these (short) links. (Hot-spot propagation driven by Joule heating would be the dominant factor in the time development of a normal region in a long line.)

This edge injection-controlled link experiment was on about as small a dimensional scale as is practical, but still did not result in sub-100 ps response. The only further means of achieving high speed in such a heavily driven nonequilibrium device is to substantially lower the carrier density. To estimate the requirement, we note that for substantial gap suppression the nonequilibrium quasiparticle density must be of order the critical density $n_c \approx 0.4 \times 2N(0)\Delta(0)$, where $N(0)$ and $\Delta(0)$ are the density of states at the Fermi level and the zero-temperature energy gap of the film. The required injection (input) current is $J_{in} = en_c d/\tau$, where $d$ is the thickness of the perturbed film and $\tau$ is the effective relaxation time for the excess quasiparticle population, which should be of order 10 ps. The film thickness has some practical lower limit, say $d \sim 10$ nm. For a reasonably high quality tunnel injector, $J_{in}$ is

limited to $\sim 10^5$ A/cm$^2$, so that the product $N(0)\Delta(0)$ must be less than $\approx 8 \times 10^{18}$ cm$^{-3}$. For a low-$T_c$ material, $\Delta(0) \sim 2$ meV so that $N(0)$ would have to be about $4 \times 10^{21}$ cm$^{-3}$eV$^{-1}$, which is relatively low, but well within the range of $BaPb_{1-x}Bi_xO_3$ with $N(0) \approx 10^{21}$ cm$^{-3}$eV$^{-1}$ [121]. For a high-$T_c$ material, $\Delta(0)$ should exceed 20 mV, so that $N(0)$ must be less than $4 \times 10^{20}$ cm$^{-3}$eV$^{-1}$, which is somewhat below the measured mobile carrier densities of $2 \times 10^{21}$ cm$^{-3}$eV$^{-1}$ that are representative of $La_{1.85}Sr_{.15}CuO_4$, $YBa_2Cu_3O_{7-x}$, and $Bi_2Sr_2CaCu_2O_8$ (the 80 K phase) [122]. Nevertheless, superconductors with carrier densities close to what would make these devices interesting certainly exist, but it is less clear that device structures with sufficiently high quality elements, e.g., high current density tunnel junctions, can be made with such materials.

With regard to using the high temperature superconductors in nonequilibrium superconducting devices, the lack of any experimental work makes it worthwhile to make only a few additional comments. In general, the times involved for nonequilibrium effects get faster as temperature increases. This implies improved device performance, but it also means that it becomes harder to decouple the electronic excitations from the many additional lattice and other modes that exist on larger energy scales and have considerably more heat capacity at high temperature. This may mean that only heating effects will be possible. For devices such as injection-controlled superconducting links that rely on the resistivity of the superconducting material when it is in the normal state, the high resistivity of the oxide superconductors might be an additional advantage.

### 3.4. *Conclusions on Nonequilibrium Devices*

The most vigorously pursued nonequilibrium superconducting devices, the quiteron and injection-controlled links, do not function like the fluid-actuated valve that characterizes true transistor-like action. Both of these also involve superconductors driven far from equilibrium. The reciprocity evident in the quiteron rules it out as being of much interest; injection-controlled links might be viable with low carrier density oxide superconductors (low-$T_c$ and high-$T_c$), but there are serious technological obstacles to incorporating films of these materials in useful device configurations. It may be that basing device operation on superconductors being driven so far from equilibrium will always lead to the slow time constants associated with substantial heating.

Two ways of operating stacked junction devices—by controlled tunneling through the gap of a superconductor or by a tunneling analog of the metal

base transistor and SUBSIT—give true transistor action and do not involve driving superconductors so far from equilibrium. Both of these require high current density junctions on very thin electrodes that are of a higher quality than has yet been demonstrated. Further research is required to assess whether or not such high current density, high quality junctions, and the devices they would enable are really viable, and this research appears to be best carried out in a low-$T_c$ context.

## 4. Magnetic and Other Devices

Superconducting logic gates, beginning with the cryotron and continuing through the use of single Josephson junctions to interferometers (SQUIDs), have relied heavily on magnetic control of supercurrents to provide a pseudo third terminal. However Josephson-based elements are still two-terminal devices, relying on the addition of currents to exceed a threshold value (the use of a magnetic field to reduce the threshold is formally equivalent to simply adding currents). An interesting variation of this type of device is the Super-CIT (Superconducting Current Injection Transistor), proposed and studied by van Zeghbroeck [123], and currently under active investigation by Nordman *et al.* [124]. The device, discussed in Ref. [1], is electrically a dual of the FET, with a reversal of the roles of current and voltage, magnetic and electric fields, resistance and conductance, etc. Thus, the input voltage, rather than the input current is zero (infinite voltage, rather than current, gain). These devices do not fit the fluid analogy; an appropriate analogy would use flow to control pressure, and the resulting device would have to be used in an entirely new way to do logic. Also, although magnetic devices of this type tend to be very long, restricting their potential application in advanced digital cricuits, analog applications are more appropriate [124]. Finally, this device is related to the vortex flow transistor [125], which is also currently under investigation [126].

Given the difficulties in using magnetic fields to control fast microelectronic devices, the question arises of whether control by magnetic fields can be ruled out on fundamental grounds. For example, the relatively large spatial extent of the quantum of magnetic flux compared to that of an electron has significance for microelectronic devices. Nevertheless, a general dismissal does not come easily, as recognized years ago by Landauer [4]. So it is not surprising that device schemes based upon magnetic control continue to be advanced. Some of these devices may prove useful in applications in which high circuit density is not required.

One novel type of device, proposed by Mannhart *et al.* [127], uses a magnetic field to control filamentary current flow during avalanche breakdown in a semiconductor (making this a type of superconductor–semiconductor hybrid). In a lightly doped semiconductor, avalanche breakdown occurs at low electric fields, and current flows in well-defined filamentary channels. A perpendicular magnetic field is used to control these currents via the Lorentz force. The device is another magnetic analog of the FET, with nearly zero input impedence. Although operation in the GHz range may be possible, there has been no discussion of the use of these devices in truly high speed circuits, where they presumably suffer from the limitations similar to other magnetic FET analogs [1]. Also, in experiments to date, these devices operate on a scale of volts, and it is not clear that the operating voltage and current can be brought into suitable ranges with voltage and current gain.

Three-terminal devices based on the magnetoelectric effect have also been proposed [128,129]. Goldman [128] suggested a two-junction thin film sandwich, one junction of which contained a magnetoelectric barrier. Switching that junction into the voltage state would produce a magnetic field that is coupled into the other junction. In principle, such a device could be quite fast ($\sim 10$ ps switching time), although the relevant time constant has not been experimentally measured. Unfortunately, the small size of the magnetoelectric coefficient in known magnetoelectric materials makes the required device size rather large (of order mm) and the device margin requirement rather stringent, since the desired junction voltage of order mV limits the available electric field. Prospects for this device would be markedly improved if better magnetoelectric materials were available (the magnetoelectric coefficients of known materials are far from the theoretical upper limit). Sobolewski and Hsiang [129] demonstrated this device experimentally, using a thick magnetoelectric barrier, which had a high input impedence but required several volts on the input to produce switching. Given the known problems with this device, the prospects for a low voltage version appear to be rather bleak.

Finally, there has been considerable recent interest in an area that appears to touch on some of the ultimate limits for such electronic devices, tunnel junctions in which an external electrode controls the transfer of single electrons or Cooper pairs. Three-terminal devices based on these concepts have been proposed in which single electrons control device properties. Fundamental questions remain to be answered prior to any serious discussion of practical applications of such devices. We limit ourselves to referring the

reader to the brief discussion of this subject in the chapter in this book by K.K. Likharev, V.K. Semenov, and A.B. Zorin and to the related work of Sugahara and co-workers [130].

## 5. Conclusions

We have described a number of approaches that have been used in attempts to develop three-terminal superconducting devices, none of which has produced a truly successful device to date. However, the total amount of experimental work in this area is still limited, and the motivation behind attempts to develop these devices remains strong. In some cases, the prospects are very limited; while in others future success depends upon answering several fundamental questions.

Further work towards potential high performance devices based on conventional superconductors driven far from equilibrium does not appear justified. There may be prospects for stacked-junction devices that operate close to equilibrium but require very high quality, high current density junctions. Also, more device research should be directed at exploiting low carrier density superconductors. Some oxide superconductors may have carrier densities low enough to fit into this category.

Hybrid superconductor–semiconductor devices appear promising, but they are in a very early stage of development. It is in this area that progress has been the most significant in the last five years. Based on recent advances in exploratory semiconductor technologies, including FETs and HETs, this progress is likely to continue. SUBSIT is based on an interesting principle, but relies on a special superconductor–semiconductor contact that has yet to be demonstrated. With JOFETs, the major issue is the disparity between input voltage scale and output voltage range over which superconductivity is important, and to what extent this gap can be narrowed.

Other proposed devices are in very rudimentary stages of understanding. Magnetic devices continue to appear, flux flow transistors in particular, that may be useful for specialized analog applications. Explorations of devices based on ultrasmall tunnel junctions are in a very early stage.

Finally, experimental and theoretical explorations related to devices are of interest beyond the potential device applications, as they address fundamentally important issues such as nonequilibrium superconductivity, the proximity effect and the physics of metal–semiconductor and superconductor–semiconductor interfaces.

**Acknowledgements**

The authors have collaborated with B. Bumble, A. Davidson, C. Jessen, D.P. Kern, T.N. Jackson, D. McInturff, D. Pettit, S.I. Raider, F. Rammo, H. Schmid, and J.M. Woodall in work relating to various aspects of this paper, and wish to acknowledge valuable conversations with R.A. Buhrman, D. Frank, and S. Tiwari.

Partial support of this work was provided by the U.S. Office of Naval Research under contract N00014-85-C-0361.

**References**

1. Gallagher, W.J. *IEEE Trans. Magn.* **21**, 709 (1985).
2. Nisenoff, M. *Cryogenics* **28**, 47 (1988).
3. Van Duzer, T. *Cryogenics* **28**, 527 (1988).
4. Landauer, R. *Physics Today* **23**, 22 (1970).
5. Keyes, R. *Science* **230**, 138 (1985); *Adv. Electronics and Electron Phys.* **70**, 159 (1987).
6. Keyes, R., Harris, E.P., and Konnerth, K. *Proc. IEEE* **58**, 1914 (1970).
7. Kirschman, R.K., ed. "Low-Temperature Electronics." IEEE Press, New York, 1986.
8. Raider, S.I., Kirschman, R.K., Hayakawa, H., and Ohta, H., eds. "Low Temperature Electronics and High Temperature Superconductors." Electrochem. Soc., Pennington, New Jersey, 1988.
9. Solomon, P.M. *Proc. IEEE* **70**, 489 (1982).
10. Wolf, P. *In* "SQUID '85: Superconducting Quantum Interference Devices and their Applications" (H.D. Halbohm and H. Lübbig, eds.), p. 1127. W. de Gruyter, Berlin, 1985.
11. Kleinsasser, A.W. Superconductor–silicon heterostructures. *In* "Heterostructures on Si: One Step Further with Silicon" (Y.T. Nissim, ed.). Kluwer, The Netherlands, 1988.
12. Frank, D.J., and Davidson, A. *In* "Proc. 5th Intl. Workshop on Future Electron Devices," Miyagi-Zao, Japan, 1988.
13. Chang, L.L., and Esaki, L. *Appl. Phys. Lett.* **31**, 687 (1977).
14. Gueret, P., Kaufmann, U., and Marclay, E. *Electron. Lett.* **8**, 344 (1985).
15. Capasso, F., and Kiehl, R. *J. Appl. Phys.* **58**, 1366 (1985).
16. Yokoyama, N., Imamura, K., Muto, S., Hiyamizu, S., and Nishi, H. *Japan. J. Appl. Phys. Lett.* **24**, L583 (1985); *Sol. State Electron.* **31**, 577 (1988).
17. Hess, K., Morkoc, H., Shichijo, H., and Streetman, B.G. *Appl. Phys. Lett.* **35**, 469 (1979).
18. Kastalsky, A., and Luryi, S. *IEEE Electron Dev. Lett.* **31**, 832 (1983).
19. Dennard, R.H., and Wordeman, M.W. *Physica B* **129**, 3 (1985).
20. Sze, S.M. "Physics of Semiconductor Devices," p. 248. Wiley, New York, 1981.

21. Mead, C.A. *Proc. IRE* **48**, 359 (1960).
22. Heiblum, M. *Sol. State Electron.* **24**, 343 (1981).
23. Luryi, S., and Kastalsky, A. *Physica B* **134**, 453 (1985).
24. Heiblum, M., and Fischetti, M. *In* "Physics of Quantum Electron Devices" (F. Capasso, ed.). Springer-Verlag, Berlin, 1987.
25. Dumke, W.P. *In* "Low Temperature Electronics and High Temperature Superconductors" (S.I. Raider, R. Kirschman, H. Hayakawa, and H. Ohta, eds.), p. 449. Electrochem. Soc., Pennington, New Jersey, 1988.
26. Bozler, C.O., and Alley, G.D. *IEEE Trans. Electron Dev.* **26**, 619 (1980).
27. Malik, R.J., AuCoin, T.R., Ross, R.L., Board, K., Wood, C.E.C., and Eastman, L.F. *Electron. Lett.* **16**, 836 (1980).
28. Seo, K., Heiblum, M., Knoedler, C.M., Oh, J.E., Pamulapati, J., Bhattacharya, P., *IEEE Electron Dev. Lett.* **10**, 73 (1989).
29. Palevski, A., Heiblum, M., Umbach, C.P., Knoedler, C.M., Broers, A.N., and Koch, R.H. *Phys. Rev. Lett.* **62**, 1776 (1989). Palevski, A., Umbach, C.P., and Heiblum, M. *Appl. Phys. Lett.*, **55**, 1421 (1989).
30. Levy, A.F.J. *Appl. Phys. Lett.* **48**, 1609 (1985).
31. Luryi, S. *IEEE Electron Dev. Lett.* **6**, 178 (1985).
32. Levy, A.F.J., and Chiu, T.H. *Appl. Phys. Lett.* **51**, 984 (1987).
33. Sze, S.M., and Gummel, H.K. *Solid State Electron.* **9**, 751 (1966).
34. Tonouchi, M., Sakai, H., and Kobayashi, T. *Japan J. Appl. Phys.* **25**, 705 (1986).
35. Crowell, C.R., and Sze, S. *J. Appl. Phys.* **37**, 2683 (1966).
36. Sakai, H., Kurita, Y., Tonouchi, M., and Kobayashi, T., *Japan J. Appl. Phys.* **25**, 835 (1986).
37. Kobayashi, T., Sakai, H., Kurita, Y., Tonouchi, M., and Okada, M. *Japan J. Appl. Phys.* **25**, 402 (1986).
38. Rosencher, E., Delage, S., Campidelli, Y., and Arnaud d'Avitaya, F. *Electron Lett.* **20**, 762 (1984). Rosencher, E., Badoz, P.A., Pfister, J.C., Arnaud d'Avitaya, F., Vincent, G., and Delage, S. *Appl. Phys. Lett.* **49**, 271 (1986). Hensel, J.C., Levi, A.F.J., Tung, R.T., and Gibson, J.M. *Appl. Phys. Lett.* **47**, 151 (1985). Hensel, J.C. *Appl. Phys. Lett.* **49**, 522 (1986).
39. Tonouchi, M., Hashimoto, K., Sakaguchi, Y., Kita, S., and Kobayashi, T. *Japan J. Appl. Phys.*, to be published (1989).
40. Brosious, P.R., Heiblum, M., and Kleinsasser, A.W. Unpublished work (1984).
41. Heiblum, M., Kleinsasser, A.W., and Woodall, J.M. Unpublished work (1985).
42. Gueret, P., Baratoff, A., Bending, S., Meier, H., Marclay, E., and Py, M. *In* "Proc. Intl. Conf. on High Speed Electronics" (B. Kallback and H. Beneking, eds.), Springer Series on Electronics and Photonics, Vol. 22, p. 24, 1986.
43. Kleinsasser, A.W., Woodall, J.M., Pettit, G.D., Jackson, T.N., Tang, J.Y.-F., and Kirchner, P.D. *Appl. Phys. Lett.* **46**, 1168 (1985).
44. Frank, D.J., Brady, M.J., and Davidson, A. *IEEE Trans. Magn.* **21**, 721 (1985).
45. Davidson, A., Brady, M.J., Frank, D.J., Woodall, J.M., and Kleinsasser, A.W. *IEEE Trans. Magn.* **23**, 727 (1987).
46. Tamura, H., Hasuo, S., and Yamaoka, T. *Japan J. Appl. Phys.* **24**, L709 (1985).
47. Yoshida, A., Tamura, H., Fujii, T., and Hasuo, S. *In* "Proc. 1987 Intl. Superconductivity Electronics Conf.," Tokyo, Japan, 1987.

48. Tamura, H., Fujimaki, N., and Hasuo, S. *J. Appl. Phys.* **60**, 711 (1986).
49. Silver, A.H., Chase, A.B., McColl, M., and Millea, M.F. *In* "Future Trends in Superconductive Electronics," (B.S. Deaver, C.M. Falco, J.H. Harris, and S.A. Wolf, eds.), p. 364. American Institute of Physics, New York, 1978.
50. Clark, T.D., Prance, R.J., and Grassie, A.D.C. *J. Appl. Phys.* **51**, 2736 (1980). Clark, T.D. PhD Thesis, University of London, 1971.
51. Likharev, K.K. *Rev. Mod. Phys.* **51**, 101 (1979).
52. Van Duzer, T., and Turner, C.W. "Principles of Superconductive Devices and Circuits," p. 302. Elsevier, New York, 1981.
53. Deutscher, G., and de Gennes, P.G. *In* "Superconductivity" (R.D. Parks, ed.), Vol. 2, p. 1005. Marcel Dekker, New York, 1969.
54. Kleinsasser, A.W., and Jackson, T.N. *IEEE Trans. Magn.* **25**, 1274 (1989).
55. Klapwijk, T., Heslinga, D.R., and van Huffelen, W.M. *In* "Proc. NATO Adv. Study Institute on Superconducting Electronics," Il Ciocco, Italy, June 26–July 6, 1988.
56. Glasser, L. *IEEE J. Sol. State Ckts.*, to be published (1989).
57. Nishino, T., Miyake, M., Harada, Y., and Kawabe, U. *IEEE Electron Dev. Lett.* **6**, 297 (1985).
58. Nishino, T., Yamada, E., and Kawabe, U. *Phys. Rev. B* **33**, 2042 (1986).
59. Kleinsasser, A.W. *Phys. Rev. B* **35**, 8753 (1987).
60. Takayanagi, H., and Kawakami, T. *Phys. Rev. Lett.* **54**, 2449 (1985).
61. Takayanagi, H., and Kawakami, T. *In* "Intl. Electron Dev. Mtg. Digest," p. 98. IEEE, Piscataway, New Jersey, 1985.
62. Kleinsasser, A.W., Jackson, T.N., Pettit, G.D., Schmid, H., Woodall, J.M., and Kern, D.P. *Appl. Phys. Lett.* **49**, 1741 (1986).
63. Kleinsasser, A.W., Jackson, T.N., McInturff, D., Pettit, G.D., and Woodall, J.M. Unpublished work (1987).
64. Kawakami, T., Akazaki, T., and Takayanagi, H. *In* "Proc. 1987 Intl. Superconductivity Electronics Conf.," p. 174. Tokyo, Japan, 1987.
65. Ivanov, Z., and Claeson, T. *Japan J. Appl. Phys.* **26**, suppl. 26-3, 1617 (1987).
66. Hiraki, M., and Sugano, T. *In* "Proc. 1987 Intl. Superconductivity Electronics Conf.," p. 218. Tokyo, Japan, 1987.
67. Nishino, T., Hatano, M., Hasegawa, H., Murai, F., Kure, T., Hirawa, A., Yagi, K., and Kawabe, U. *IEEE Electron Dev. Lett.* **10**, 61 (1989).
68. Kleinsasser, A.W., Jackson, T.N., McInturff, D., Pettit, G.D., Rammo, F., and Woodall, J.M. *Appl. Phys. Lett.* **55**, 1909 (1989).
69. Kroger, H. *IEEE Trans. Electron Dev.* **27**, 2016 (1980).
70. Seto, J., and Van Duzer, T. *In* "Proc. 13th Intl. Conf. on Low Temp. Phys.," Vol. 3, p. 328. Plenum, New York, 1972.
71. Hatano, M., Nishino, T., Murai, F., and Kawabe, U. *Appl. Phys. Lett.* **53**, 409 (1988).
72. Huang, C.L., and Van Duzer, T. *IEEE Trans. Electron Dev.* **23**, 579 (1976).
73. Gudkov, A.L., Likharev, K.K., and Makhov, V.I. *Sov. Tech. Phys. Lett.* **11**, 587 (1985). Gudkov, A.L., Zhuravlev, Yu.E., Makhov, V.I., and Tyablikov, A.V. *Sov. Tech. Phys. Lett.* **9**, 457 (1983). Huang, C.L., and Van Duzer, T. *Appl. Phys. Lett.*

25, 753 (1974); *IEEE Trans. Magn.* **11**, 766 (1975). Kändyba, P.E., Kolesnikov, D.P., Kolyasnikov, V.A., Koretskaya, S.T., Lavrishchev, V.P., Ryzhkov, V.A., Samus, A.N., and Semenov, V.K. *Sov. Microelectronics* **7**, 140 (1978). Okabe, Y., and Takatsu, M. *Japan J. Appl. Phys.* **24**, 1312 (1985). Ruby, R.C., and Van Duzer, T. *IEEE Trans. Electron Dev.* **28**, 1394 (1981). Schyfter, M., Maah-Sango, J., Raley, N., Ruby, R., Ulrich, B.T., and Van Duzer, T. *IEEE Trans. Magn.* **13**, 862 (1977). Serfaty, A., Aponte, J., and Octavio, M. *J. Low Temp. Phys.* **63**, 23 (1986); **67**, 319 (1987). Seto, J., and Van Duzer, T. *Appl. Phys. Lett.* **19**, 488 (1971).

74. Kawakami, T., and Takayanagi, H. *Appl. Phys. Lett.* **46**, 92 (1985).
75. de Gennes, P.G. *Rev. Mod. Phys.* **36**, 225 (1964).
76. Likharev, K.K. *Sov. Tech. Phys. Lett.* **2**, 12 (1976).
77. van Dover, R.B., De Lozanne, A., and Beasley, M.R., *J. Appl. Phys.* **52**, 7327 (1981).
78. Kleinsasser, A.W., and Jackson, T.N. *Japan J. Appl. Phys.* **26**, suppl. 26-3, 1545 (1987).
79. Aslamazov, L.G., and Fistul, M.V. *JETP Lett.* **30**, 213 (1979); *Sov. Phys. JETP* **54**, 206 (1981). Alfeev, V.N., and Gritsenko, N.I. *Sov. Phys. Sol. State* **22**, 1951 (1980). Itskovitch, I.F., and Shekhter, R.I. *Sov. J. Low Temp. Phys.* **7**, 418 (1981).
80. Alfeev, V.N., Verbilo, A.V., Kolesnikov, D.P., and Ryzhkov, V.A. *Sov. Phys. Semicond.* **13**, 93 (1979). Alfeev, V.N., and Gritsenko, N.I. *Sov. Phys. Sol. State* **24**, 1258 (1982); *Sov. J. Low Temp. Phys.* **9**, 290 (1983); **10**, 218 (1984).
81. Kresin, V.Z. *Phys. Rev. B* **34**, 7587 (1986). Tanaka, Y., and Tsukada, M., *Sol. St. Commun.* **61**, 445 (1987); *Phys. Rev. B* **37**, 5087 (1988); **37**, 5095 (1988).
82. Hatano, M., Nishino, T., and Kawabe, U. *Appl. Phys. Lett.* **50**, 52 (1987).
83. Silvert, W. *J. Low Temp. Phys.* **20**, 439 (1975).
84. Ref. [20], page 264.
85. Roth, L.B., Roth, J.A., and Schwartz, P.M. *In* "Future Trends in Superconductive Electronics" (B.S. Deaver, C.M. Falco, J.H. Harris, and S.A. Wolf, eds.), p. 384. American Institute of Physics, New York, 1978.
86. Boudville, W.J., and McGill, T.C. *J. Vac. Sci. Technol. B* **3**, 1192 (1985).
87. Chang, C.Y., Fang, Y.K., and Sze, S.M. *Sol. St. Electron.* **14**, 541 (1971).
88. Nishino, T., Hatano, M., and Kawabe, U. *Japan J. Appl. Phys.* **26**, suppl. 26-3, 1543 (1987).
89. For a review of Josephson phenomena see, for example, Barone, A., and Paterno, G. "Physics and Applications of the Josephson Effect." Wiley, New York, 1982.
90. McColl, M., Millea, M.F., and Silver, A.H. *Appl. Phys. Lett.* **23**, 263 (1973).
91. Heslinga, D.R., and Klapwijk, T. *Appl. Phys. Lett.* **54**, 1048 (1989).
92. Gurvitch, M., Kastalsky, A., Schwartz, S., Hwang, D.M., Butherus, D., Pearton, S., and Gardner, C.R. *J. Appl. Phys.* **60**, 3204 (1986).
93. Fukuyama, H., and Maekawa, S. *J. Phys. Soc. Japan* **55**, 1360 (1986).
94. Glover, R.E., and Sherrill, M.D. *Phys. Rev. Lett.* **5**, 248 (1960); and references contained in Ref. [1].
95. Hebard, A.F., Fiory, A.T., and Eick, R.H. *IEEE Trans. Magn.* **23**, 1279 (1987).
96. Gurvitch, M., Stormer, H.L., Dynes, R.C., Graybeal, J.M., and Jacobsen, D.C.

*In* "Superconducting Materials Extended Abstracts." Mat. Res. Soc., Pittsburg, Pennsylvania, 1986.
Brazovskii, S.A., and Yakovenko, V.M. *Phys. Lett. A* **132**, 290 (1988).
Giaever, I. U.S. Patent No. 3,116,427 (1963).
Gallagher, W.J., Kleinsasser, A.W., and Raider, S.I. *IBM Technical Disclosure Bulletin* **27**, 6721 (1985).
Gray, K.E. *Appl. Phys. Lett.* **32**, 392 (1978).
Faris, S.M. U.S. Patent 4,334,158; *Physica B* **126**, 165 (1984). Faris, S.M., Raider, S.I., Gallagher, W.J., and Drake, R.E. *IEEE Trans. Magn.* **19**, 807 (1983).
Wong, T.-W., Yeh, J.T.C., and Langenberg, D.N. *Phys. Rev. Lett.* **37**, 150 (1976); *IEEE Trans. Magn.* **13**, 743 (1977).
Buhrman, R.A. Three-terminal non-equilibrium superconducting devices. *In* "SQUID '85: Superconducting Quantum Interference Devices and their Applications" (H.D. Halbohm and H. Lübbig, eds.), pp. 171–188. Walter de Gruyter, Berlin, 1985.
Gray, K. Tunneling: A probe of non-equilibrium superconductivity. *In* "Nonequilibrium Superconductivity, Phonons, and Kapitza Boundaries" (K.E. Gray, ed.), pp. 131–168. Plenum, New York, 1981.
Frank, D.J., Davidson, A., and Klapwjk, T.M. *Appl. Phys. Lett.* **46**, 603 (1985).
Booth, N.E. *App. Phys. Lett.* **50**, 293 (1987).
Iguchi, I., and Kashimura, H. *In* "SQUID '85: Superconducting Quantum Interference Devices and their Applications" (H.D. Halbohm and H. Lübbig, eds.), pp. 191–195. Walter de Gruyter, Berlin, 1985.
Hatano, M., Hatano, Y., Nishino, T., Harada, Y., and Kawabe, U. *IEEE Trans. Elect. Dev.* **33**, 1286 (1986).
Gallagher, W.J. *In* "Proc. 17th Int. Conf. on Low Temp. Phys." (U. Eckern, A. Schid, W. Weber, and H. Wühl, eds.), p. 441. Elsevier, 1984.
Frank, D.J., *J. Appl. Phys.* **56**, 2553 (1984).
Iguchi, I. *J. Appl. Phys.* **59**, 533 (1986).
Hunt, B.D., and Buhrman, R.A. *IEEE Trans. Magn.* **19**, 1155 (1983).
Hunt, B.D., Rabertazzi, R., and Buhrman, R.A. *IEEE Trans. Magn.* **21**, 717 (1985).
Raider, S.I. *IEEE Trans. Magn.* **21**, 110 (1985).
Gallagher, W.J. Unpublished (1989).
Tedrow, P.M., and Meservey, R. *Phys. Rev. B* **7**, 318 (1973).
Moodera, J.S., Hao, X., Gibson, G.A., and Meservey, R. *Phys. Rev. Lett.* **61**, 637 (1988).
Takeuchi, K., and Okabe, Y. *IEEE Trans. Magn.* **25**, 1282 (1989).
Sprik, R., Gallagher, W.J., Raider, S.I., Bumble, B., and Chi, C.-C. *Appl. Phys. Lett.*, **55**, 489 (1989).
Tinkham, M. Heating and dynamic enhancement in metallic weak links. *In* "Nonequilibrium Superconductivity, Phonons, and Kapitza Boundaries" (K.E. Gray, ed.), pp. 231–262. Plenum, New York, 1981.
Batlogg, B. *Physica B* **126**, 275 (1984).
Shafer, M.W., Penney, T., Olson, B.L., Greene, R.L., and Koch, R.H. *Phys. Rev. B* **39**, 2914 (1989).

123. van Zeghbroeck, B.J. *Appl. Phys. Lett.* **42**, 736 (1984); *IEEE Trans. Magn.* **21**, 916 (1984).
124. McGinnis, J.P., Beyer, J.B., and Nordman, J.E. *IEEE Trans. Magn.* **25**, 1262 (1989); and references therein.
125. Rajeevakumar, T.V. *Appl. Phys. Lett.* **39**, 439 (1981).
126. McGinnis, J.P., Hohenwarter, G.K.G., and Nordman, J.E. *IEEE Trans. Magn.* **25**, 1258 (1989). Hashimoto, T., Enkupu, K., and Yoshida, K. *IEEE Trans. Magn.* **25**, 1266 (1989).
127. Mannhart, J., Huebener, R.P., Parisi, J., and Peinke, J. *Sol. State Commun.* **58**, 323 (1986); Mannhart, J., and Huebener, R.P. *J. Appl. Phys.* **60**, 1829 (1986); Mannhart, J., Parisi, J., Mayer, K.M., and Huebener, R.P. *IEEE Trans. Electron. Dev.* **34**, 1802 (1987).
128. Goldman, A.M. *IEEE Trans. Magn.* **21**, 928 (1985).
129. Sobolewski, R., and Hsiang, T.Y. *In* "Proc. 1987 Intl. Superconductivity Electronics Conf.," p. 167. Tokyo, Japan, 1987.
130. Sugahara, M., Yoshikawa, N., and Murakami, T. *IEEE Trans. Magn.* **25**, 1278; 1286 (1989); and references therein.